

# EXPANDED AROMATIC MONOMERS FOR FUNCTIONAL POROUS POLYMERS

by

Arosha Aruni Kumari Karunathilake



APPROVED BY SUPERVISORY COMMITTEE:

---

Dr. Ronald A. Smaldone, Chair

---

Dr. Michael C. Biewer

---

Dr. John W. Sibert

---

Dr. Yves J. Chabal

Copyright 2017

Arosha Aruni Kumari Karunathilake

All Rights Reserved

*To my loving parents*  
*and to my loving husband, Eranda*

EXPANDED AROMATIC MONOMERS FOR FUNCTIONAL POROUS POLYMERS

by

AROSHA ARUNI KUMARI KARUNATHILAKE, BS

DISSERTATION

Presented to the Faculty of

The University of Texas at Dallas

in Partial Fulfillment

of the Requirements

for the Degree of

DOCTOR OF PHILOSOPHY IN

CHEMISTRY

THE UNIVERSITY OF TEXAS AT DALLAS

May 2017

## ACKNOWLEDGMENTS

First and foremost, I would like to acknowledge my research advisor and mentor, Dr. Ronald A. Smaldone, for his endless scientific guidance, unwavering support and enthusiasm throughout the years. His guidance and encouragement were always behind my success. I thank members of my supervisory committee Dr. Michael C. Biewer, Dr. John W. Sibert and Dr. Yves J. Chabal for their constructive advice and new ideas. Their advice and comments helped me to add value to my research work and to come up with high quality outputs.

I respect and appreciate all my colleagues from the Smaldone group, both past and present: Dr. Christina Thompson for getting me started in the lab and introducing me to projects, Dr. Sumudu Wijenayake for enduring friendship and technical expertise, Fei Li for his support and encouragement at my early years, Sampath Alhakoon for his valuable discussions and always being there to help me, Gayan Adikari for his friendship, support and encouragement, Yinhuwan Xie for positive attitude and sense of humor, Vicky, Josh, Daniel and Grant for their helpful nature and company. I also thank my undergraduate lab mates Amy, Quang, Dorothy, Cathy, Ivana, and Ethan for their hard work and assistance, and all the other undergraduate and high school lab mates for their support at various tasks.

Special thanks to Dr. John Ferraris for the collaboration on electrochemical experiments and for his guidance and advice and to my friend and collaborator Sahila Peranathen for her expertise, relentless spirit and valuable discussion and assistance over the years. I would like to extend my acknowledgement to Dr. Sung Joon Kim and team of collaborators at Baylor University for their support with solid state NMR.

My Special thanks goes to the Chemistry Department staff members Betty, Linda, Kelli, Deb, Lydia for always being helpful and pleasant, to UTD NanoTech Institute, UTD Cleanroom Research Laboratory and Department of Materials Science and Engineering for their instrumentations and to Dr. George McDonald, Dr. Hien Nguyen, Dr. Greg McCandless, Dr. Winston Layne, Dr. Roger Robinsons, Dr. Ben Bachelor and Dr. Samsuddin Faisal for their expertise and availability whenever I needed help.

I thank all my friends at UTD for their warm friendship, support and encouragement which contributed to my academic success and made life at UTD memorable.

I am grateful to my parents, for their endless love, guidance and encouragement throughout my journey. I am also thankful to my loving brother, my parents-in-law, sister-in-law and brother-in-law for their caring, love and inspiration which helped me to achieve this goal. Finally, it is with deepest gratitude I thank my husband, Eranda. I would not have made it this far if not for his unwavering love, patience, continuous encouragement and guidance over the last five years.

March 2017

## EXPANDED AROMATIC MONOMERS FOR FUNCTIONAL POROUS POLYMERS

Arosha Aruni Kumari Karunathilake, PhD  
The University of Texas at Dallas, 2017

Supervising Professor: Dr. Ronald A. Smaldone

Porous materials have attracted immense attention in the scientific community due to their excellent performance in a variety of applications such as gas adsorption, separation and catalysis. In the last few years utilizing expanded aromatic monomers for porous polymers has emerged as a method of designing and synthesizing functional porous polymers. As described in Chapter 1, expanded aromatic scaffolds such as hexaphenylbenzene (HEX), hexabenzocoronene (HBC) and corannulene have unique chemical structures and electronic properties that could be used to improve the performance of porous materials for applications in energy storage. Their unique symmetry and shape can be used to introduce novel topologies and conjugated  $\pi$  systems to porous polymers which provides improved gas binding ability. Chapter 2 describes a series of novel corannulene based porous organic polymers (BB-POPs) that retain the inherent redox activity of corannulene when incorporated into the porous system. These materials are the first reported POPs based on corannulene. Chapter 3 describes the synthesis and characterization of novel HEX and HBC based POPs (HEX-POP-93 and HBC-POP-98) for volatile organic compounds (VOCs) adsorption. Interestingly, while both POPs have moderate BET surface areas ( $687$  and  $548 \text{ m}^2 \text{ g}^{-1}$  respectively), they both show an excellent selectivity for organic vapors over water, with a high

benzene adsorption capacity of 99.9 wt.% for HEX-POP-93. Presented in Chapter 4 is the bottom-up synthesis of nanographene based porous organic polymers. Nanographenes (NGs) such as HBC are observed to readily adopt  $\pi$ -stacked arrangements. As such, stable  $\pi$ -stacked conformations between the HBC units are likely a major directing force for the POP structure. Since these interactions cause the  $\pi$ -surfaces within the polymer to be blocked, they limit the gas and VOCs adsorption capability. Thus, pre-synthesized HEX based POPs were post-synthetically cyclodehydrogenated to obtain NG based POPs with good surface areas and high CO<sub>2</sub> binding ability (22 wt. %). The overall findings presented in this dissertation suggest that the expanded aromatic structures introduce novel properties to porous materials while the careful design will enhance the ultimate properties.



## TABLE OF CONTENTS

ACKNOWLEDGMENTS.....	v
ABSTRACT.....	vii
LIST OF FIGURES.....	xi
LIST OF TABLES.....	xv
CHAPTER 1 INTRODUCTION TO FUNCTIONAL POROUS MATERIALS BASED ON HEXAPHENYLBENZENE, HEXABENZOCORONENE AND CORANNULENE.....	1
1.1 Abstract .....	1
1.2 Porous Materials .....	1
1.3 Goal: Expanded aromatic monomers for functional porous materials .....	7
1.4 Porous materials synthesized with HEX, HBC and Corannulene .....	13
1.5 Significance of porous materials synthesized with HEX, HBC and BB .....	19
1.6 Conclusion .....	22
1.7 References .....	22
CHAPTER 2 ELECTROCHEMICALLY ACTIVE POROUS ORGANIC POLYMERS BASED ON CORANNULENE.....	28
2.1 Abstract .....	29
2.2 Introduction .....	29
2.3 Experimental .....	31
2.4 Result and discussion .....	35
2.5 Conclusion .....	44
2.6 Acknowledgements .....	45
2.7 References .....	45
CHAPTER 3 HEXAPHENYLBENZENE AND HEXABENZOCORONENE-BASED POR- OUS POLYMERS FOR THE ADSORPTION OF VOLATILE ORGANIC COMPOUNDS .....	50
3.1 Abstract .....	51
3.2 Introduction .....	51
3.3 Experimental .....	53

3.4	Result and discussion .....	56
3.5	Conclusion .....	67
3.6	Acknowledgements .....	67
3.7	References .....	67
CHAPTER 4 HYPERCROSSLINKED NANOGRAFENE BASED POROUS POLYMERS VIA POST SYNTHETIC MODIFICATIONS .....		74
4.1	Abstract .....	75
4.2	Introduction .....	75
4.3	Experimental .....	79
4.4	Result and Discussion .....	83
4.5	Porosity and surface area .....	87
4.6	Conclusion .....	92
4.7	Acknowledgements .....	93
4.8	References .....	93
BIOGRAPHICAL SKETCH.....		96
CURRICULUM VITAE		

## LIST OF FIGURES

Figure 1-1. Classification of porous materials .....	2
Figure 1-2. (a) A typical approach to MOF synthesis, (b) unit cell of MOF-5 (MOF-5 structure is reproduced from J. Mater. Chem., 2006, 16, 2464–2472 (Reference 12) with permission of The Royal Society of Chemistry) .....	3
Figure 1-3. (a) Some common reversible reactions that have been successfully developed for the construction of COF materials, (b) synthesis of 2D hexagonal COF-5 .....	5
Figure 1-4. (a), (b) and (c) represent different methods of synthesizing HCPs .....	6
Figure 1-5. A representative polymer of intrinsic microporosity .....	6
Figure 1-6. (a) Some common reactions that have been successfully used for synthesis of CMPs and PAFs, (b) synthesis of CMP-1 (X = Br or I) and (c) synthesis of PAF-1 (X = Br or I) .....	7
Figure 1-7. Structures of hexaphenylbenzene, hexabenzocoronene and corannulene .....	8
Figure 1-8. Examples of PPB core structures .....	9
Figure 1-9. (a) Several common simple PAHs, (b) graphene and nanographenes and (c) buckminsterfullerene and curved PAHs .....	10
Figure 1-10. Common methods for the synthesis of hexaphenylbenzene (HEX) and hexa-peri hexabenzocoronene (HBC) .....	11
Figure 1-11. Methods for the synthesis of corannulene .....	12
Figure 1-12. Reported HEX and HBC based POPs .....	15
Figure 1-13. HEX based PAFs with Yamamoto-Ullmann cross coupling and Scholl oxidation ..	16
Figure 1-14. HEX and HBC based COFs and MOFs (Pbz-MOF-1 structure is reprinted with permission from J. Am. Chem. Soc. 2016, 138, 12767-12770 (reference 56) copyright 2016 American Chemical Society) .....	17
Figure 1-15. Corannulene-based porous materials .....	18
Figure 2-1. Structure of corannulene .....	29
Figure 2-2. Synthesis of BB-POPs 1-3 and model compound (BB-PA) from Sonogashira copolymerization condition: Pd(PPh <sub>3</sub> ) <sub>4</sub> , CuI, Et <sub>3</sub> N, toluene, 90 °C .....	31

Figure 2-3. Synthesis of 1,4-diethynylbenzene (DEB), 1,3,5-trisethynylbenzene (TEB), tetrakis(4-ethynyl)-tetraphenylmethane (TPM), and 1,2,5,6-tetrabromocorannulene (TBC) .....	34
Figure 2-4. IR spectra of tetrakis(4-ethynyl)-tetraphenylmethane (TPM) and BB-POPs. ....	36
Figure 2-5. SEM images of BB-POPs: BB-POP-1 (left), BB-POP-2 (middle) and BB-POP-3 (right) .....	37
Figure 2-6. TGA curves of BB-POPs .....	37
Figure 2-7. PXRD patterns of BB-POPs.....	38
Figure 2-8. Normalized emission spectra in CH <sub>2</sub> Cl <sub>2</sub> with excitation at 300 nm .....	38
Figure 2-9. (a) Nitrogen adsorption at 77 K (solid symbols) and desorption (open symbols) isotherms .....	39
Figure 2-10. Differential (line) and cumulative (dash) pore size distributions of BB-POP-1 (blue), BB-POP-2 (green), BB-POP-3 (red) .....	40
Figure 2-11. CO <sub>2</sub> adsorption isotherms adsorption (filled circles) desorption (open circles) for BB-POP-1 (blue), BB-POP-2 (green) and BB-POP-3 (red) at (a) 273 K (b) 298 K and (c) Heat of adsorption for CO <sub>2</sub> .....	41
Figure 2-12. H <sub>2</sub> adsorption isotherms at 77 K for BB-POP-1 (blue), BB-POP-2 (green) and BB-POP-3 (red) .....	42
Figure 2-13. Cyclic voltammograms of BB-POP-2 and 3, corannulene (1 mM), BB-PA (1 mM) and reference (bare gold electrode) in 0.1 M tetrabutylammonium hexafluorophosphate /DMF using Pt mesh as the counter electrode, Ag/Ag <sup>+</sup> as the reference electrode and Au as the working electrode .....	43
Figure 2-14. Cyclic voltammograms of corannulene (1 mM), BB-PA (1 mM), BB-POP-2 and 3 in 0.1 M tetrabutylammonium hexafluorophosphate/DMF using Pt mesh as the counter electrode, Ag/Ag <sup>+</sup> as the reference electrode and Au as the working electrode.....	44
Figure 3-1. Structure of hexaphenylbenzene (HEX) and hexabenzocoronene (HBC) .....	53
Figure 3-2. Reaction conditions for the synthesis of HEX-POP-93 and HBC-POP-98 .....	53
Figure 3-3. Synthesis of hexa(4-iodophenyl)benzene (HPB-6I) and hexakis(4-iodo)-peri-hexabenzocoronene (HBC-6I) .....	56
Figure 3-4. IR spectra of starting material: TPM and two POPs: HEX-POP-93 and HBC-POP-98 .....	58

Figure 3-5. Solid state $^{13}\text{C}$ -CPMAS and $^{13}\text{C}$ -NQS NMR spectra.....	58
Figure 3-6. Carbon and iodine EDAX maps of HEX-POP-93 and HBC-POP-98 .....	59
Figure 3-7. TGA curves of HEX-POP-93 and HBC-POP-98.....	59
Figure 3-8. PXRD patterns of HEX-POP-93 and HBC-POP-98 .....	60
Figure 3-9. Nitrogen adsorption (solid symbols) and desorption (open symbols) isotherms at 77 K and pore size distribution (solid line) and cumulative pore volume (dash) .....	61
Figure 3-10. $\text{CO}_2$ adsorption desorption isotherms at 273 K (circle) and 298 K (triangle).....	62
Figure 3-11. Adsorption and desorption isotherms of (A) benzene, (B) toluene, (C) cyclohexane and (D) methanol vapour for HEX-POP-93 and HBC-POP-98 at 298 K.....	63
Figure 3-12. Adsorption isotherms of cyclohexane, benzene, toluene, methanol and water vapours at 298 K for (a) HEX-POP-93 and (b) HBC-POP-98 .....	64
Figure 3-13. Adsorption weight percent of cyclohexane, benzene, toluene, methanol and water vapours at 298 K for HEX-POP-93 (red) and HBC-POP-98 (blue) .....	65
Figure 4-1. Structures of graphene, hexabenzocoronene (HBC) and hexaphenylbenzene (HEX) and synthesis of HBC via cyclodedrogenation of HEX.....	77
Figure 4-2. Different approaches for the synthesis of nanographene based POP via Friedel Crafts polymerization .....	78
Figure 4-3. Synthesis of HEX-FC, HEX-SO and nanographene based POPs of each via cyclodehydrogenation .....	79
Figure 4-4. Synthesis of Hexaphenylbenzene.....	80
Figure 4-5. Raman spectra of polymers .....	85
Figure 4-6. FT-IR spectra of polymers .....	86
Figure 4-7. Powder X-ray diffraction (PXRD) of polymers .....	86
Figure 4-8. TGA of polymers .....	86
Figure 4-9. SEM images if of initial polymers and corresponding NG polymers .....	87
Figure 4-10. Nitrogen adsorption (solid symbols) and desorption (open symbols) isotherms at 77 K and pore size distribution (solid line) and cumulative pore volume (dash) of POPs.....	89

Figure 4-11. CO <sub>2</sub> adsorption isotherms at (a) 273 K, (b) 298 K and (c) heat of adsorption for CO <sub>2</sub>	92
Figure 4-12. CH <sub>4</sub> adsorption isotherms at (a) 273 K and (b) 298 K	92

## LIST OF TABLES

Table 1-1. Reported HEX, HBC and BB based porous materials and their properties. ....	20
Table 2-1. Elemental ratios in BB-POPs based on EDX .....	37
Table 2-2. Pore structure parameters of polymers obtained by N <sub>2</sub> adsorption .....	39
Table 2-3. Reduction potentials vs Ag/Ag <sup>+</sup> of corannulene, BB-PA and BB-POPs in DMF/Bu <sub>4</sub> NPF <sub>6</sub> (0.1 M) .....	43
Table 3-1. Elemental ratios in HEX-POP-93 and HBC-POP-98 for carbon, iodine, and palladium based on EDX analysis .....	59
Table 3-2. Surface area and pore structure properties of polymers obtained by N <sub>2</sub> adsorption ....	61
Table 3-3. Adsorption capacities for POPs in this work and other materials .....	65
Table 4-1. I <sub>D</sub> /I <sub>G</sub> ratio based on Raman analysis .....	85
Table 4-2. Pore structure parameters of polymers obtained by N <sub>2</sub> adsorption .....	88

# **CHAPTER 1**

## **INTRODUCTION TO FUNCTIONAL POROUS MATERIALS BASED ON HEXAPHENYLBENZENE, HEXABENZOCORONENE AND CORANNULENE**

### **1.1 Abstract**

Rational design and synthesis of porous materials with controlled architecture and functionality have gained considerable attention over the last few years. Size, geometry and inherent properties of monomers play a vital role in the structure and functionality of porous materials. While simple benzenoid derivatives with four or fewer benzene rings have been widely employed as monomers, expanded  $\pi$  aromatics molecules are currently emerging as potential monomers for the synthesis of porous materials with interesting structures and properties. They expect to have excellent gas and energy storage properties due to extended  $\pi$  conjugations. Further, inherent electronics of these molecules has the potential of introducing electronic functionalities to porous materials. Hexaphenylbenzene (HEX), hexabenzocoronene (HBC) and corannulene (BB) are three expanded  $\pi$  aromatics monomers with unique shapes, symmetries and electronic properties. Herein, a summary of the potential and recent progress of these three molecules on synthesizing functional porous materials is provided.

### **1.2 Porous Materials**

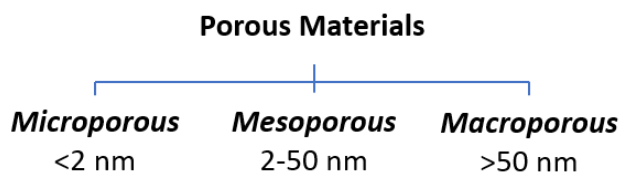
Porous materials, solid state materials with void spaces, have been of great interest over the last two decades due to their structural morphology and diverse applications.<sup>1-4</sup> They have shown promising implementations in varied applications in separation chemistry, gas and energy storage, sensing, catalysis, electronic devices and drug delivery.<sup>5,6</sup> Current research in the field is focused



on understanding structure-function correlation, leading to the efficient synthesis of porous materials with designed properties and functionality.<sup>7</sup>

Porous materials can be classified as macro (>50 nm), meso (2-50 nm) and microporous (< 2 nm) or sometimes collectively identified as nanoporous materials (Figure 1-1).<sup>2</sup> Numerous types of nanoporous materials have been synthesized with inorganic and organic building units *via* coordination or covalent chemistry. The resulting solids can be crystalline or amorphous depending on the nature of the bond formation that occurs during the synthesis.<sup>8-10</sup> If the synthesis is *via* a coordination bond or reversible covalent bond formation, then it allows for error correction during the network formation to produce thermodynamically favorable networks which are generally crystalline. Conversely, materials formed under kinetic control typically result in amorphous materials.

#### Depending on pore size



#### Building Units

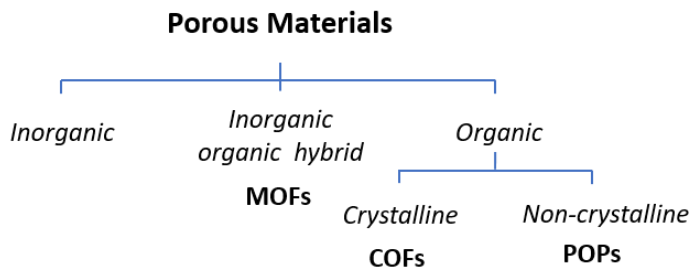


Figure 1-1. Classification of porous materials

The most common classification of modern nanoporous materials is based on the type of building units used, which are classified as: metal organic frameworks (MOFs), covalent organic frameworks (COFs) and porous organic polymers (POPs) (Figure 1-1). MOFs and COFs are crystalline materials while POPs are amorphous. POPs are further classified as polymers of intrinsic microporosity (PIMs), conjugated microporous polymers (CMPs), porous aromatic frameworks (PAFs) and hypercrosslinked porous polymers (HCPs), *etc.*<sup>2</sup> However, these classifications are not consistent and some materials can be categorized under more than one class.

### 1.2.1 Metal-organic frameworks (MOFs)

Metal-organic frameworks (MOFs)<sup>8,11</sup> are crystalline porous materials which are synthesized *via* copolymerization of organic linkers with metal ions (Figure 1-2).<sup>12</sup> Generally organic units are multidentate organic carboxylates or another negative functionality. Metal ions form metal containing clusters which are known as secondary building units (SBUs). The reversible nature of the coordination bond formation between metal cations/cluster and organic linkers facilitates the formation of crystalline frameworks.

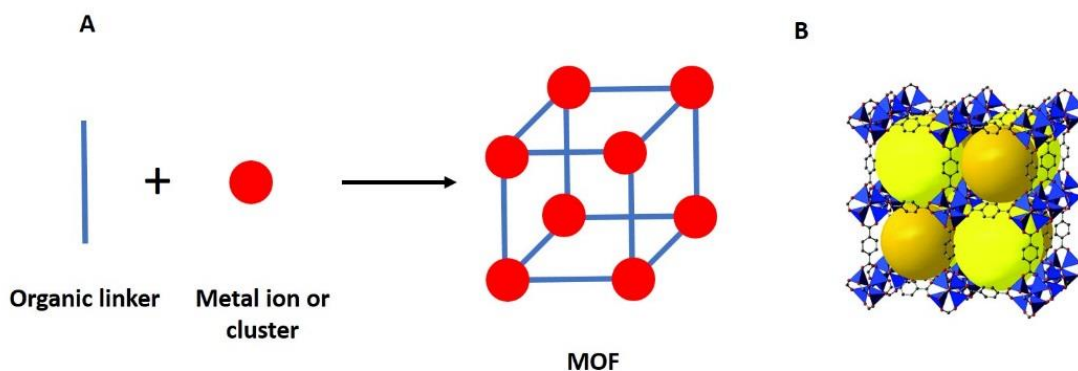


Figure 1-2. (a) A typical approach to MOF synthesis, (b) unit cell of MOF-5 (MOF-5 structure is reproduced from *J. Mater. Chem.*, **2006**, *16*, 2464–2472 (Reference 12) with permission of The Royal Society of Chemistry)

More than 20,000 different MOFs with various geometries and functionalities have been synthesized by varying the building units, giving MOFs a greater structural diversity greater than any other class of porous material.<sup>13</sup> The Brunauer, Emmett and Teller (BET) surface area of MOFs can go as high as 7000 m<sup>2</sup>/g,<sup>14</sup> exceeding those of traditional porous materials such as zeolites and activated carbons or modern materials such as COFs and POPs. MOFs have found applications in gas storage, purification and separation, as well catalysis, sensing and drug delivery applications.<sup>15</sup>

### **1.2.2 Covalent organic frameworks (COFs)**

Covalent organic frameworks (COFs)<sup>16</sup> are crystalline and can be synthesized by covalently linking organic monomers. The linkers are generally connected using reversible dynamic bonds, such as boronic esters, azines, imines, or hydrazones. Thus, they consist of only of light elements such as carbon, hydrogen, oxygen and boron or nitrogen (Figure 1-3). The crystallinity observed in these materials is due to the reversible nature of the covalent bond formation, while the aromatic interactions and electronics of the organic linkers can facilitate the thermodynamic control of covalent bond formation. With varying building units, 2D and 3D COFs have been synthesized using solvothermal, ionothermal and mechanochemical methods. The highest reported BET surface area of COFs is 4210 m<sup>2</sup> g<sup>-1</sup>.<sup>17</sup> COFs are used in a variety of applications that range from gas separation to capacitive energy storage to explosive sensing.<sup>16</sup>

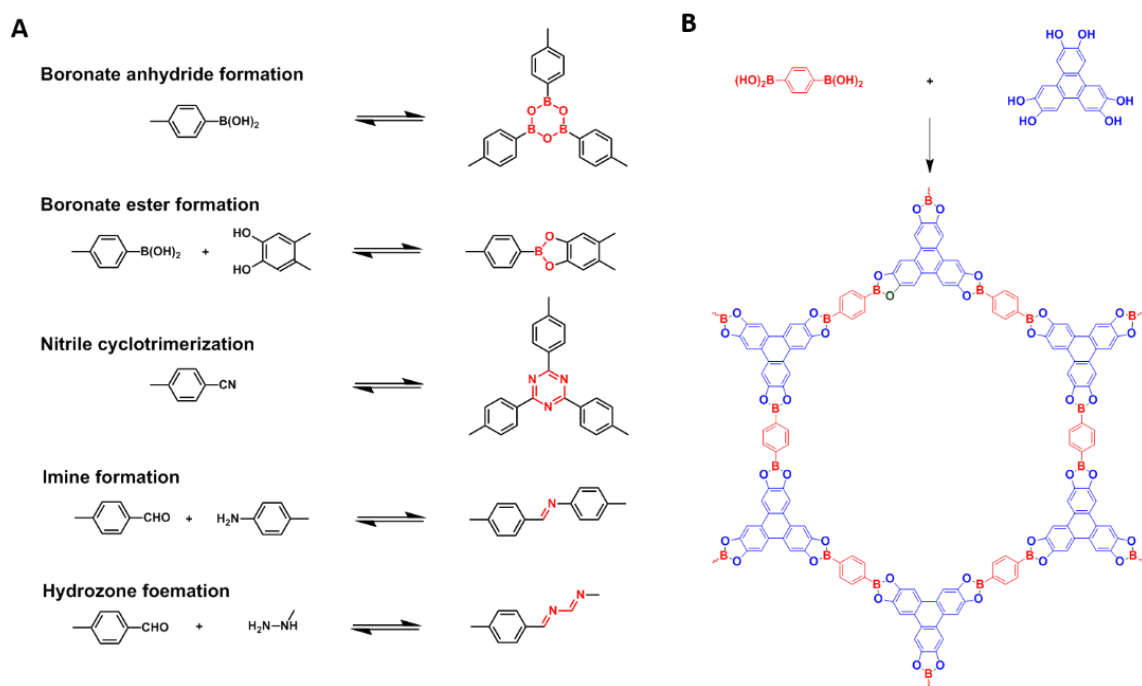


Figure 1-3. (a) Some common reversible reactions that have been successfully developed for the construction of COF materials, (b) synthesis of 2D hexagonal COF-5

### 1.2.3 Porous organic polymers (POPs)

Porous organic polymers (POPs) are amorphous porous materials which are synthesized by covalently linking organic monomers via various kinetically controlled organic reactions such as C-C cross coupling reactions and Friedel-Crafts reactions. In generally, most POPs have excellent thermal and moisture stability (typically better than MOFs and COFs).<sup>7</sup> Also, they can be synthesized with various reactions and monomers.<sup>2</sup> Thus, there are different types of POPs based on synthesis method and network morphology such as HCPs, PIMs, CMPs and PAFs.

Hypercrosslinked polymers (HCPs) are extensively crosslinked polymer networks with permanent porosity. HCPs can be produced in three ways (Figure 1-4): (a) intermolecular and intramolecular crosslinking of preformed polymer chains, (b) direct step growth polycondensation of suitable monomers and (c) knitting of aromatic compounds using an external cross-linker to form a

polymer.<sup>18</sup> Today, knitting of aromatic compounds via Friedel-Crafts reactions with Lewis acids such as  $\text{FeCl}_3$  is considered to be one of the most cost-effective methods of synthesizing porous materials.<sup>19</sup>

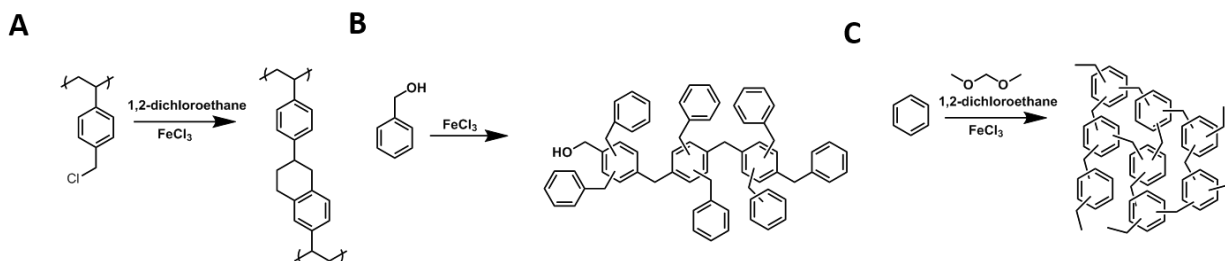


Figure 1-4. (a), (b) and (c) represent different methods of synthesizing HCPs

Polymers of intrinsic microporosity (PIMs) are a class of solution processable porous polymers and generally obtained through aromatic substitution polymerization (Figure 1-5). Their fused-ring structures prevent the polymer chains packing efficiently, hence obtaining a porous structure. Other than gas adsorption applications they can easily be developed into gas selective membranes and sensors as these materials are solution processable.<sup>20</sup>

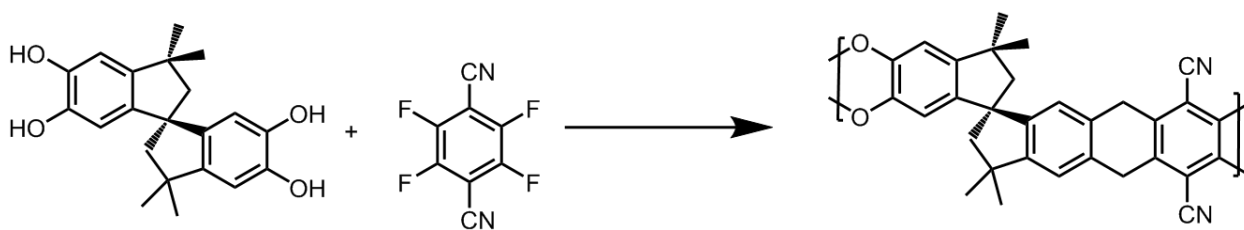


Figure 1-5. A representative polymer of intrinsic microporosity

Conjugated microporous polymers (CMPs)<sup>21,22</sup> are typically prepared via metal-catalyzed cross-coupling of di- or trihalo aromatics with di- or triethynyl aromatics while other methods such as cyclotrimerization or oxidative coupling have also been employed (Figure 1-6). CMPs possess interesting optoelectronic properties due to their conjugated network structure. Therefore, other

than gas storage and separation applications they are suitable for various electronic device applications.

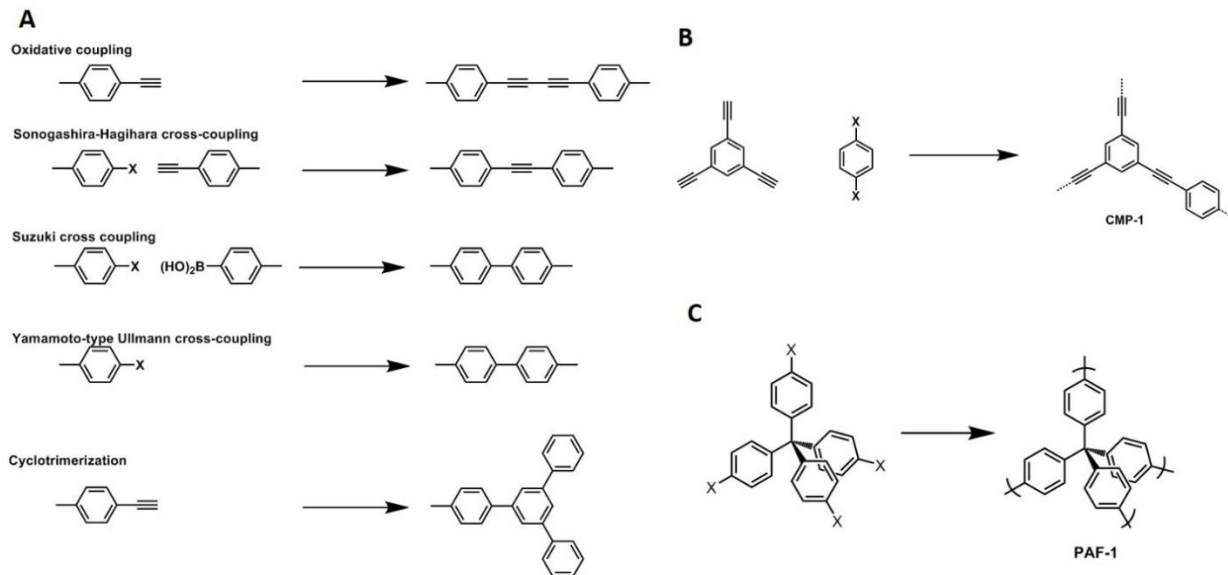


Figure 1-6. (a) Some common reactions that have been successfully used for synthesis of CMPs and PAFs, (b) synthesis of CMP-1 (X = Br or I) and (c) synthesis of PAF-1 (X = Br or I)

Porous aromatic frameworks (PAFs) are synthesized through the homocoupling of aromatic bromides *via* nickel(0)-catalyzed Yamamoto-type homocoupling (Figure 1-6). Recently, the Scholl oxidation was introduced as a low-cost alternative for synthesizing PAFs. The PAF known as PAF-1 has the highest recorded BET surface for any porous organic polymer, of 5640 m<sup>2</sup> g<sup>-1</sup>.

1,23,24

### 1.3 Goal: Expanded aromatic monomers for functional porous materials

Most of the porous materials are built with benzenoid organic linkers.<sup>7</sup> However, only simple benzenoid derivatives with four or fewer benzene rings are mostly incorporated, while extended benzenoid systems such as polyphenylbenzenes (PPBs) and polycyclic aromatic hydrocarbons (PAHs) are rarely used. The expanded aromatic scaffolds have interesting structural and functional

properties which can introduce novel topologies and functionalities into porous materials such as improved gas binding, energy storage and electronic properties. Herein, we are discussing the potential of using three expanded aromatic scaffolds: hexaphenylbenzene (HEX,  $C_{42}H_{30}$ ), hexabenzocoronene (HBC,  $C_{42}H_{18}$ ) and corannulene (BB,  $C_{20}H_{10}$ ) (Figure 1-7) in porous materials.

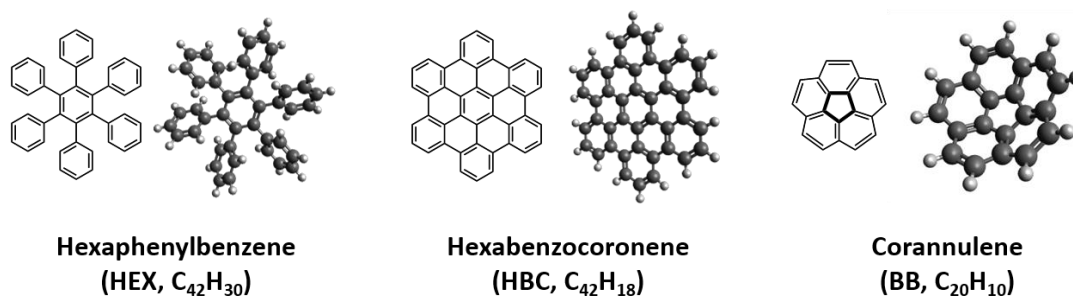


Figure 1-7. Structures of hexaphenylbenzene, hexabenzocoronene and corannulene

### 1.3.1 Extended $\pi$ conjugation for improved gas and energy storage.

When designing porous materials for gas or vapor adsorption and separation, improving the quality of the non-covalent interactions between the pore surface and binding substance is important. Materials with highly conjugated surfaces such as carbon nanotubes and porous graphene have demonstrated strong adsorption of gases like hydrogen.<sup>25</sup> Further, studies with PAHs have proven that their  $\pi$  surface have higher gas binding abilities.<sup>26</sup> Hence, porous materials synthesized with extended aromatic monomers will possess higher gas/energy storage capacities.

### 1.3.2 Symmetry and shape for novel topologies and controlled pore size.

HEX, HBC and corannulene represent three interesting classes of aromatic compounds: PPB, planar PAHs and curved PAHs, respectively. Further, they have diverse symmetries and shapes with the potential of introducing interesting structural morphologies in porous materials.

PPBs<sup>27</sup> (Figure 1-8) are benzene derivatives with phenyl substituents attached around a central benzene ring and general precursor for PAHs. Hexaphenylbenzene (HEX),<sup>28</sup> is the most popular PPB with a six-fold symmetry and propeller-like nonplanar conformation due to the steric hindrance between the peripheral phenyl rings.

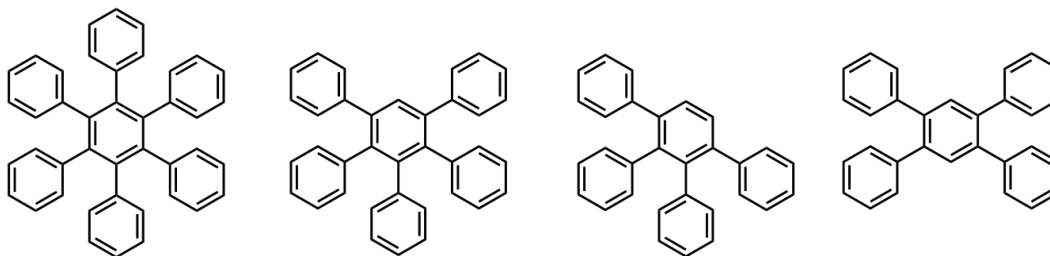


Figure 1-8. Examples of PPB core structures

PAHs, compounds consisting of fused aromatic rings (Figure 1-9a), are sometimes described as “nanographenes” as they resemble a fragment of graphene. Hexa-*peri*-hexabenzocoronene (HBC, “super-benzene”) (Figure 1-9b) is a simple PAH which is considered to be the smallest nanographene<sup>29</sup> and has a planar structure with six-fold symmetry.

The discovery of buckminsterfullerene ( $C_{60}$ ) has inspired another class of PAHs known as curved PAHs (Figure 1-9c). While graphene consists of all 6-membered rings,  $C_{60}$  has incorporated 5-membered rings resulting in a spherical structure. Similarly, curved PAHs consist with 5-membered ring resulting in a five-fold symmetry.<sup>30</sup> Corannulene is the smallest curved PAHs. The arrangement of the five benzene rings around the central five-membered ring induces the nonplanarity to corannulene with a bowl depth of 0.87 Å. Corannulene consists of one third of buckminsterfullerene, thus known as the smallest buckybowl (BB).<sup>30</sup>



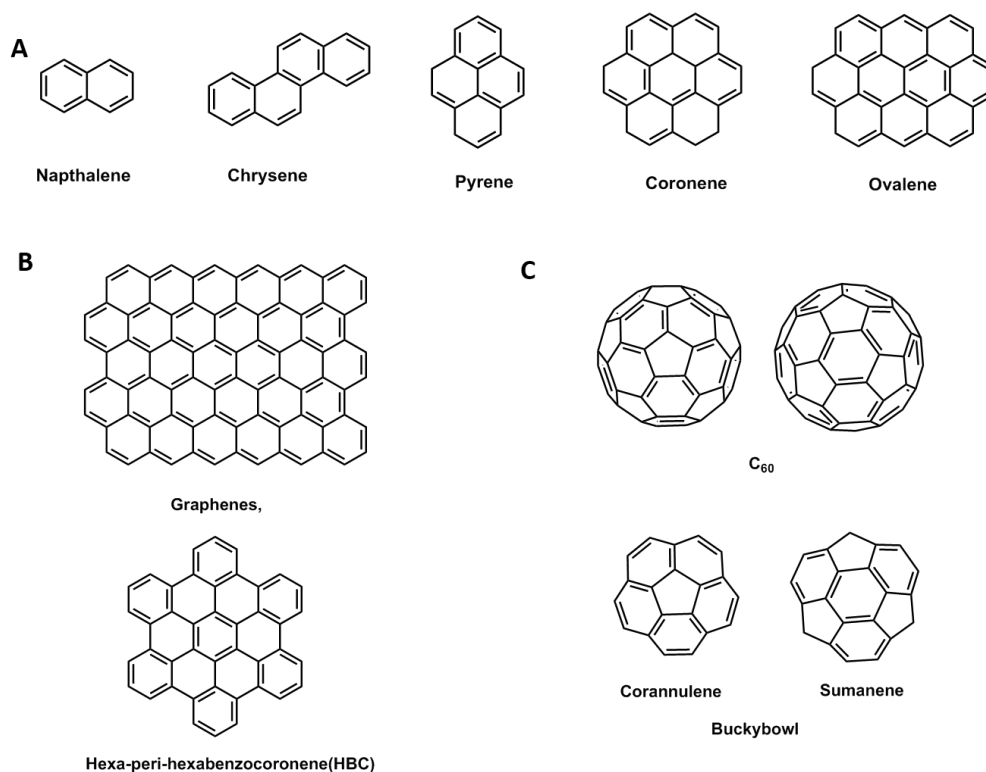


Figure 1-9. (a) Several common simple PAHs, (b) graphene and nanographenes and (c) buckminsterfullerene and curved PAHs

### 1.3.3 Convenient synthesis and functionalization methods for large scale synthesis of porous materials

Convenient large scale synthesis and functionalization methods are available for the synthesis of HEX, HBC and corannulene due to extensive research over several decades. HEX was first reportedly synthesized as early as 1933 and currently using common method of HEX synthesis was introduced by Louis F. Fieser in 1966 *via* a Diels-Alder reaction between tetraphenylcyclopentadienone and diphenylacetylene.<sup>31</sup> HBC was first reported by Clar and Ironside in 1958<sup>32</sup> and later synthesized and studied extensively since the development of synthetic route *via* oxidative cyclodehydrogenation (Scholl oxidation) of HEX by Müllen and coworkers.<sup>33,34</sup> For cyclodehydrogenation, iron (III) chloride ( $FeCl_3$ ) or dichlorodicyano-*p*-

benzoquinone (DDQ) is used as the oxidant. To date there are several ways of synthesizing HEX and HBC (Figure 1-10). Methods for functionalization of HEX and HBC with various substituents are also developed.<sup>35</sup> Corannulene was first synthesized in 1966 by Barth and Lawton with an 18-step synthesis.<sup>36</sup> However, it gained considerable attention only after the discovery of fullerenes due to the structural similarities and as a potential synthetic precursor. Since then, syntheses, structures, and properties of corannulene and related buckybowls were highly interesting topics. Thus, more practical methods for the synthesis were developed over two decades including a three step flash vacuum pyrolysis method<sup>37</sup> and an eight step solution phase synthesis which has recently been scaled up to the kilogram scale<sup>38</sup> (Figure 1-11). The availability of these methods is the basis for the design and large scale synthesis of porous materials based on these expanded aromatic scaffolds.

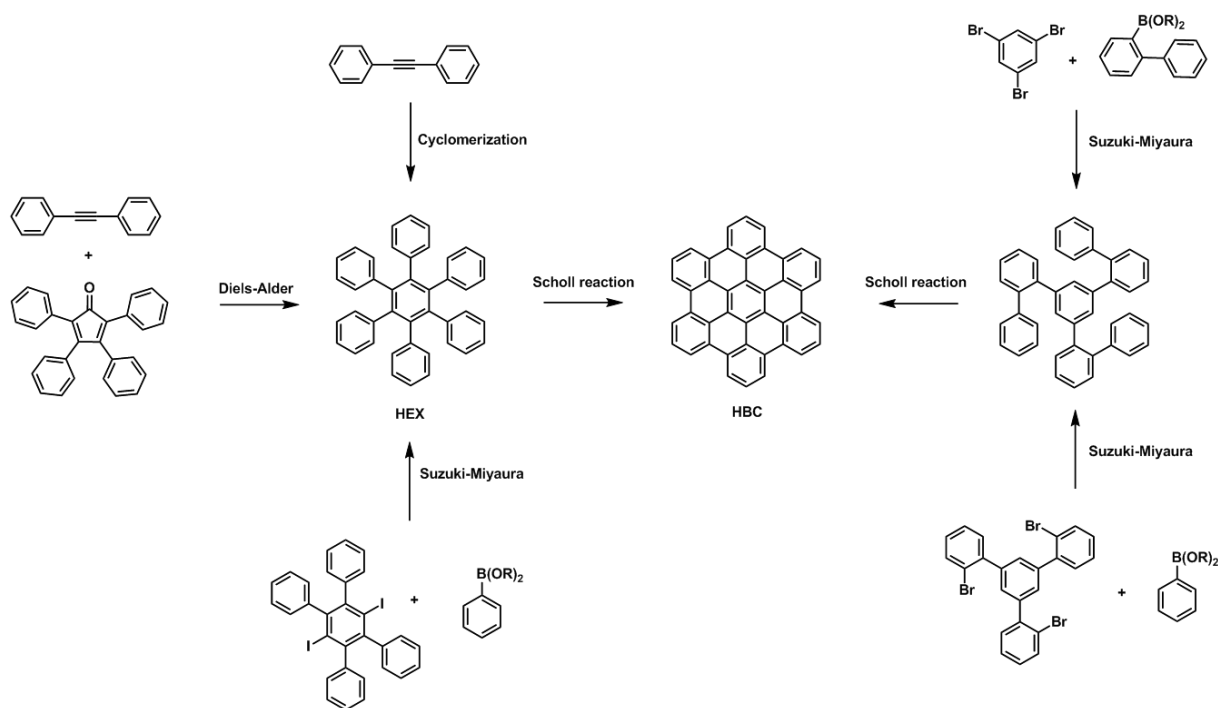
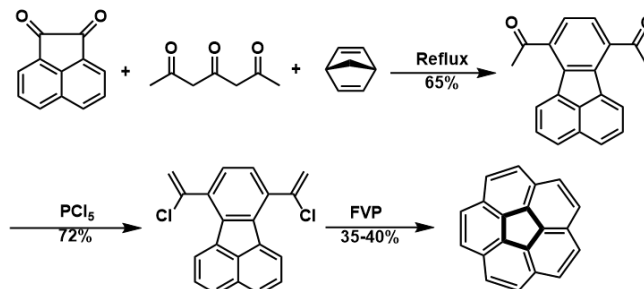


Figure 1-10. Common methods for the synthesis of hexaphenylbenzene (HEX) and hexa-*peri* hexabenzocoronene (HBC)

### Flash Vacuum Pyrolysis



### Solution Phase Kg scale synthesis

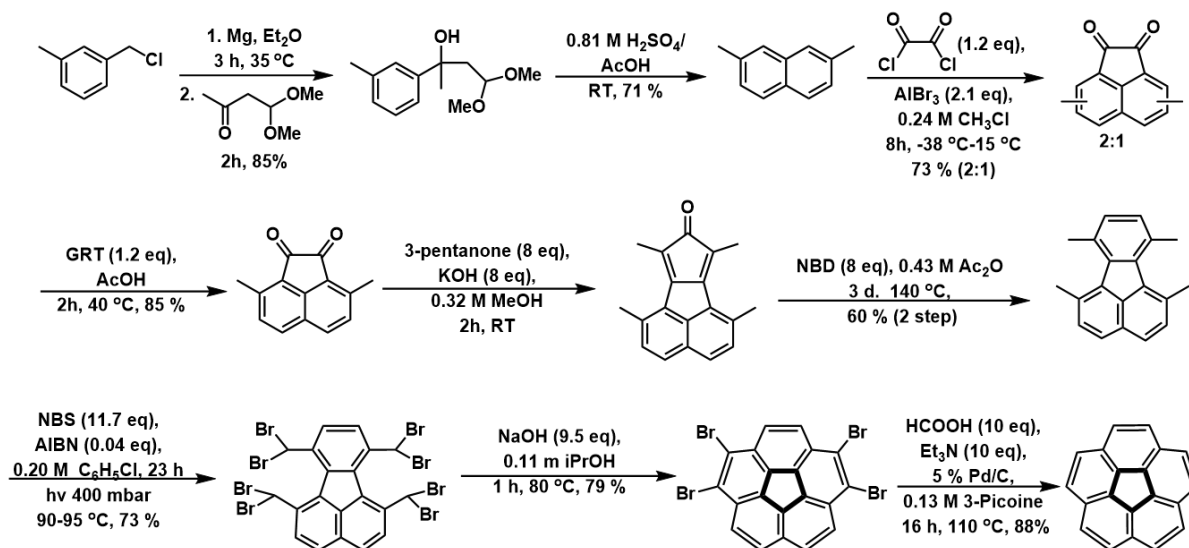


Figure 1-11. Methods for the synthesis of corannulene

### 1.3.4 Inherent electronic properties for functional porous materials

Owing to their extended  $\pi$  electronic system and shapes of these molecules possess interesting functional properties which led to intensive research for various applications such as organic electronics. For instance, HEX has been known for applications such as organic light emitting diodes (OLEDs) and field-effect transistors, catalysis, enzyme simulation and biologically active compounds.<sup>28</sup> HBC and other PAHs possess strong  $\pi$ - $\pi$  stacking interactions which make them insoluble in most of the organic solvents. Peripheral substitution can increase the solubility in

HBC. Further, functionalized HBCs show high thermal and chemical stability and are incorporated in various applications such as in liquid crystalline systems, sensor materials and organic semiconductors.<sup>35</sup> The redox chemistry<sup>39</sup>, metal coordination<sup>40,41</sup> and photophysical properties of corannulene have been intensively studied. Further, corannulene has been successfully investigated for numerous potential applications in a wide range of systems including liquid crystalline materials, polymers, dendrimers, molecular tweezers, photovoltaic cells, organic field effect transistors, and light emitting diodes.<sup>42-44</sup> The synthesis of porous materials with these molecules can introduce these properties to the porous materials resulting in added functionality porous materials for beneficial applications.

#### **1.4 Porous materials synthesized with HEX, HBC and Corannulene**

Due to these potentials, synthesis of porous materials with these extended aromatic scaffolds has emerged as an interesting field over past 6 years. HEX is the most widely studied material among the three molecules of interest while other two have only a few examples yet.

The first HEX based porous material reported was a PIM (HPB-PIM).<sup>45</sup> Later, a series of HEX based PIMs (PIM-HPBs) (Figure 1-12) were prepared into cast films which are suitable for gas permeation studies.<sup>46</sup> This approach has shown to be useful for tuning the performance of membranes for gas separation, particularly those involving CO<sub>2</sub> as it had shown high CO<sub>2</sub> selectivity. Next HEX based POPs (HPOP-1 and 2) (Figure 1-12) were prepared via palladium-catalyzed C-C coupling polymerization. BET surface area for these polymers are 742 and 1148 m<sup>2</sup> g<sup>-1</sup> while the adsorption capacity for hydrogen is up to 1.5 wt.% at 1.13 bar and 77 K.<sup>47</sup> Another organic microporous polymer HTP (Figure 1-12) has been synthesized from a HEX with triptycene, which combine the benefit of propeller shape of triptycene with HEX. HTP displays a

high BET surface area of  $1151 \text{ m}^2 \text{ g}^{-1}$  and reversibly adsorbs 12.5 wt.% of  $\text{CO}_2$  at 1.0 bar and 273 K and high thermal stability.<sup>48</sup>

Our group has successfully prepared and evaluated the first set of permanently porous HBC containing polymers (HBC-POPs) (Figure 1-12) via a Sonogashira polymerization with tetrakis(4-ethynyl)tetraphenylmethane (TPM).<sup>49</sup> These polymers have demonstrated permanent porosity and moderate surface area ( $550\text{-}670 \text{ m}^2 \text{ g}^{-1}$ ), but good  $\text{CO}_2$  adsorption capacities (8-9 wt.%) and excellent adsorption enthalpies for  $\text{CO}_2$  relative to their surface areas. Even though these polymers are formed under kinetic conditions they have shown to exhibit strong  $\pi$ -stacking interactions, which may be the major driving force in the structure of these HBC based polymers. Further, availability of accessible highly conjugated  $\pi$ -surfaces in these POPs were proven with fluorescence quenching studies with buckminsterfullerene. HEX and HBC can easily be functionalized with various substituent groups. That allowed the synthesis of a series of POPs based on HEX and HBC (Figure 1-12) with varying peripheral substitution.<sup>50</sup> These show BET surface areas ranging from  $320\text{-}1140 \text{ m}^2 \text{ g}^{-1}$ . Due to these structural modifications, significant effects on the properties were observed in both their gas-sorption performance and the microscopic structure. Size of the side group and  $\pi$ -stacking ability were more important factors. Also, we have recently studied<sup>51</sup> (chapter 3) the ability of adsorbing volatile organic compounds (VOCs) in to HEX and HBC based POPs with two novel POPs (HEX-POP-93 and HBC-POP-98). Both polymers possess moderate surface areas ( $687$  and  $548 \text{ m}^2 \text{ g}^{-1}$ ), but good organic vapor adsorption capacities with excellent benzene adsorption capacity (99.9 wt. %) with preference for benzene over water ( $< 1 \text{ wt.}\%$ ).

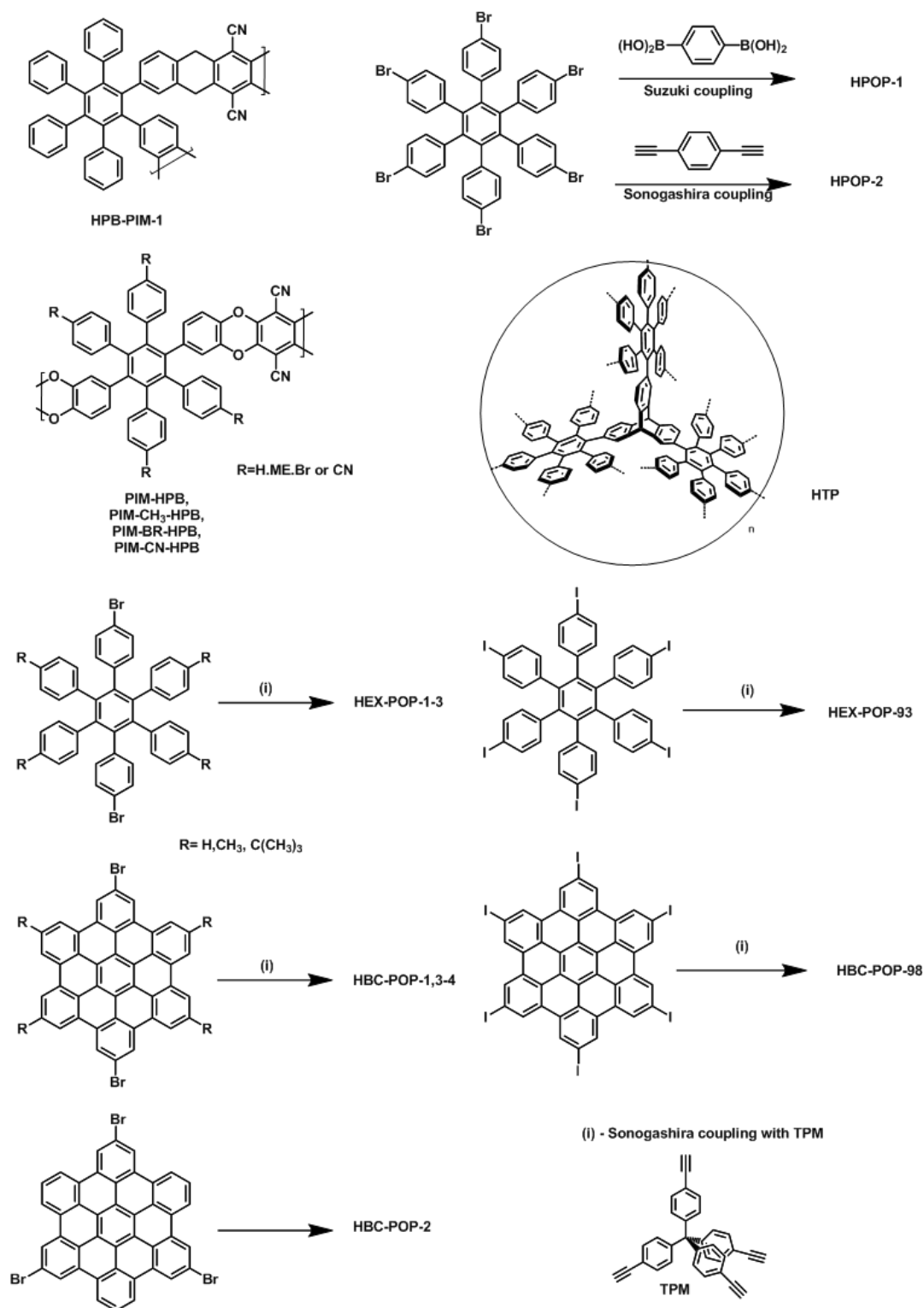


Figure 1-12. Reported HEX and HBC based POPs

The highest reported BET surface area ( $1790 \text{ m}^2 \text{ g}^{-1}$ ) with any HEX based POP is obtained from the Scholl oxidation of HEX in the presence of  $\text{AlCl}_3$  and dichloromethane (DCM) (Figure 1-13).<sup>52</sup> We have increased the BET surface area up to  $2222 \text{ m}^2 \text{ g}^{-1}$  for the POP synthesized under similar Scholl oxidation condition (unreported data, chapter 4) with excellent  $\text{CO}_2$  adsorption capacity (20.7 wt.%). A similar PAF, named HP obtained from Yamamoto-Ullmann cross coupling of hexakisbromohexaphenylbenzene, has a BET surface area of only  $675 \text{ m}^2 \text{ g}^{-1}$  (Figure 1-13).

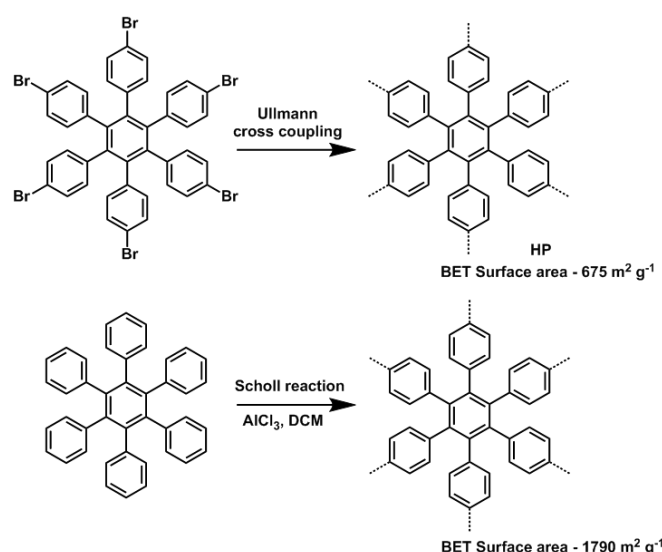


Figure 1-13. HEX based PAFs with Yamamoto-Ullmann cross coupling and Scholl oxidation

Donglin Jiang *et. al* reported the first set of COFs with HEX and HBC scaffolds.<sup>53</sup> They have used HEX and HBC to introduce the triangular topology to the COFs with small pore sizes of  $12 \text{ \AA}$ , which is among the smallest pores for COFs reported, and high  $\pi$ -column densities of up to  $0.25 \text{ nm}^{-2}$ . Further, these crystalline COFs facilitate  $\pi$ -cloud delocalization and high conductivity, with a hole mobility that is among the highest reported for COFs. The next HEX based COF, HEX based azine linked COF (HEX-COF 1) was reported by our group which has even smaller pore size of  $11 \text{ \AA}$  with a higher surface area in excess of  $1200 \text{ m}^2 \text{ g}^{-1}$ .<sup>54</sup> Also it shows an excellent

sorption capability for carbon dioxide (20 wt.%) and methane (2.3 wt.%) at 273 K and 1 atm (Figure 1-14).

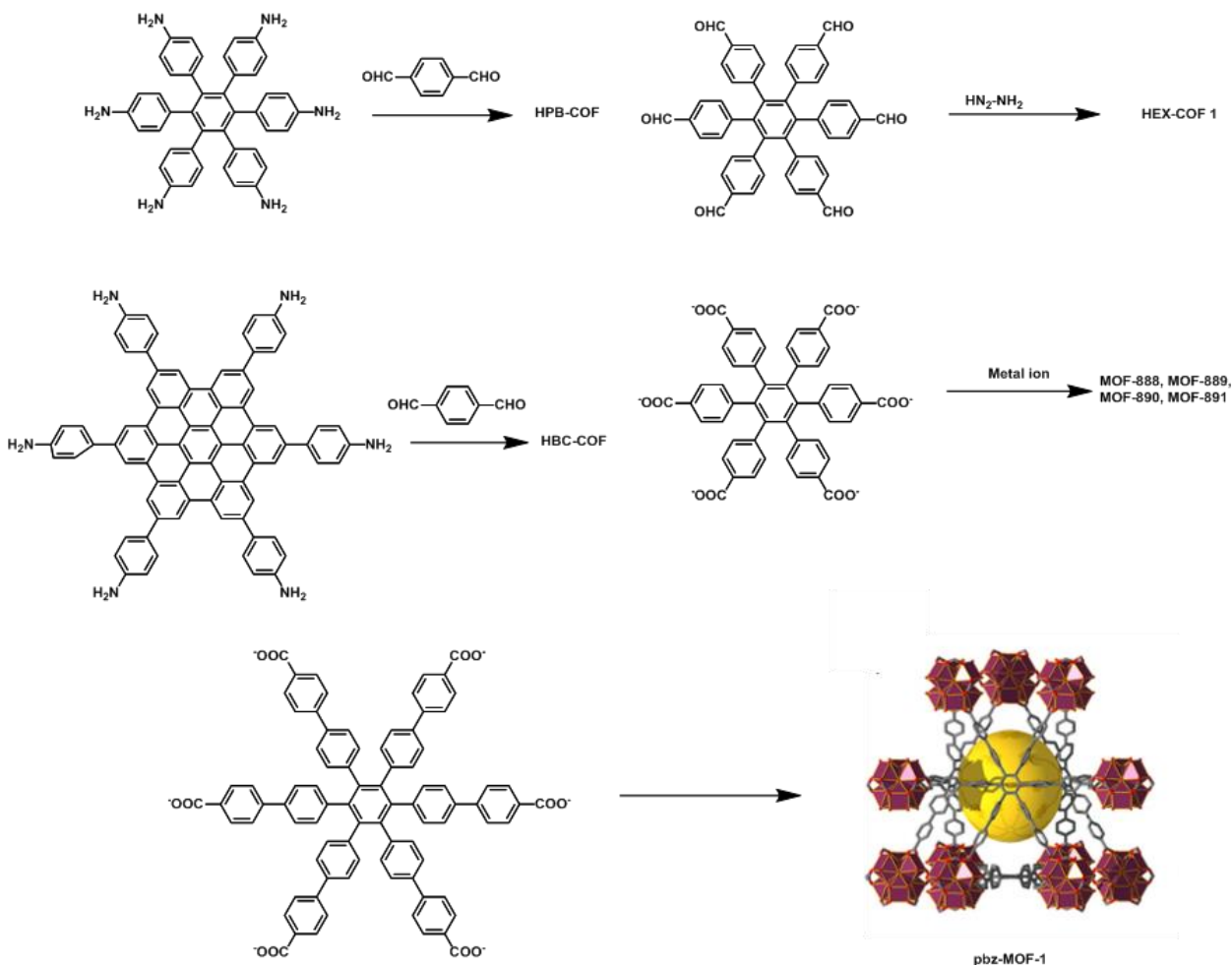


Figure 1-14. HEX and HBC based COFs and MOFs (Pbz-MOF-1 structure is reprinted with permission from *J. Am. Chem. Soc.* **2016**, 138, 12767-12770 (reference 56) copyright 2016 American Chemical Society)

Four MOF structures (MOF 888 to 891), based on a HEX based hexatopic linker, 1',2',3',4',5',6'-hexakis(4-carboxyphenyl)-benzene, has been synthesized while two of them have introduced new topologies, namely, htp and hhp, to the field of MOF chemistry.<sup>55</sup> Gas adsorption measurements revealed that though they have low surface areas (38-295 m<sup>2</sup> g<sup>-1</sup>) they exhibited moderately high



CO<sub>2</sub> adsorptions and selectivity over N<sub>2</sub> and CH<sub>4</sub>. Very recently another MOF based on HEX was reported (pbz-MOF-1) as the first example of Zr(IV)-based MOF with polybenzene (pbz) or “cubic graphite” topology (Figure 1-14).<sup>56</sup> Rational design and the propeller shaped of HEX allow the synthesis of cubic graphene like structure which was only a postulated structure so far.

A curved PAH corannulene has been reported for a theoretical MOF (IRMOF-M8)<sup>57</sup> and for a redox active crystalline MOF.<sup>58</sup> This latest report which contains a crystalline corannulene scaffold proved to remain the corannulene bowl inside the prepared rigid matrix based on X-ray diffraction studies, thus obtained an array of buckybowls. Also, it retains the inherent redox activity of corannulene. Recently, we have reported<sup>59</sup> (chapter 2) the first set of POPs based on corannulene (BB-POPs) which were synthesized via Sonogashira co-polymerization of 1,2,5,6-tetrabromocorannulene and alkyne linkers. BB-POP-3 exhibits the highest BET surface area of 560 m<sup>2</sup> g<sup>-1</sup> and CO<sub>2</sub> adsorption of 11.7 wt. %. BB-POPs also retain the redox properties of its corannulene monomers (Figure 1-15).

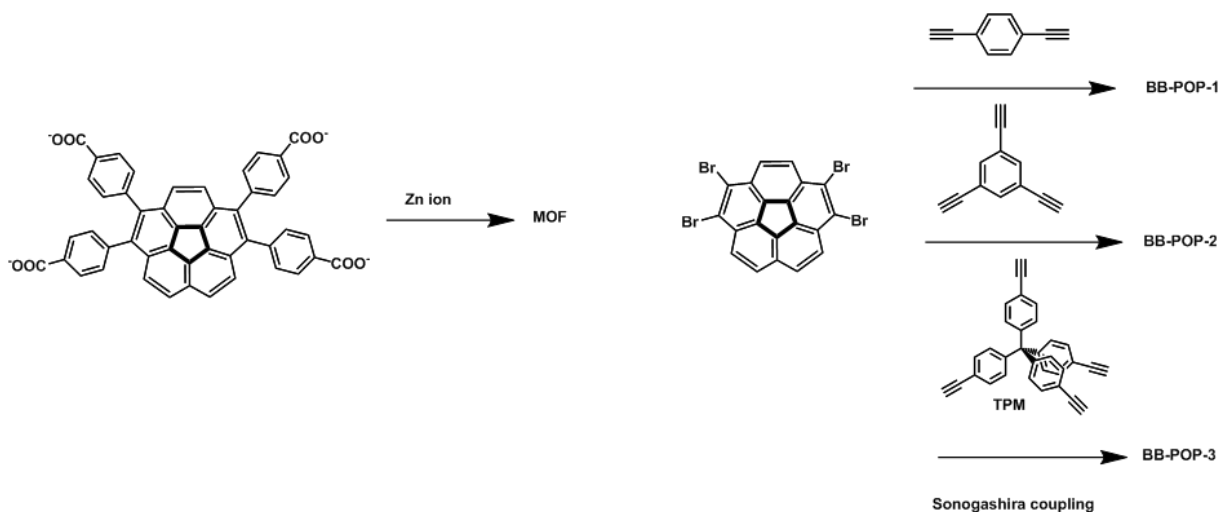


Figure 1-15. Corannulene-based porous materials

## 1.5 Significance of porous materials synthesized with HEX, HBC and BB

The highest reported BET surface area of  $2415 \text{ m}^2 \text{ g}^{-1}$  for any porous materials based on HEX is for the recently reported pbz-MOF-1.<sup>56</sup> However, with HBC and corannulene it reached only a moderate BET surface areas of  $670 \text{ m}^2 \text{ g}^{-1}$  (HBC-POP-1)<sup>49</sup> and  $556 \text{ m}^2 \text{ g}^{-1}$  (BB-POP-3)<sup>59</sup> (Table 1-1).

All the materials studied here have reported good  $\text{CO}_2$  adsorption capacities (up to 20 wt.%)<sup>54</sup>, heat of adsorption and selectivity compared to smaller aromatic scaffolds. It suggests that there could be a contribution of the extended  $\pi$  conjugation towards improved  $\text{CO}_2$  adsorption and selectivity (Table 1-1). Also, these materials demonstrate excellent  $\text{CH}_4$  (HEX-COF-1)<sup>54</sup> and VOCs adsorption capacities (HEX-POP-93) as well.<sup>51</sup>

Interestingly, all these porous materials retain the initial structure and symmetry, introducing novel topologies to porous materials. The hexagonal symmetry of HEX and HBC have introduced a novel triangular topology to COFs.<sup>53,54</sup> Also, HEX has been introduced new topologies, namely, htp and hhp,<sup>55</sup> and polybenzene (pbz)<sup>56</sup> to the field of MOFs.

Similarly, these porous materials retain the inherent properties such as electronics and redox activities from initial aromatic scaffolds. Thus, other than the gas storage and selectivity due to inheriting of properties of initial monomers, these polymers demonstrate the potential of being used in other applications such as organoelectronics. As an example, HPB-COF and HBC-COF show photoconductive and high hole mobility properties.<sup>53</sup> Corannulene based MOF and POPs (BB-POP-2 and 3) shows the inheriting of redox activity elaborating potential applications in supercapacitors and batteries<sup>59</sup> (Table 1-1).

Table 1-1. Reported HEX, HBC and BB based porous materials and their properties.

Aromatic scaffold	Type	Porous material	BET	CO <sub>2</sub>	Other properties	Ref
			surface area	ads		
			(m <sup>2</sup> g <sup>-1</sup> )	wt%		
HEX	POP	HPB-PIM-1	425	-	Good CO <sub>2</sub> selectivity	45
		HPB-PIM-2	527	-		
		PIM-HPB	537	-		
		PIM-CH <sub>3</sub> -HPB	560	-		
		PIM-Br-HPB	410	-		
		PIM-CN-HPB	440	-		
		HPOP-1	1148	-	1.5 wt% H <sub>2</sub> adsorption at 1.13 bar and 77 K	47
		HPOP-2	742	-		
		HP	675	8.0		
		HTP	1151	12.5		
		HEX-POP-1	610			
		HEX-POP-2	600		99.9 wt.% Benzene adsorption	51
		HEX-POP-3	1140	18		
		HEX-POP-93	687	8.8		
		Scholl oxidation	1790	19.8		
						52

	COF	HPB-COF	965	-		53
		HEX-COF-1	1214	20	CH <sub>4</sub> adsorption 2.3 wt%	54
	MOF	MOF-888	38	4.7	High CO <sub>2</sub> heat of	55
		MOF-889	144	10.8	adsorption and CO <sub>2</sub>	
		MOF-890	295	11.3	selectivity	
		MOF-891	200	11.3		
		Pbz-MOF-1	2415	-	High storage capacity	56
					of CH <sub>4</sub> at high pressure	
HBC	POP	HBC-POP-1	670	9		49
		HBC-POP-2	500	8		
		HBC-POP-3	360	-		50
		HBC-POP-4	320	-		
		HBC-POP-98	548	8.0	Good VOCs	51
					adsorptions	
	COF	HBC-COF	469			53
BB	MOF		224	-	Redox active	58
	POP	BB-POP-1	56	7.4		59
		BB-POP-2	130	8.5		
		BB-POP-3	556	11.7		

## 1.6 Conclusion

Over the past six years, using extended aromatic scaffold such as HEX, HBC and corannulene for porous materials has introduced interesting properties and topologies to porous materials. There is an increasing trend in exploring these molecules, as well an improvement of properties of these porous materials. HEX has been studied more than HBC and corannulene. The challenge of poor solubility of HBC and related compounds could be the reason for lack of studies. On the other hand, unusual bowl shape and the symmetry of corannulene is expected to introduce novel topologies to porous materials. However, it requires a rational design especially in designing MOFs and COFs and we are concentrating on this strategy. Further, other than HEX, HBC and corannulene there are several other related compounds which are yet to be explored in order to expand this field of study. It can be expected that in the next decade, extended aromatic scaffold research in porous materials will introduce materials with novel properties for new applications.

## 1.7 References

1. Davis, M. E. Ordered porous materials for emerging applications. *Nature* **2002**, *417*, 813-821.
2. Dawson, R.; Cooper, A. I.; Adams, D. J. Nanoporous organic polymer networks. *Prog. Poly. Sci.* **2012**, *37*, 530-563.
3. Tian, J.; Thallapally, P. K.; McGrail, B. P. Porous organic molecular materials. *Cryst. Eng. Comm.* **2012**, *14*, 1909-1919.
4. Xiang, Z.; Cao, D. Porous covalent-organic materials: synthesis, clean energy application and design. *J. Mater. Chem. A* **2013**, *1*, 2691-2718.
5. Li, B.; Wen, H.; Zhou, W.; Chen, B. Porous Metal-Organic Frameworks for Gas Storage and Separation: What, How, and Why? *J. Phys. Chem. Lett.* **2014**, *5*, 3468-3479.

6. Morris, R.; Wheatley, P. Gas Storage in Nanoporous Materials. *Angew. Chem. Int. Ed.* **2008**, *47*, 4966-4981.
7. Das, S.; Heasman, P.; Ben, T.; Qiu, S. Porous Organic Materials: Strategic Design and Structure Function Correlation. *Chem. Rev.* **2016**.
8. Dey, C.; Kundu, T.; Biswal, B. P.; Mallick, A.; Banerjee, R. Crystalline metal-organic frameworks (MOFs): synthesis, structure and function. *Acta Crystallogr. B. Struct. Sci. Cryst. Eng. Mater.* **2014**, *70*, 3-10.
9. Holst, J. R.; Trewin, A.; Cooper, A. I. Porous organic molecules. *Nat. Chem.* **2010**, *2*, 915-920.
10. Jiang, S.; Jones, J. T. A.; Hasell, T.; Blythe, C. E.; Adams, D. J.; Trewin, A.; Cooper, A. I. Porous organic molecular solids by dynamic covalent scrambling. *Nat. Commun.* **2011**, *2*, 207.
11. Zhou, H.; Long, J. R.; Yaghi, O. M. Introduction to Metal-Organic Frameworks. *Chem. Rev.* **2012**, *112*, 673-674.
12. Hermes, S.; Schroder, F.; Amirjalayer, S.; Schmid, R.; Fischer, R. A. Loading of porous metal-organic open frameworks with organometallic CVD precursors: inclusion compounds of the type [LnM]a@MOF-5. *J. Mater. Chem.* **2006**, *16*, 2464-2472.
13. Peplow, M. Materials science: The hole story. *Nature* **2015**, *520*, 148-150.
14. Farha, O. K.; Eryazici, I.; Jeong, N. C.; Hauser, B. G.; Wilmer, C. E.; Sarjeant, A. A.; Snurr, R. Q.; Nguyen, S. T.; Yazaydin, A. Ö.; Hupp, J. T. Metal-Organic Framework Materials with Ultrahigh Surface Areas: Is the Sky the Limit? *J. Am. Chem. Soc.* **2012**, *134*, 15016-15021.
15. Silva, P.; Vilela, S. M. F.; Tome, J. P. C.; Almeida Paz, F. A. Multifunctional metal-organic frameworks: from academia to industrial applications. *Chem. Soc. Rev.* **2015**, *44*, 6774-6803.
16. Ding, S.; Wang, W. Covalent organic frameworks (COFs): from design to applications. *Chem. Soc. Rev.* **2013**, *42*, 548-568.
17. El-Kaderi, H.; Hunt, J. R.; Mendoza-Cortes, J. L.; Cote, A. P.; Taylor, R. E.; O'Keeffe, M.; Yaghi, O. M. Designed Synthesis of 3D Covalent Organic Frameworks. *Science* **2007**, *316*, 268.
18. Xu, S.; Luo, Y.; Tan, B. Recent development of hypercrosslinked microporous organic polymers. *Macromol. Rapid Commun.* **2013**, *34*, 471-484.

19. Li, B.; Gong, R.; Wang, W.; Huang, X.; Zhang, W.; Li, H.; Hu, C.; Tan, B. A New Strategy to Microporous Polymers: Knitting Rigid Aromatic Building Blocks by External Cross-Linker. *Macromolecules* **2011**, *44*, 2410-2414.
20. McKeown, N. B. Polymers of Intrinsic Microporosity. *ISRN Mater. Sci.* **2012**, *2012*, 16.
21. Xu, Y.; Jin, S.; Xu, H.; Nagai, A.; Jiang, D. Conjugated microporous polymers: design, synthesis and application. *Chem. Soc. Rev.* **2013**, *42*, 8012-8031.
22. Liu, Q.; Tang, Z.; Wu, M.; Zhou, Z. Design, preparation and application of conjugated microporous polymers. *Polym. Int.* **2014**, *63*, 381-392.
23. Ben, T.; Ren, H.; Ma, S.; Cao, D.; Lan, J.; Jing, X.; Wang, W.; Xu, J.; Deng, F.; Simmons, J.; Qiu, S.; Zhu, G. Targeted Synthesis of a Porous Aromatic Framework with High Stability and Exceptionally High Surface Area. *Angew. Chem.* **2009**, *121*, 9621-9624.
24. Ben, T.; Qiu, S. Porous aromatic frameworks: Synthesis, structure and functions. *Cryst. Eng. Comm.* **2013**, *15*, 17-26.
25. Lu, Y.; Feng, Y. P. Adsorptions of hydrogen on graphene and other forms of carbon structures: First principle calculations. *Nanoscale* **2011**, *3*, 2444-2453.
26. Hussain, M. A.; Vijay, D.; Sastry, G. N. Buckybowls as adsorbents for CO<sub>2</sub>, CH<sub>4</sub>, and C<sub>2</sub>H<sub>2</sub>: Binding and structural insights from computational study. *J. Comput. Chem.* **2016**, *37*, 366-377.
27. Lima, C. F. R. A. C.; Rocha, M. A. A.; Melo, A.; Gomes, L.; Low, J. N.; Santos, L. M. N. B. F. Structural and Thermodynamic Characterization of Polyphenylbenzenes. *J. Phys. Chem. A* **2011**, *115*, 11876-11888.
28. Vij, V.; Bhalla, V.; Kumar, M. Hexaarylbenzene: Evolution of Properties and Applications of Multitalented Scaffold. *Chem. Rev.* **2016**, *116*, 9565-9627.
29. Narita, A.; Wang, X.; Feng, X.; Mullen, K. New advances in nanographene chemistry. *Chem. Soc. Rev.* **2015**, *44*, 6616-1643.
30. Sygula, A. Chemistry on a Half-Shell: Synthesis and Derivatization of Buckybowls. *Euro. J. Org. Chem.* **2011**, *2011*, 1611-1625.
31. Fieser, L. F. Hexaphenylbenzene. *Org. Synth.* **1966**, *46*, 44.
32. Clar, E.; Ironside, C. T. Hexabenzocoronene. *Proc. Chem. Soc.* **1958**, 150-150

33. Feng, X.; Wu, J.; Enkelmann, V.; Müllen, K. Hexa-peri-hexabenzocoronenes by Efficient Oxidative Cyclodehydrogenation: The Role of the Oligophenylene Precursors. *Org. Lett.* **2006**, *8*, 1145-1148.
34. Zhai, L.; Shukla, R.; Rathore, R. Oxidative C-C Bond Formation (Scholl Reaction) with DDQ as an Efficient and Easily Recyclable Oxidant. *Org. Lett.* **2009**, *11*, 3474-3477.
35. Seyler, H.; Purushothaman, B.; Jones, D.; Holmes, A.; Wong, W. Hexa-peri-hexabenzocoronene in organic electronics. *Pure App. Chem.* **2012**, *84*(4), 1047-1067.
36. Barth, W. E.; Lawton, R. G. Dibenzo[ghi,mno]fluoranthene. *J. Am. Chem. Soc.* **1966**, *88*, 380-381.
37. Scott, L. T.; Cheng, P.; Hashemi, M. M.; Bratcher, M. S.; Meyer, D. T.; Warren, H. B. Corannulene. A Three-Step Synthesis1. *J. Am. Chem. Soc.* **1997**, *119*, 10963-10968.
38. Butterfield, A. M.; Gilomen, B.; Siegel, J. S. Kilogram-Scale Production of Corannulene. *Org. Process Res. Dev.* **2012**, *16*, 664-676.
39. Bruno, C.; Benassi, R.; Passalacqua, A.; Paolucci, F.; Fontanesi, C.; Marcaccio, M.; Jackson, E. A.; Scott, L. T. Electrochemical and Theoretical Investigation of Corannulene Reduction Processes. *J. Phys. Chem. B* **2009**, *113*, 1954-1962.
40. Petrukhina, M. A.; Scott, L. T. Coordination chemistry of buckybowls: from corannulene to a hemifullerene. *Dalton Trans.* **2005**, 2969-2975.
41. Zabula, A. V.; Filatov, A. S.; Spisak, S. N.; Rogachev, A. Y.; Petrukhina, M. A. A Main Group Metal Sandwich: Five Lithium Cations Jammed Between Two Corannulene Tetraanion Decks. *Science* **2011**, *333*, 1008-1011.
42. Lu, R.; Xuan, W.; Zheng, Y.; Zhou, Y.; Yan, X.; Dou, J.; Chen, R.; Pei, J.; Weng, W.; Cao, X. A corannulene-based donor-acceptor polymer for organic field-effect transistors. *RSC Adv.* **2014**, *4*, 56749-56755.
43. Lu, R.; Zheng, Y.; Zhou, Y.; Yan, X.; Lei, T.; Shi, K.; Zhou, Y.; Pei, J.; Zoppi, L.; Baldrige, K. K.; Siegel, J. S.; Cao, X. Corannulene derivatives as non-fullerene acceptors in solution-processed bulk heterojunction solar cells. *J. Mater. Chem. A* **2014**, *2*, 20515-20519.
44. Scott, L. T.; Jackson, E. A.; Zhang, Q.; Steinberg, B. D.; Bancu, M.; Li, B. A Short, Rigid, Structurally Pure Carbon Nanotube by Stepwise Chemical Synthesis. *J. Am. Chem. Soc.* **2012**, *134*, 107-110.



45. Short, R.; Carta, M.; Bezzu, C. G.; Fritsch, D.; Kariuki, B. M.; McKeown, N. B. Hexaphenylbenzene-based polymers of intrinsic microporosity. *Chem. Commun.* **2011**, 47, 6822-6824.
46. Carta, M.; Bernardo, P.; Clarizia, G.; Jansen, J. C.; McKeown, N. B. Gas Permeability of Hexaphenylbenzene Based Polymers of Intrinsic Microporosity. *Macromolecules* **2014**, 47, 8320-8327.
47. Chen, Q.; Luo, M.; Wang, T.; Wang, J.; Zhou, D.; Han, Y.; Zhang, C.; Yan, C.; Han, B. Porous Organic Polymers Based on Propeller-Like Hexaphenylbenzene Building Units. *Macromolecules* **2011**, 44, 5573-5577.
48. Zhang, C.; Peng, L.; Li, B.; Liu, Y.; Zhu, P.; Wang, Z.; Zhan, D.; Tan, B.; Yang, X.; Xu, H. Organic microporous polymer from a hexaphenylbenzene based triptycene monomer: synthesis and its gas storage properties. *Polym. Chem.* **2013**, 4, 3663-3666.
49. Thompson, C. M.; Li, F.; Smaldone, R. A. Synthesis and sorption properties of hexa-(peri)-hexabenzocoronene-based porous organic polymers. *Chem. Commun.* **2014**, 50, 6171-6173.
50. Thompson, C. M.; McCandless, G. T.; Wijenayake, S. N.; Alfarawati, O.; Jahangiri, M.; Kokash, A.; Tran, Z.; Smaldone, R. A. Substituent Effects on the Gas Sorption and Selectivity Properties of Hexaphenylbenzene and Hexabenzocoronene Based Porous Polymers. *Macromolecules* **2014**, 47, 8645-8652.
51. Karunathilake, A. A. K.; Chang, J.; Thompson, C. M.; Nguyen, C. U.; Nguyen, D. Q.; Rajan, A.; Sridharan, A.; Vyakaranam, M.; Adegboyega, N.; Kim, S. J.; Smaldone, R. A. Hexaphenylbenzene and hexabenzocoronene-based porous polymers for the adsorption of volatile organic compounds. *RSC Adv.* **2016**, 6, 65763-65769.
52. Msayib, K. J.; McKeown, N. B. Inexpensive polyphenylene network polymers with enhanced microporosity. *J. Mater. Chem. A* **2016**, 4, 10110-10113.
53. Dalapati, S.; Addicoat, M.; Jin, S.; Sakurai, T.; Gao, J.; Xu, H.; Irle, S.; Seki, S.; Jiang, D. Rational design of crystalline supermicroporous covalent organic frameworks with triangular topologies. *Nat. Commun.* **2015**, 6.
54. Alahakoon, S. B.; Thompson, C. M.; Nguyen, A. X.; Occhialini, G.; McCandless, G. T.; Smaldone, R. A. An azine-linked hexaphenylbenzene based covalent organic framework. *Chem. Commun.* **2016**, 52, 2843-2845.
55. Nguyen, P. T. K.; Nguyen, H. T. D.; Pham, H. Q.; Kim, J.; Cordova, K. E.; Furukawa, H. Synthesis and Selective CO<sub>2</sub> Capture Properties of a Series of Hexatopic Linker-Based Metal-Organic Frameworks. *Inorg. Chem.* **2015**, 54, 10065-10072.

56. Alezi, D.; Spanopoulos, I.; Tsangarakis, C.; Shkurenko, A.; Adil, K.; Belmabkhout, Y.; O'Keeffe, M.; Eddaoudi, M.; Trikalitis, P. N. Reticular Chemistry at Its Best: Directed Assembly of Hexagonal Building Units into the Awaited Metal-Organic Framework with the Intricate Polybenzene Topology, pbz-MOF. *J. Am. Chem. Soc.* **2016**, *138*, 12767-12770.
57. Warmbier, R.; Quandt, A.; Seifert, G. Dielectric Properties of Selected Metal-Organic Frameworks. *J. Phys. Chem. C* **2014**, *118*, 11799-11805.
58. Fellows, W. B.; Rice, A. M.; Williams, D. E.; Dolgoplova, E. A.; Vannucci, A. K.; Pellechia, P. J.; Smith, M. D.; Krause, J. A.; Shustova, N. B. Redox-Active Corannulene Buckybowls in a Crystalline Hybrid Scaffold. *Angew. Chem. Inter. Ed.* **2016**, *55*, 2195-2199.
59. Karunathilake, A. A. K.; Thompson, C. M.; Peranathan, S.; Ferraris, J. P.; Smaldone, R. A. Electrochemically active porous organic polymers based on corannulene. *Chem. Commun.* **2016**, *52*, 12881-12884.

**CHAPTER 2**  
**ELECTROCHEMICALLY ACTIVE POROUS ORGANIC POLYMERS BASED ON**  
**CORANNULENE**

Authors: Arosha A. K. Karunathilake, Christina M. Thompson, Sahila Peranathan, John P.  
Ferraris and Ronald A. Smaldone

Department of Chemistry and Biochemistry, The University of Texas at Dallas,  
800 W Campbell Rd, Richardson, Texas, 75080

Reprinted (adapted) from Karunathilake, A. A. K.; Thompson, C. M.; Peranathan, S.; Ferraris, J. P.; Smaldone, R. A. Electrochemically active porous organic polymers based on corannulene. *Chem. Commun.* **2016**, 52, 12881-12884 with permission of The Royal Society of Chemistry.

## 2.1 Abstract

For the first time, porous organic polymers (POPs) based on the smallest buckybowl, corannulene (BB-POPs) have been synthesized. Three POPs were synthesized via Sonogashira copolymerization of 1,2,5,6-tetrabromocorannulene and alkyne linkers. BB-POP-3 exhibits the highest surface area ( $S_{\text{BET}} = 560 \text{ m}^2 \text{ g}^{-1}$ ) and  $\text{CO}_2$  adsorption of 11.7 wt%, while they retain the redox properties of corannulene.

## 2.2 Introduction

Corannulene ( $\text{C}_{20}\text{H}_{10}$ ) (Figure 2-1) is a bowl-shaped polycyclic aromatic hydrocarbon (PAH), known as the smallest “buckybowl” (BB) and comprises one third of a  $\text{C}_{60}$  fullerene with hydrogen termination.<sup>1-3</sup> First synthesized in 1966,<sup>4</sup> there have been multiple subsequent syntheses of corannulene,<sup>5-9</sup> including its production on kilogram scale.<sup>10</sup> Its curved topography and unique chemical structure give corannulene interesting and potentially useful physical properties, including metal coordination capability<sup>11,12</sup> and redox activity.<sup>13</sup> These properties, combined with relatively facile synthetic pathways, have led numerous research activities to incorporate corannulene into a wide range of systems including polymers,<sup>14</sup> dendrimers,<sup>15</sup> molecular tweezers,<sup>16</sup> liquid crystalline materials,<sup>17</sup> and as a precursor of carbon nanotubes.<sup>18</sup>

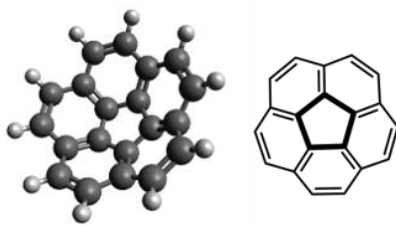


Figure 2-1. Structure of corannulene

The inherent redox activity of corannulene has led to great interest in developing materials incorporating it for electrochemical applications such as photovoltaic cells,<sup>19</sup> organic field effect transistors,<sup>20-23</sup> and light emitting diodes.<sup>24</sup> It has also been postulated that corannulene's ability to form tessellated stacks, along with its ability to bind metals such as lithium, could make it valuable in lithium ion battery research.<sup>25</sup> Recently a redox active metal organic framework (MOF) based on corannulene was reported.<sup>26</sup>

Porous materials such as MOFs,<sup>27</sup> covalent organic frameworks (COFs),<sup>28</sup> and porous organic polymers (POPs)<sup>29</sup> have garnered interest as materials for applications ranging from gas storage and separation to electronic device fabrication. Important advantages of porous materials include high surface areas, tunable pore-sizes, and a wide range of potential functional group incorporation. Unlike MOFs, POPs are fully organic, amorphous materials comprised of all covalent bonds. Importantly, this gives them higher thermal and chemical stability than MOFs, while maintaining high surface areas and great structural tunability.<sup>30-32</sup> Our group has previously reported a range of POPs<sup>33-35</sup> and a COF<sup>36</sup> based on two PAHs: planar hexabenzocoronene (HBC) and propeller-shaped hexaphenylbenzene (HEX). We report herein the first example of a porous organic polymer containing the curved PAH structure, corannulene.

To the best of our knowledge, there has been only one report on the N<sub>2</sub> adsorption properties of a corannulene containing system<sup>26</sup> with all other investigations being theoretical in nature<sup>37-43</sup> or consisting of non-functionalized corannulene samples.<sup>37</sup> These studies illustrate the potential of corannulene for the adsorption and storage of gases such as H<sub>2</sub>, CO<sub>2</sub>, and CH<sub>4</sub> as its curvature provides multiple surfaces to bind gas molecules. To study these theoretical predictions in more detail, we have synthesized three POPs (BB-POPs) containing corannulene. Polymeric networks

have been generated through Sonogashira copolymerization between 1,2,5,6-tetrabromocorannulene (TBC) and di, tri, and tetra-functionalized alkyne monomers, 1,4-diethynylbenzene (DEB), 1,3,5-trisubstituted benzene (TEB), tetrakis(4-ethynyl)-tetraphenylmethane (TPM), respectively (Figure 2-2) and their adsorption capacities for nitrogen, carbon dioxide and hydrogen have been measured. Further, we have investigated the electrochemical properties of the synthesized BB-POPs via cyclic voltammetry to explore the success of incorporating these redox properties of corannulene into a porous polymer.

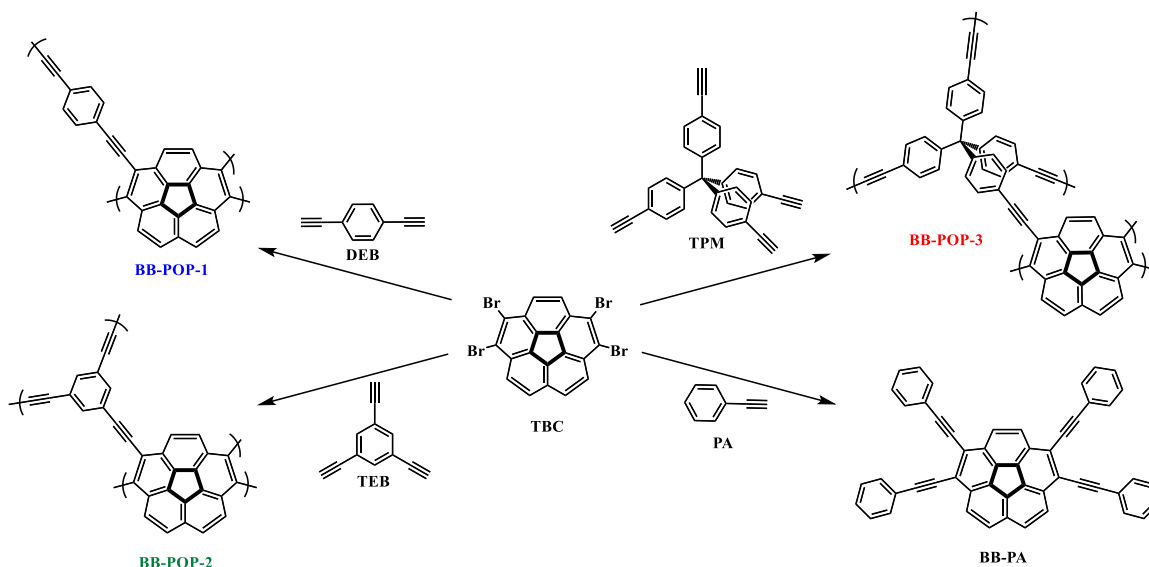


Figure 2-2. Synthesis of BB-POPs 1-3 and model compound (**BB-PA**) from Sonogashira copolymerization condition:  $\text{Pd(PPh}_3)_4$ , CuI,  $\text{Et}_3\text{N}$ , toluene,  $90^\circ\text{C}$

## 2.3 Experimental

### 2.3.1 Materials and methods

All reagents were purchased from commercial suppliers (Sigma-Aldrich and Fisher Scientific) and used as received. Low-pressure gas adsorption experiments (up to 760 torr) were carried out on a Micromeritics ASAP 2020 surface area analyzer. Ultrahigh purity grade  $\text{N}_2$ ,  $\text{CO}_2$  and  $\text{H}_2$  were

obtained from Airgas Corporation. Samples were degassed under dynamic vacuum for 12 h at 150 °C prior to each measurement. N<sub>2</sub>, CO<sub>2</sub> and H<sub>2</sub> isotherms were measured using a liquid nitrogen bath (77 K) and CO<sub>2</sub> was measured in a room temperature water bath (298 K) and using an ice water bath (273 K). Pore size distributions were calculated from the adsorption curve using the nonlocal density function theory (NLDFT) carbon slit-pore model in the Micromeritics software package and heats of adsorption values were computed by the Micromeritics ASAP software package using a variant of the Clausius-Clapeyron equation. Fourier transform infrared (FT-IR) spectra were taken on a Nicolet 380 FT-IR with a Smart Orbit diamond attenuated total reflectance (ATR) cell. The thermogravimetric analyses (TGA) were performed using a TA Instrument SDT Q600 Analyzer under nitrogen atmosphere with a heating rate of 10 °C min<sup>-1</sup> from 30-800 °C. Powder X-ray diffraction (PXRD) of polymers was carried out on a Bruker D8 Advance diffractometer with a sealed tube radiation source (Cu K $\alpha$ ,  $\lambda$  = 1.54184 Å), a no background sample holder, and a Lynxeye XE detector. Scanning electron microscope (SEM) images were acquired with Zeiss-LEO model 1530 SEM instrument and energy dispersive X-ray spectroscopy (EDX) were acquired on a Zeiss SUPRA40 SEM instrument. The samples were prepared on 15 mm aluminum stubs using double-sided adhesive copper tapes. For EDX uncoated samples were imaged at a working distance of 10 mm and a voltage of 15 kV using a secondary electron detector. Fluorescence measurements were carried out on a Perkin-Elmer LS-50B Luminescence Spectrophotometer with a suspension of BB-POPs (1 mg) in dichloromethane (3 mL). Cyclic voltammetry (CV) was performed using a Potentiostat/Galvanostat (EG&G Princeton Applied Research 273A) in an anhydrous DMF solution of Bu<sub>4</sub>NPF<sub>6</sub> (0.1 M). Voltammograms of corannulene and BB-PA were obtained in the solution phase by dissolving them in the electrolyte.

The insoluble BB-POPs were dispersed in acetone with polytetrafluoroethylene (PTFE, 5-15 %) as a binder, drop cast onto the gold working electrode and dried. Platinum mesh was used as a counter electrode and potentials were recorded versus Ag/Ag<sup>+</sup> (0.01M) as a reference electrode. The scan rate was 100 mV s<sup>-1</sup>.

### 2.3.2 Monomer and Model compound synthesis

Monomers: TBC, DEB, TEB and TBC, corannulene and model compound: 1,2,5,6-Tetra(phenylethynyl)corannulene (BB-PA) were synthesized using previously reported protocols (Figure 2-3).<sup>10,44-47</sup>

### 2.3.3 Polymer Synthesis

**BB-POP-1:** To a pressure tube containing **TBC** (40 mg, 0.071mmol) and **DEB** (17.9 mg, 0.142 mmol) were added toluene (2 mL) and Et<sub>3</sub>N (4 mL). This was purged with nitrogen for 15 min before Pd(PPh<sub>3</sub>)<sub>4</sub> (15.0 mg, 0.014mmol) and CuI (2.6 mg, 0.014 mmol) were added and the tube was sealed. The reaction was then heated at 90 °C for 18 h. After that time a brown solid had formed which was collected by filtration, and washed with CH<sub>2</sub>Cl<sub>2</sub> (100 mL) and methanol (100 ml), followed by sonication (20 min) in CH<sub>2</sub>Cl<sub>2</sub> twice after which time the solid was collected by filtration. The polymer was then sonicated in 5 mL of hot toluene for five minutes before being filtered. This washing procedure was repeated a total of five times in hot toluene followed by five washings in 5 mL hot DMSO. The solid was finally washed with acetone (100 mL). Yield = 27 mg (77%).



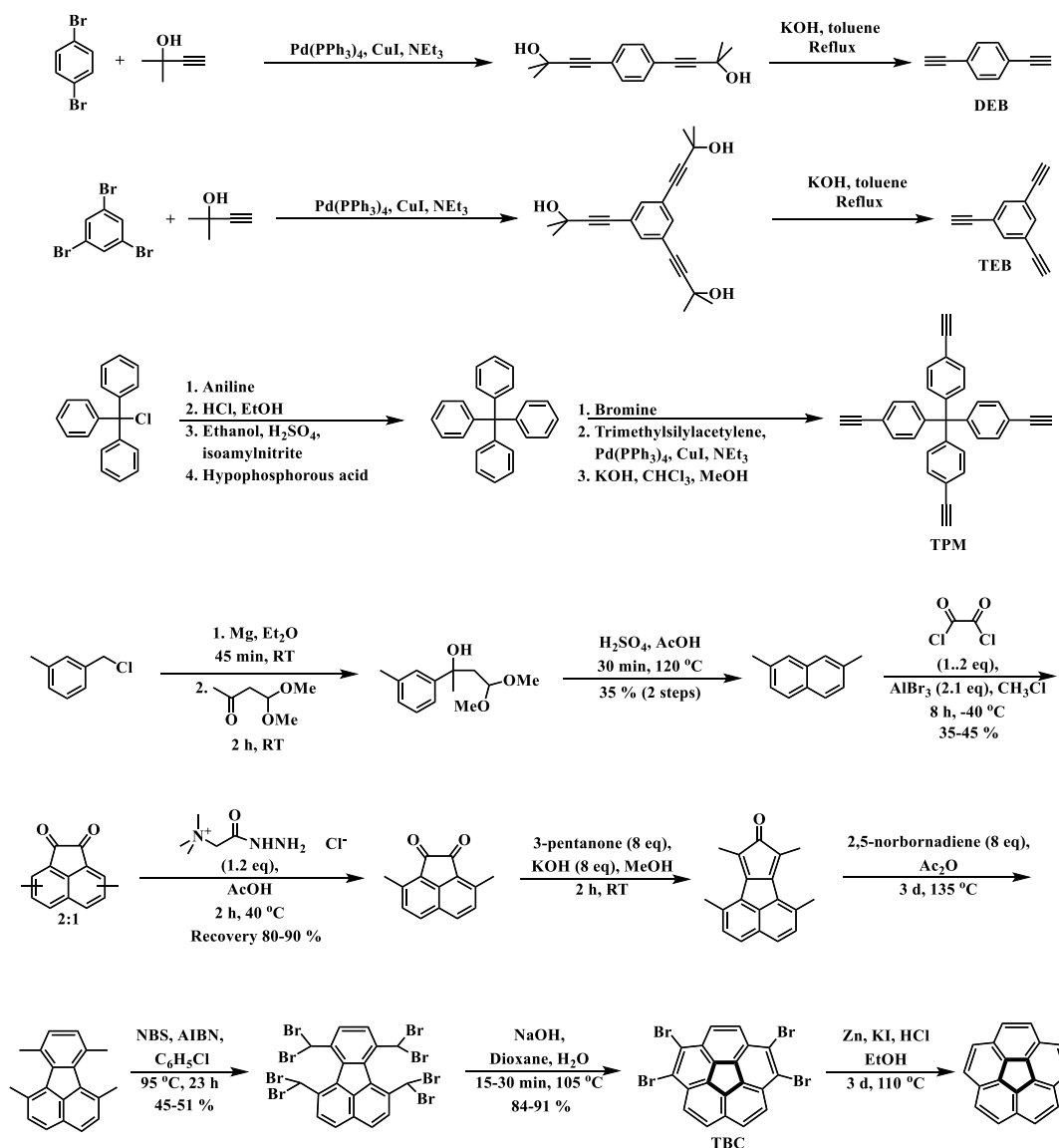


Figure 2-3. Synthesis of 1,4-diethynylbenzene (**DEB**), 1,3,5-trisubstituted ethynylbenzene (**TEB**), tetrakis(4-ethynyl)-tetraphenylmethane (**TPM**), and 1,2,5,6-tetrabromocorannulene (**TBC**)

**BB-POP-2:** To a pressure tube containing **TBC** (40 mg, 0.071 mmol) and **TEB** (14.2 mg, 0.094 mmol) were added toluene (2 mL) and  $\text{Et}_3\text{N}$  (4 mL). This was purged with nitrogen for 15 min before  $\text{Pd(PPh}_3)_4$  (16.33 mg, 0.014 mmol) and  $\text{CuI}$  (2.76 mg, 0.014 mmol) were added and the tube was sealed. The reaction was then heated at  $90^\circ\text{C}$  for 18 h. After that time a brown solid had formed which was collected by filtration, and washed with  $\text{CH}_2\text{Cl}_2$  (100 mL) and methanol

(100 ml), followed by sonication (20 min) in  $\text{CH}_2\text{Cl}_2$  twice and then the solid was collected by filtration. The polymer was then sonicated in 5 mL of hot toluene for five minutes before being filtered. This washing procedure was repeated a total of five times in hot toluene followed by five washings in 5 mL hot DMSO. The solid was finally washed with acetone (100 mL). Yield = 25 mg (80%).

**BB-POP-3:** To a pressure tube containing **TBC** (40 mg, 0.071mmol) and **TPM** (29.4 mg, 0.071 mmol) were added toluene (2 mL) and  $\text{Et}_3\text{N}$  (4 mL). This was purged with nitrogen for 15 min before  $\text{Pd}(\text{PPh}_3)_4$  (16.33 mg, 0.014mmol) and  $\text{CuI}$  (2.8 mg, 0.014 mmol) were added and the tube was sealed. The reaction was then heated at 90 °C for 18 h. After that time a brown solid had formed which was collected by filtration, and washed with  $\text{CH}_2\text{Cl}_2$  (100 mL) and methanol (100 ml), followed by sonication (20 min) with  $\text{CH}_2\text{Cl}_2$  for twice and filtered. The polymer was then sonicated in 5 mL of hot toluene for five minutes before being filtered. This washing procedure was repeated a total of five times in hot toluene followed by five washings in 5 mL hot DMSO. The solid was finally washed with acetone (100 mL). Yield = 43 mg, (92%).

## 2.4 Result and discussion

### 2.4.1 Synthesis and characterization

Three BB-POPs were obtained as brown powders via Sonogashira polymerization (Figure 2-2). Each of the polymers is insoluble in common organic solvents indicating the formation of a hyper-crosslinked polymeric structure. FT-IR spectra show a significant reduction of alkyne C-H stretching (Figure 2-4) confirming the polymerization.

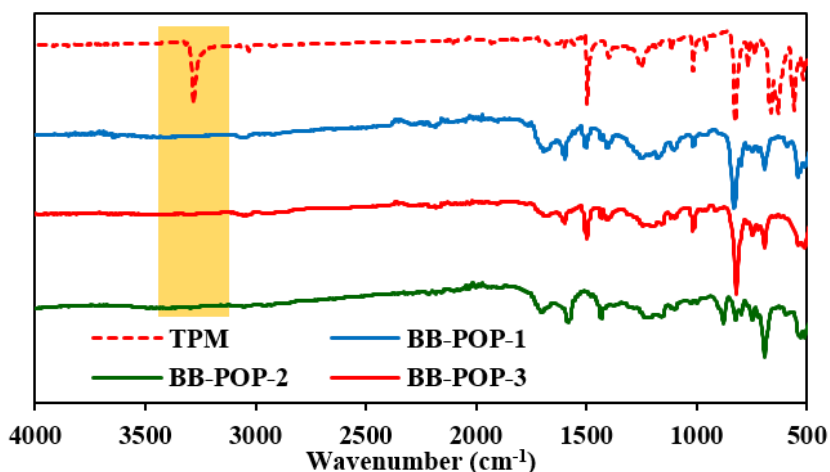


Figure 2-4. IR spectra of tetrakis(4-ethynyl)-tetraphenylmethane (TPM) and BB-POPs.

Energy-dispersive X-ray spectroscopy (EDX) analysis indicates that is only 0.6-0.7 unreacted Br atoms per corannulene core in these POPs, that is approximately about C:Br atomic ratio of 98:2 (Table 2-1). This measurement is indicative of high conversion. SEM analysis indicate the rod shape morphology of polymers (Figure 2-5). Thermogravimetric analysis of POPs indicates polymers are thermally stable with less than 20 wt.% up to 800 °C at N<sub>2</sub> atmosphere (Figure 2-6). The powder X-ray diffraction (PXRD) patterns (Figure 2-7) show that all three POPs have largely amorphous structures and lack the prominent peaks attributed to  $\pi$  stacking that we have previously observed in POPs containing large PAH monomers.<sup>33,35</sup> We hypothesize that this could be due to the unusual symmetry of the 1,2,5,6 functionalization pattern of the corannulene and its curved shape creating a polymer where these  $\pi$ -stacking interactions are unable to form in the solid state. The luminescent properties of the BB-POPs were investigated (Figure 2-8) and compared with a model compound 1,2,5,6-tetra(phenylethynyl)corannulene (**BB-PA**). The emission maximum of corannulene was located at 453 nm while that of **BB-PA** was red shifted by 23 nm. The photoluminescence maxima BB-POP-1 exhibits a larger red shift of about 77 nm ( $\lambda_{\text{max}} = 530$  nm)

indicating that the extension of conjugation may be longer due to the linear shape of the **DEB** co-monomer as compared with BB-POP-2 and 3 whose conjugation is limited by either out of plane rotations enforced by steric effects (BB-POP-2) or the existence of an  $sp^3$  carbon (BB-POP-3).

Sample	Weight %			Atomic %		
	C%	Br%	Pd%	C%	Br%	Pd%
BB-POP-1	88.15	10.01	1.84	98.09	1.67	0.23
BB-POP-2	87.50	9.98	2.52	98.00	1.68	0.32
BB-POP-3	91.00	7.47	1.52	98.60	1.22	0.19

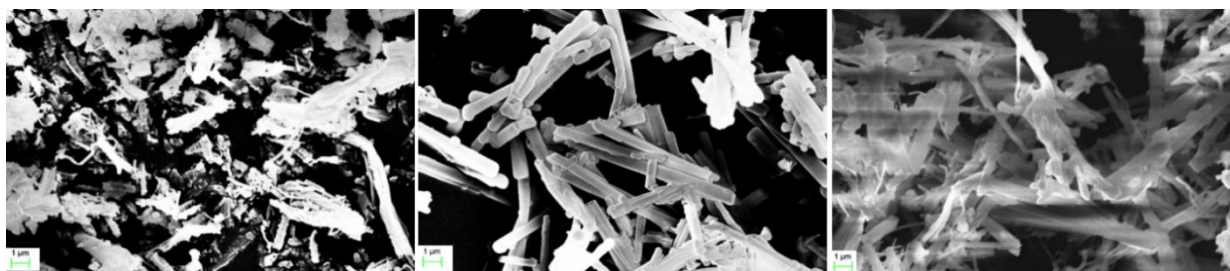


Figure 2-5. SEM images of BB-POPs: BB-POP-1 (left), BB-POP-2 (middle) and BB-POP-3 (right)

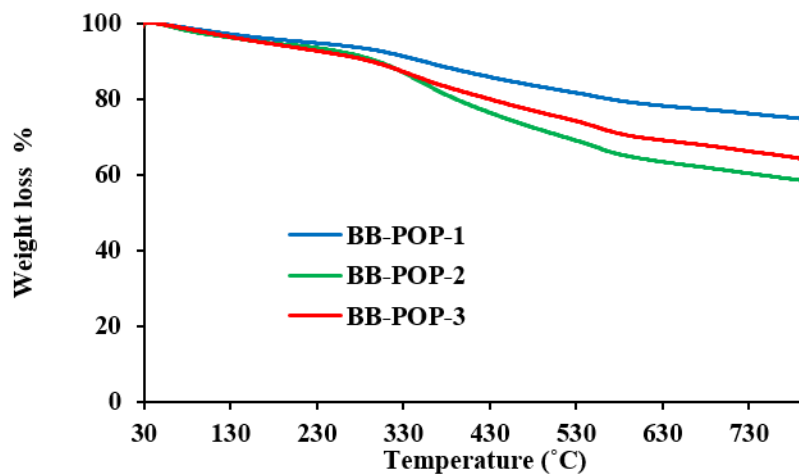


Figure 2-6. TGA curves of BB-POPs

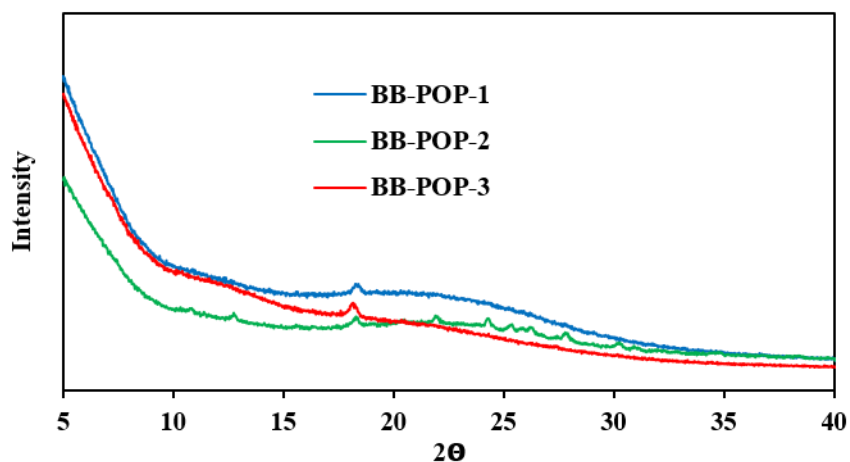


Figure 2-7. PXRD patterns of BB-POPs

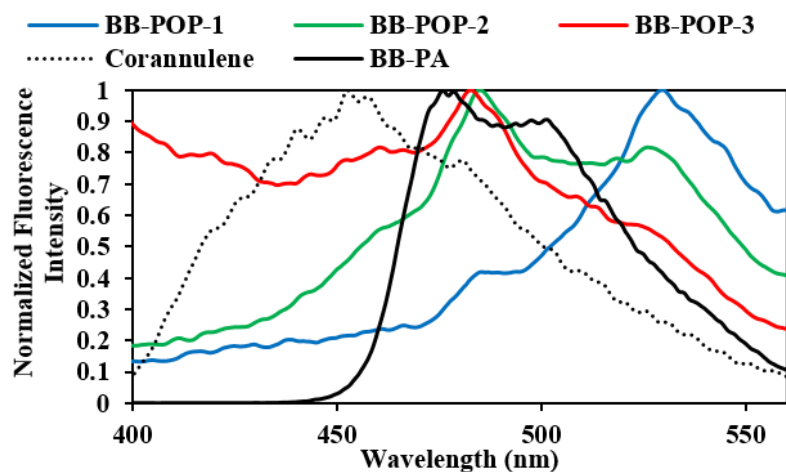


Figure 2-8. Normalized emission spectra in  $\text{CH}_2\text{Cl}_2$  with excitation at 300 nm

#### 2.4.2 Porosity measurements and gas uptake

The accessible surface areas (SAs) and pore size distributions were determined for all three POPs using  $\text{N}_2$  adsorption measurements at 77 K (Figure 2-9). As shown in Figure, BB-POP-3 has a moderate  $\text{N}_2$  uptake capacity, ( $284 \text{ cm}^3/\text{g}$ ) which is much higher than that of BB-POP-1 and BB-POP-2 ( $84$  and  $89 \text{ cm}^3/\text{g}$ , respectively). The Brunauer, Emmett and Teller (BET) and Langmuir surface areas for the POPs were calculated using the  $\text{N}_2$  adsorption in the low-pressure range ( $P/P_0$  0.01-0.1) (Table 2-2). BB-POP-3 shows a moderate BET surface area of  $556 \text{ m}^2/\text{g}$ , whereas the

other two polymers show low surface areas of 56 and 130 m<sup>2</sup>/g for BB-POP-1 and BB-POP-2, respectively. Thus, as expected, the N<sub>2</sub> adsorption data confirm that incorporating the three dimensional monomer **TPM** results in a higher surface area than the other co-monomers **TEB** and **DEB**. The N<sub>2</sub> isotherms show rapid N<sub>2</sub> uptake at low relative pressures ( $P/P_0 < 0.01$ ), which is typical for microporous materials. Pore size distributions (Figure 2-10) also indicate BB-POPs are predominantly microporous (pore width < 2 nm).

Table 2-2. Pore structure parameters of polymers obtained by N<sub>2</sub> adsorption

Sample	BET surface area (m <sup>2</sup> /g)	Langmuir	Horvath Kawazoe
		surface area (m <sup>2</sup> /g)	Pore Volume (cm <sup>3</sup> /g)
BB-POP-1	56	62	0.13
BB-POP-2	130	143	0.14
BB-POP-3	556	609	0.44

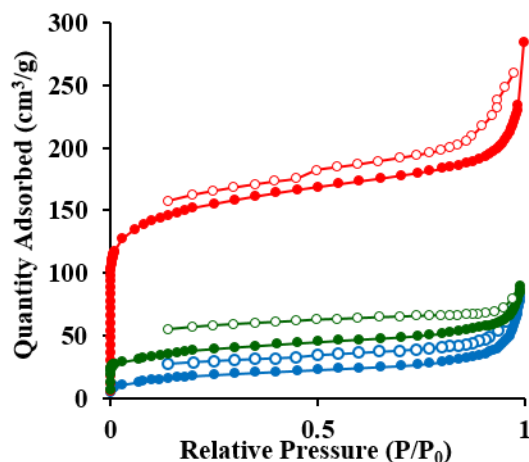


Figure 2-9. (a) Nitrogen adsorption at 77 K (solid symbols) and desorption (open symbols) isotherms

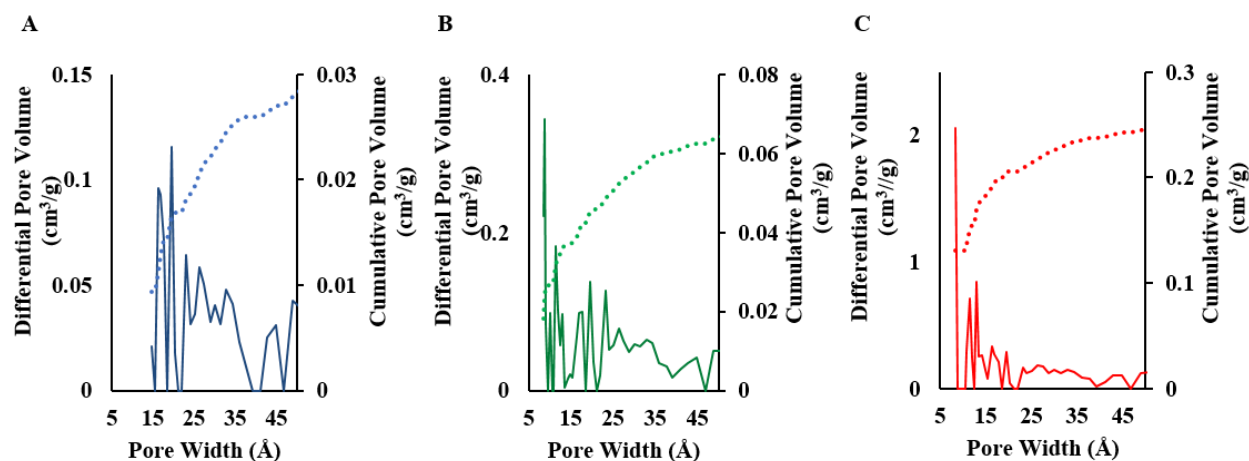


Figure 2-10. Differential (line) and cumulative (dash) pore size distributions of BB-POP-1 (blue), BB-POP-2 (green), BB-POP-3 (red)

The CO<sub>2</sub> adsorption isotherms of BB-POPs were measured at 273 K (Figure 2-11a) and 298 K (Figure 2-11b). BB-POP-3 shows the highest CO<sub>2</sub> uptake capacity, 57 cm<sup>3</sup>/g (11.7 wt. %) at 273 K and 900 mmHg. In spite of its moderate surface area, the CO<sub>2</sub> capacities of the BB-POPs compete with (or even surpass) a variety of other porous materials, for example PAF-1 (Network A) (11.7 wt. %  $S_{\text{BET}}=4077 \text{ m}^2 \text{ g}^{-1}$ ),<sup>48</sup> COF-5 (5.9 wt %,  $S_{\text{BET}}=1670 \text{ m}^2 \text{ g}^{-1}$ ),<sup>49</sup> COF-103 (7.6 wt %,  $3530 \text{ m}^2 \text{ g}^{-1}$ )<sup>49</sup> and BLP-1H (7.4 wt %,  $1360 \text{ m}^2 \text{ g}^{-1}$ ).<sup>50</sup> Despite their low porosity, BB-POP-1 and 2 also demonstrate considerable CO<sub>2</sub> adsorption capacities of 7.4 wt. % and 8.5 wt. %, respectively. Despite its lower surface area of  $130 \text{ m}^2 \text{ g}^{-1}$ , BB-POP-2 built with **TBC** and **TEB**, has a similar storage capacity to CMP-1 (9.0 wt %,  $S_{\text{BET}}= 837 \text{ m}^2 \text{ g}^{-1}$ )<sup>31</sup> which is made out of 1,4-diiodobenzene and **TEB**, indicating the potential involvement of corannulene in CO<sub>2</sub> adsorption. Further, CO<sub>2</sub> adsorption capacities exceeded that of our previously reported **HBC** based POPs synthesized in a similar manner with **TPM**: HBC-POP-1 (9 wt.%), HBC-POP-2 (8 wt.%), and HBC-POP-98 (8 wt.%).<sup>33,35</sup> These results are consistent with the findings of computational studies,

which show that the concave surface of corannulene may exhibit higher affinity for small molecules like CO<sub>2</sub> compared to planar coronenes.<sup>43</sup>

To gain further insight into these interactions, isosteric heats of adsorption ( $Q_{st}$ ) were calculated based on adsorption data at 273 K and 298 K (Figure 2-11). The initial  $Q_{st}$  of BB-POP-2 is 28.8 kJ mol<sup>-1</sup> and is among the highest values reported to date for a hydrocarbon-based porous organic material. However, the  $Q_{st}$  decreases rapidly for BB-POP-1 and 2 and this rapid reduction is probably due to the depletion of available surface area for adsorption, owing to the low surface area. On the other hand, BB-POP-3 shows a stabilizing trend of the  $Q_{st}$  with good initial  $Q_{st}$  value of 24.0 kJ mol<sup>-1</sup>.

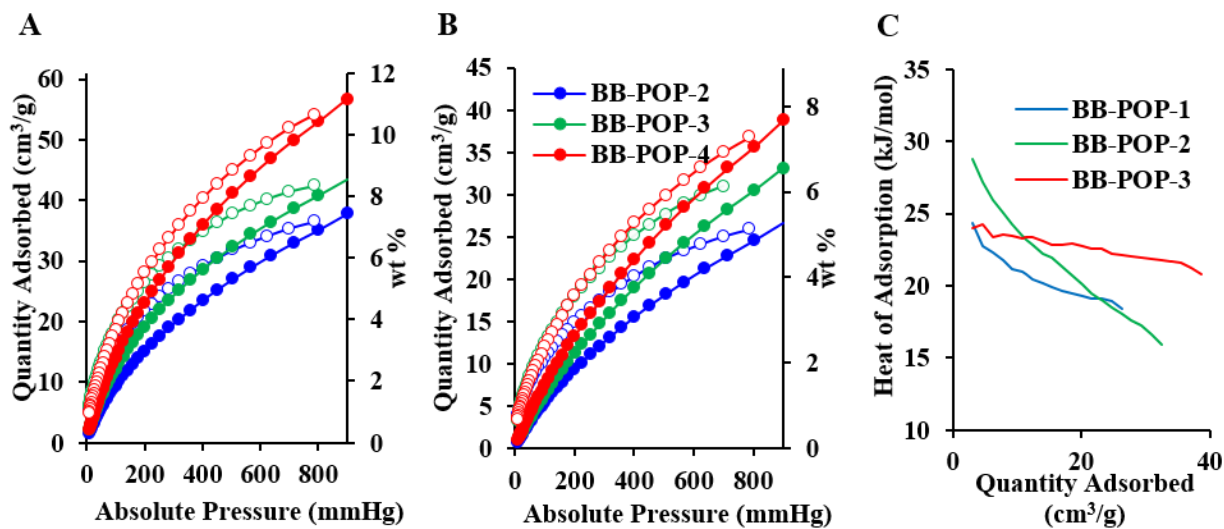


Figure 2-11. CO<sub>2</sub> adsorption isotherms adsorption (filled circles) desorption (open circles) for BB-POP-1 (blue), BB-POP-2 (green) and BB-POP-3 (red) at (a) 273 K (b) 298 K and (c) Heat of adsorption for CO<sub>2</sub>

The H<sub>2</sub> adsorption isotherms of BB-POPs were also measured at 77 K (Figure 2-12). BB-POP-3 shows moderate H<sub>2</sub> uptakes of 1.08 wt.% at saturation pressure. Two lower surface area POPs: BB-POP-1 and 2 also demonstrate competitive H<sub>2</sub> adsorption capacities 0.78 wt.% and 0.76 wt.%.



However, the H<sub>2</sub> adsorption capacity of BB-POP-3 is higher than that of the planar analogue: HBC based HBC-POP-1 and 2 (0.8 wt.%) which were also built with **TPM**.<sup>34</sup>

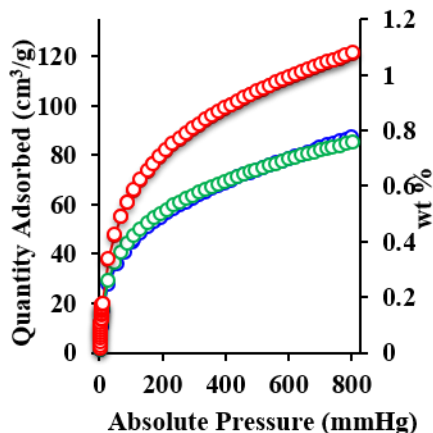


Figure 2-12. H<sub>2</sub> adsorption isotherms at 77 K for BB-POP-1 (blue), BB-POP-2 (green) and BB-POP-3 (red)

### 2.4.3 Electrochemical properties

To determine whether the redox capability of corannulene is retained upon its incorporation into a POP, cyclic voltammetry (CV) of BB-POP-2 and 3 was carried out (Figure 2-13, Figure 2-14, Table 2-3). BB-POP-2 shows three distinct reduction events its peak potentials of -1.38 V, -1.76 V, and -2.55 V. BB-POP-3 shows four distinct reduction events at -1.61 V, -1.91 V, -2.42 V, and -2.73 V. Reduction potentials of the model compound **BB-PA** are less negative than corannulene which illustrates stronger electron accepting behavior in comparison with unfunctionalized corannulene. The first two reduction potentials of BB-POP-2 are also less negative than that of corannulene. These CV curves of POPs resemble the shape of corannulene and BB-PA, indicating that the redox properties of corannulene are retained after incorporation into a POP, although they are shifted slightly in comparison with both control compounds and with respect to one another. It is likely that the nature of the porous polymer structure contributes to these changes. Future

studies will attempt to gain more detailed insight into how an enforced porous microenvironment can affect the redox properties of corannulene-based materials.

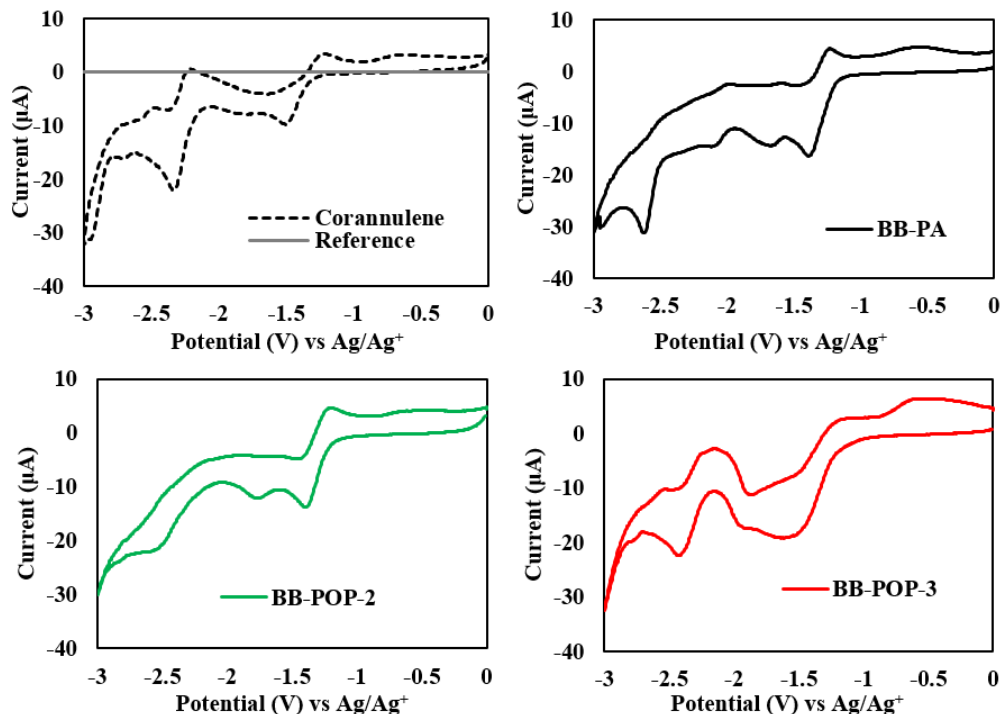


Figure 2-13. Cyclic voltammograms of BB-POP-2 and 3, corannulene (1 mM), BB-PA (1 mM) and reference (bare gold electrode) in 0.1 M tetrabutylammonium hexafluorophosphate /DMF using Pt mesh as the counter electrode,  $\text{Ag}/\text{Ag}^+$  as the reference electrode and Au as the working electrode

Table 2-3. Reduction potentials vs  $\text{Ag}/\text{Ag}^+$  of corannulene, **BB-PA** and BB-POPs in DMF/ $\text{Bu}_4\text{NPF}_6$  (0.1 M)

Sample	$E_p$ (I) /V	$E_p$ (II) /V	$E_p$ (III) /V	$E_p$ (IV) /V
Corannulene	-1.50	-1.78	-2.35	-2.72
BB-PA	-1.39	-1.68	-2.11	-2.62
BB-POP-2	-1.39	-1.76	-2.55	n/o
BB-POP-3	-1.62	-1.91	-2.43	-2.83

n/o = not observed

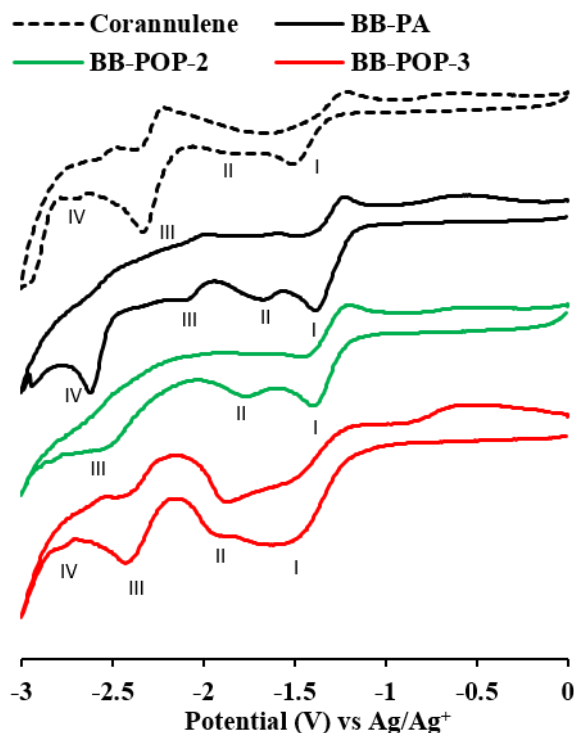


Figure 2-14. Cyclic voltamograms of corannulene (1 mM), **BB-PA** (1 mM), BB-POP-2 and 3 in 0.1 M tetrabutylammonium hexafluorophosphate/DMF using Pt mesh as the counter electrode,  $\text{Ag}/\text{Ag}^+$  as the reference electrode and Au as the working electrode

## 2.5 Conclusion

In summary, we have succeeded in the design and preparation of a corannulene based porous polymer via Sonogashira copolymerization between 1,2,5,6-tetrabromocorannulene (**TBC**) and both planar (**DEB**, **TEB**) and tetrahedral (**TPM**) alkyne monomers, resulting in polymers with microporous structures and  $\text{CO}_2$  adsorption properties that are higher than expected given their moderate surface areas. Furthermore, the corannulene units of the polymers retain their redox activity, demonstrating potential as robust materials for electrochemical applications such as supercapacitors and batteries. This combination of porosity and redox activity could also create

new opportunities for the application of porous materials as electrochemical sensors or redox catalysts.

## 2.6 Acknowledgements

This research was carried out with the support of University of Texas at Dallas, and the American Chemical Society Petroleum Research Fund (52906-DNI10). We would like to acknowledge Fei Li, Dr. Sumudu N. Wijenayake and Dr. Gregory McCandless for helpful discussion and PXRD.

## 2.7 References

1. Wu, Y.; Siegel, J. S. Aromatic Molecular-Bowl Hydrocarbons: Synthetic Derivatives, Their Structures, and Physical Properties. *Chem. Rev.* **2006**, *106*, 4843-4867.
2. Tsefrikas, V. M.; Scott, L. T. Geodesic Polyarenes by Flash Vacuum Pyrolysis. *Chem. Rev.* **2006**, *106*, 4868-4884.
3. Sygula, A. Chemistry on a Half-Shell: Synthesis and Derivatization of Buckybowls. *Eur. J. Org. Chem.* **2011**, *2011*, 1611-1625.
4. Barth, W. E.; Lawton, R. G. Dibenzo[ghi,mno]fluoranthene. *J. Am. Chem. Soc.* **1966**, *88*, 380-381.
5. Lawton, R. G.; Barth, W. E. Synthesis of corannulene. *J. Am. Chem. Soc.* **1971**, *93*, 1730-1745.
6. Mehta, G.; Panda, G. A new synthesis of corannulene. *Tetrahedron Lett.* **1997**, *38*, 2145-2148.
7. Scott, L. T.; Hashemi, M. M.; Meyer, D. T.; Warren, H. B. Corannulene. A convenient new synthesis. *J. Am. Chem. Soc.* **1991**, *113*, 7082-7084.
8. Scott, L. T.; Cheng, P.; Hashemi, M. M.; Bratcher, M. S.; Meyer, D. T.; Warren, H. B. Corannulene. A Three-Step Synthesis<sup>1</sup>. *J. Am. Chem. Soc.* **1997**, *119*, 10963-10968.
9. Sygula, A.; Rabideau, P. W. Non-Pyrolytic Syntheses of Buckybowls: Corannulene, Cyclopentacorannulene, and a Semibuckminsterfullerene. *J. Am. Chem. Soc.* **1999**, *121*, 7800-7803.

10. Butterfield, A. M.; Gilomen, B.; Siegel, J. S. Kilogram-Scale Production of Corannulene. *Org. Process Res. Dev.* **2012**, *16*, 664-676.
11. Petrukhina, M. A.; Scott, L. T. Coordination chemistry of buckybowl: from corannulene to a hemifullerene. *Dalton Trans.* **2005**, 2969-2975.
12. Filatov, A. S.; Petrukhina, M. A. Probing the binding sites and coordination limits of buckybowl in a solvent-free environment: Experimental and theoretical assessment. *Coord. Chem. Rev.* **2010**, *254*, 2234-2246.
13. Bruno, C.; Benassi, R.; Passalacqua, A.; Paolucci, F.; Fontanesi, C.; Marcaccio, M.; Jackson, E. A.; Scott, L. T. Electrochemical and Theoretical Investigation of Corannulene Reduction Processes. *J. Phys. Chem. B* **2009**, *113*, 1954-1962.
14. Stuparu, M. C. Rationally Designed Polymer Hosts of Fullerene. *Angew. Chem. Inter. Ed.* **2013**, *52*, 7786-7790.
15. Pappo, D.; Mejuch, T.; Reany, O.; Solel, E.; Gurram, M.; Keinan, E. Diverse Functionalization of Corannulene: Easy Access to Pentagonal Superstructure. *Org. Lett.* **2009**, *11*, 1063-1066.
16. Sygula, A.; Fronczek, F. R.; Sygula, R.; Rabideau, P. W.; Olmstead, M. M. A Double Concave Hydrocarbon Buckycatcher. *J. Am. Chem. Soc.* **2007**, *129*, 3842-3843.
17. Miyajima, D.; Tashiro, K.; Araoka, F.; Takezoe, H.; Kim, J.; Kato, K.; Takata, M.; Aida, T. Liquid Crystalline Corannulene Responsive to Electric Field. *J. Am. Chem. Soc.* **2009**, *131*, 44-45.
18. Scott, L. T.; Jackson, E. A.; Zhang, Q.; Steinberg, B. D.; Bancu, M.; Li, B. A Short, Rigid, Structurally Pure Carbon Nanotube by Stepwise Chemical Synthesis. *J. Am. Chem. Soc.* **2012**, *134*, 107-110.
19. Lu, R.; Zheng, Y.; Zhou, Y.; Yan, X.; Lei, T.; Shi, K.; Zhou, Y.; Pei, J.; Zoppi, L.; Baldrige, K. K.; Siegel, J. S.; Cao, X. Corannulene derivatives as non-fullerene acceptors in solution-processed bulk heterojunction solar cells. *J. Mater. Chem. A* **2014**, *2*, 20515-20519.
20. Shi, K.; Lei, T.; Wang, X.; Wang, J.; Pei, J. A bowl-shaped molecule for organic field-effect transistors: crystal engineering and charge transport switching by oxygen doping. *Chem. Sci.* **2014**, *5*, 1041-1045.
21. Lu, R.; Xuan, W.; Zheng, Y.; Zhou, Y.; Yan, X.; Dou, J.; Chen, R.; Pei, J.; Weng, W.; Cao, X. A corannulene-based donor-acceptor polymer for organic field-effect transistors. *RSC Adv.* **2014**, *4*, 56749-56755.

22. Lu, R.; Zhou, Y.; Yan, X.; Shi, K.; Zheng, Y.; Luo, M.; Wang, X.; Pei, J.; Xia, H.; Zoppi, L.; Baldrige, K. K.; Siegel, J. S.; Cao, X. Thiophene-fused bowl-shaped polycyclic aromatics with a dibenzoa,g]corannulene core for organic field-effect transistors. *Chem. Commun.* **2015**, *51*, 1681-1684.
23. Chen, R.; Lu, R.; Shi, K.; Wu, F.; Fang, H.; Niu, Z.; Yan, X.; Luo, M.; Wang, X.; Yang, C.; Wang, X.; Xu, B.; Xia, H.; Pei, J.; Cao, X. Corannulene derivatives with low LUMO levels and dense convex-concave packing for n-channel organic field-effect transistors. *Chem. Commun.* **2015**, *51*, 13768-13771.
24. Mack, J.; Vogel, P.; Jones, D.; Kaval, N.; Sutton, A. The development of corannulene-based blue emitters. *Org. Biomol. Chem.* **2007**, *5*, 2448-2452.
25. Zabula, A. V.; Filatov, A. S.; Spisak, S. N.; Rogachev, A. Y.; Petrukhina, M. A. A Main Group Metal Sandwich: Five Lithium Cations Jammed Between Two Corannulene Tetraanion Decks. *Science* **2011**, *333*, 1008-1011.
26. Fellows, W. B.; Rice, A. M.; Williams, D. E.; Dolgoplova, E. A.; Vannucci, A. K.; Pellechia, P. J.; Smith, M. D.; Krause, J. A.; Shustova, N. B. Redox-Active Corannulene Buckybowls in a Crystalline Hybrid Scaffold. *Angew. Chem. Int. Ed.* **2016**, *55*, 2195-2199.
27. Zhou, H.; Long, J. R.; Yaghi, O. M. Introduction to Metal-Organic Frameworks. *Chem. Rev.* **2012**, *112*, 673-674.
28. Ding, S.; Wang, W. Covalent organic frameworks (COFs): from design to applications. *Chem. Soc. Rev.* **2013**, *42*, 548-568.
29. Dawson, R.; Cooper, A. I.; Adams, D. J. Nanoporous organic polymer networks. *Prog. in Poly. Sci.* **2012**, *37*, 530-563.
30. Ben, T.; Qiu, S. Porous aromatic frameworks: Synthesis, structure and functions. *Cryst. Eng. Comm* **2013**, *15*, 17-26.
31. Liu, Q.; Tang, Z.; Wu, M.; Zhou, Z. Design, preparation and application of conjugated microporous polymers. *Polym. Int.* **2014**, *63*, 381-392.
32. McKeown, N. B. Polymers of Intrinsic Microporosity, *ISRN Mater. Sci.* **2012**, *2012*, 16.
33. Thompson, C. M.; Li, F.; Smaldone, R. A. Synthesis and sorption properties of hexa-(peri)-hexabenzocoronene-based porous organic polymers. *Chem. Commun.* **2014**, *50*, 6171-6173.
34. Thompson, C. M.; McCandless, G. T.; Wijenayake, S. N.; Alfarawati, O.; Jahangiri, M.; Kokash, A.; Tran, Z.; Smaldone, R. A. Substituent Effects on the Gas Sorption and

Selectivity Properties of Hexaphenylbenzene and Hexabenzocoronene Based Porous Polymers. *Macromolecules* **2014**, *47*, 8645-8652.

35. Karunathilake, A. A. K.; Chang, J.; Thompson, C. M.; Nguyen, C. U.; Nguyen, D. Q.; Rajan, A.; Sridharan, A.; Vyakaranam, M.; Adegboyega, N.; Kim, S. J.; Smaldone, R. A. Hexaphenylbenzene and hexabenzocoronene-based porous polymers for the adsorption of volatile organic compounds. *RSC Adv.* **2016**, *6*, 65763-65769.
36. Alahakoon, S. B.; Thompson, C. M.; Nguyen, A. X.; Occhialini, G.; McCandless, G. T.; Smaldone, R. A. An azine-linked hexaphenylbenzene based covalent organic framework. *Chem. Commun.* **2016**, *52*, 2843-2845.
37. Scanlon, L. G.; Balbuena, P. B.; Zhang, Y.; Sandi, G.; Back, C. K.; Feld, W. A.; Mack, J.; Rottmayer, M. A.; Riepenhoff, J. L. Investigation of Corannulene for Molecular Hydrogen Storage via Computational Chemistry and Experimentation. *J. Phys. Chem. B* **2006**, *110*, 7688-7694.
38. Zhang, Y.; Scanlon, L. G.; Rottmayer, M. A.; Balbuena, P. B. Computational Investigation of Adsorption of Molecular Hydrogen on Lithium-Doped Corannulene. *J. Phys. Chem. B* **2006**, *110*, 22532-22541.
39. Denis, P. A. Investigation of H<sub>2</sub> Physisorption on Corannulene (C<sub>20</sub>H<sub>10</sub>), Tetraindenocorannulene (C<sub>44</sub>H<sub>18</sub>), Pentaindenocorannulene (C<sub>50</sub>H<sub>20</sub>), C<sub>60</sub>, and Their Nitrogen Derivatives. *J. Phys. Chem. C* **2008**, *112*, 2791-2796.
40. Banerjee, S.; Pillai, C. G. S.; Majumder, C. Hydrogen absorption behavior of doped corannulene: A first principles study. *Int. J. Hydrogen Energy* **2011**, *36*, 4976-4983.
41. Reisi-Vanani, A.; Alihoseini, L. Computational investigation of the adsorption of molecular hydrogen on the nitrogen-doped corannulene as a carbon nano-structure. *Surf. Sci.* **2014**, *621*, 146-151.
42. Reisi-Vanani, A.; Faghih, S. Computational study of the molecular hydrogen physisorption in some of the corannulene derivatives as a carbon nanostructure. *J. Saudi Chem. Soc.* **2014**, *18*, 666-673.
43. Hussain, M. A.; Vijay, D.; Sastry, G. N. Buckybowls as adsorbents for CO<sub>2</sub>, CH<sub>4</sub>, and C<sub>2</sub>H<sub>2</sub>: Binding and structural insights from computational study. *J. Comp. Chem.* **2016**, *37*, 366-377.
44. Shu, W.; Guan, C.; Guo, W.; Wang, C.; Shen, Y. Conjugated poly(aryleneethynylsiloles) and their application in detecting explosives. *J. Mater. Chem.* **2012**, *22*, 3075-3081.

45. Pandey, P.; Farha, O. K.; Spokoyny, A. M.; Mirkin, C. A.; Kanatzidis, M. G.; Hupp, J. T.; Nguyen, S. T. A "click-based" porous organic polymer from tetrahedral building blocks. *J. Mater. Chem.* **2011**, *21*, 1700–1703.
46. Mori, T.; Grimme, S.; Inoue, Y. A Combined Experimental and Theoretical Study on the Conformation of Multiarmed Chiral Aryl Ethers. *J. Org. Chem.* **2007**, *72*, 6998-7010.
47. Sygula, A.; Xu, G.; Marcinow, Z.; Rabideau, P. W. 'Buckybowls'-introducing curvature by solution phase synthesis. *Tetrahedron* **2001**, *57*, 3637-3644.
48. Ben, T.; Ren, H.; Ma, S.; Cao, D.; Lan, J.; Jing, X.; Wang, W.; Xu, J.; Deng, F.; Simmons, J.; Qiu, S.; Zhu, G. Targeted Synthesis of a Porous Aromatic Framework with High Stability and Exceptionally High Surface Area. *Angew. Chem.* **2009**, *121*, 9621-9624.
49. Furukawa, H.; Yaghi, O. M. Storage of Hydrogen, Methane, and Carbon Dioxide in Highly Porous Covalent Organic Frameworks for Clean Energy Applications. *J. Am. Chem. Soc.* **2009**, *131*, 8875-8883.
50. Jackson, K. T.; Rabbani, M. G.; Reich, T. E.; El-Kaderi, H. Synthesis of highly porous borazine-linked polymers and their application to H<sub>2</sub>, CO<sub>2</sub>, and CH<sub>4</sub> storage. *Polym. Chem.* **2011**, *2*, 2775-2777.



**CHAPTER 3**

**HEXAPHENYLBENZENE AND HEXABENZOCORONENE-BASED POROUS  
POLYMERS FOR THE ADSORPTION OF VOLATILE ORGANIC COMPOUNDS**

Authors: Arosha A. K. Karunathilake<sup>a</sup>, James Chang<sup>b</sup>, Christina M. Thompson<sup>a</sup>, Cathy U.  
Nguyen<sup>a</sup>, Dorothy Q. Nguyen<sup>a</sup>, Aditya Rajan<sup>a</sup>, Anjali Sridharan<sup>a</sup>, Megha Vyakaranam<sup>a</sup> Nathaniel  
Adegboyega<sup>b</sup>, Sung Joon Kim<sup>b\*</sup> and Ronald A. Smaldone<sup>a\*</sup>

<sup>a</sup>Department of Chemistry and Biochemistry, The University of Texas at Dallas,  
800 W Campbell Rd, Richardson, Texas, 75080

<sup>b</sup>Department of Chemistry & Biochemistry, Baylor University,  
101 Bagby Ave., Waco, TX 76706

Reprinted (adapted) from Karunathilake, A. A. K.; Chang, J.; Thompson, C. M.; Nguyen, C. U.; Nguyen, D. Q.; Rajan, A.; Sridharan, A.; Vyakaranam, M.; Adegboyega, N.; Kim, S. J.; Smaldone, R. A. Hexaphenylbenzene and hexabenzocoronene-based porous polymers for the adsorption of volatile organic compounds. *RSC Adv.* **2016**, 6, 65763-65769 with permission of The Royal Society of Chemistry.

### 3.1 Abstract

Toxic volatile organic compounds (VOCs) including benzene and toluene that are emitted from industrial chemical processes and outdoor or indoor chemical applications are harmful to the environment and threaten human health. Porous organic polymers (POPs), which have attracted much interest during the last decade as materials for gas adsorption and separation, have only recently gained attention for the adsorption of VOCs. We synthesised two POPs based on hexaphenylbenzene (HEX-POP-93) and hexabenzocoronene (HBC-POP-98) and studied the adsorption of organic vapours. Interestingly, while both POPs have moderate BET surface areas (687 and 548 m<sup>2</sup>/g respectively), they both show an excellent affinity for organic vapours over water, with a high benzene adsorption capacity of 99.9 wt% for HEX-POP-93.

### 3.2 Introduction

Volatile organic compounds (VOCs) such as benzene, toluene, ethylbenzene, xylenes (BTEX), cyclohexane, and halogenated hydrocarbons are important industrial chemicals for a wide variety of applications including paints, cleaners, lubricants, and petrochemical fuels.<sup>1</sup> Despite their ubiquitous use, the presence of these compounds in the atmosphere can pose a direct risk to both human health and the environment, even at low concentrations.<sup>2-5</sup> Prolonged exposure to these compounds can cause various skin and eye irritations, asthma or even cancer.<sup>6-8</sup> VOCs can also contribute to the formation of secondary organic aerosols, ground level ozone, and smog.<sup>9-11</sup> Hence, during the last two decades, the removal of VOCs has gained increasing attention.<sup>12,13</sup> Among various possible removal methods including thermal or catalytic oxidation, biofiltration, and condensation, recovery of VOCs by adsorption is considered to be an efficient, convenient

and economical method. Activated carbon (AC) and its derivatives<sup>14-16</sup> are the most studied adsorbents for this purpose. Recently, metal organic frameworks (MOFs)<sup>17-19</sup> and porous organic polymers (POPs)<sup>20-22</sup> have been investigated as alternative adsorbents. ACs and MOFs are good adsorbents for many gases and vapours, but the hydroscopicity of ACs and poor moisture stability of most MOFs limit their practical applications.

In contrast, POPs, which consist of purely organic structures linked *via* covalent bonds, are exceptionally stable in water and other corrosive solvent conditions, while maintaining their sorption capability.<sup>23</sup> Numerous POPs have been reported over the last decade utilizing a diverse set of monomers and covalent linkages, allowing for the design of POP structures for specific applications.<sup>23-28</sup> Our group has previously reported the synthesis and gas sorption properties of POPs and an azine COF containing the polycyclic aromatic hydrocarbon monomers hexaphenylbenzene (HEX) and hexabenzocoronene (HBC).<sup>29-31</sup> HBC is a planar molecule with extended  $\pi$ -conjugation where as HEX has a propeller-like non-planar conformation due to steric interactions between neighbouring phenyl groups (Figure 3-1). Because of their shape, symmetry and aromatic structure both are interesting structural motifs for the construction of organic materials.<sup>32-36</sup> However, there are only a few examples of HEX and HBC-based porous materials, and none of them have been studied for VOCs adsorption.<sup>29-31,37-42</sup> Herein, we are reporting the synthesis and gas/vapour adsorption properties of two new POPs synthesised *via* Sonogashira copolymerization of tetrakis-4-ethynyl tetraphenylmethane (**TPM**) with hexaiodide functionalized monomers: **HEX-6I** and **HBC-6I** (Figure 3-2).

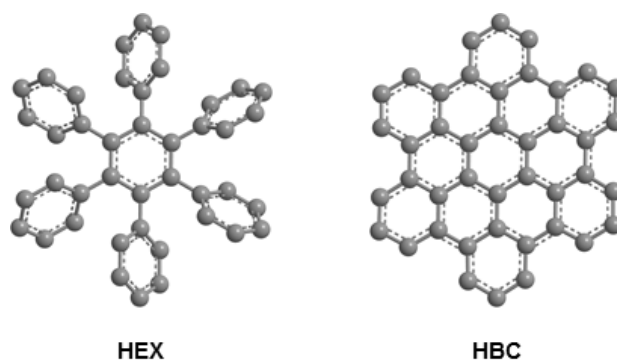


Figure 3-1. Structure of hexaphenylbenzene (**HEX**) and hexabenzocoronene (**HBC**)

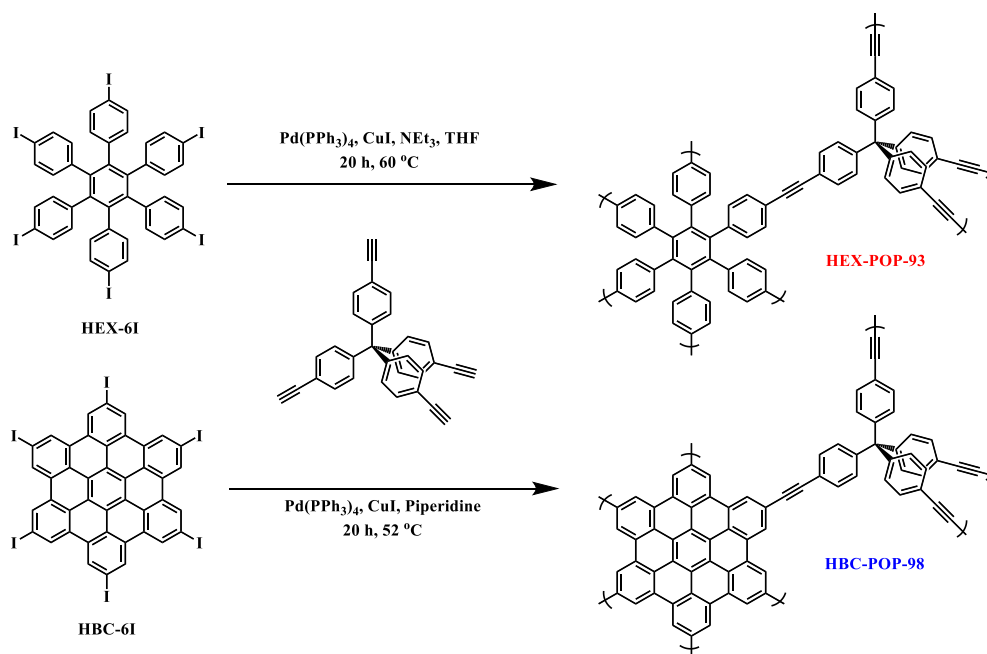


Figure 3-2. Reaction conditions for the synthesis of HEX-POP-93 and HBC-POP-98

### 3.3 Experimental

#### 3.3.1 Materials and methods

All reagents were purchased from commercial suppliers (Sigma-Aldrich and Fisher Scientific) and used as received. Low-pressure gas and vapour adsorption experiments (up to 760 torr) were carried out on a Micromeritics ASAP 2020 analyser. Ultrahigh purity grade N<sub>2</sub> and CO<sub>2</sub> were

obtained from Airgas Corporation and benzene, cyclohexane, toluene, and methanol were obtained from Fisher Scientific. Filtered, deionized H<sub>2</sub>O was used in adsorption measurements. Samples were degassed under dynamic vacuum for 12h at 100 °C prior to each measurement. N<sub>2</sub> isotherms were measured using a liquid nitrogen bath (77 K). CO<sub>2</sub>, benzene, toluene, cyclohexane, methanol, and water isotherms were measured in a room temperature water bath (298 K). CO<sub>2</sub> isotherms were also measured using an ice water bath (273 K). Pore size distributions were calculated from the adsorption branch with the nonlocal density function theory (NLDFT) carbon slit-pore model in the Micromeritics software package. Fourier transform infrared (FT-IR) spectra were taken on a Nicolet 380 FT-IR with a Smart Orbit diamond attenuated total reflectance (ATR) cell. The thermogravimetric analyses (TGA) were performed using a TA Instrument SDT Q600 Analyzer under nitrogen atmosphere with a heating rate of 10 °C min<sup>-1</sup> from 30-670 °C. Powder X-ray diffraction (PXRD) of polymers was carried out on a Bruker D8 Advance diffractometer with a sealed tube radiation source (Cu K $\alpha$ ,  $\lambda$  = 1.54184 Å), a no background sample holder, and a Lynxeye XE detector. Energy dispersive X-ray spectroscopy (EDX) analysis was carried out using scanning electron microscope (SEM) images acquired on a Zeiss SUPRA40 SEM instrument. EDX mapping was carried out using an Oxford Instruments EDX detector with Zeiss-LEO model 1530 SEM instrument. The samples were prepared on 15 mm aluminum stubs using double-sided adhesive copper tapes. The uncoated samples were imaged at a working distance of 10 mm and a voltage of 15 kV using a secondary electron detector. Solid state NMR <sup>13</sup>C-cross-polarization at magic-angle spinning (CPMAS) and <sup>13</sup>C-non-quaternary carbon suppression (NQS) NMR measurements were performed on 7.1-T (proton radio frequency of 300 MHz) on Bruker Avance III with a double resonance HX probe. The samples are contained in 4-mm outer diameter zirconia

rotor with Kel-F end-cap spinning at 12 kHz. Proton-carbon matched ramped-amplitude cross polarization, center at 50 kHz, was performed with 2-ms contact time. The proton dipolar decoupling was achieved by applying two-pulse phase modulation (TPPM15) on the  $^1\text{H}$  channel during the acquisition. The  $\pi$  pulse length was 5  $\mu\text{s}$  for  $^{13}\text{C}$  and the recycle delay was 3s. The line broadening for spectrum was 20 Hz.

### 3.3.2 Monomer synthesis

The synthesis of tetrakis(4-ethynyl)-tetraphenylmethane<sup>43</sup> (**TPM**), hexa(4-iodophenyl)benzene<sup>33,44-46</sup> (**HEX-6I**) and hexakis (4-iodo)-peri-hexabenzocoronene<sup>33</sup> (**HBC-6I**) were performed using previously reported protocols (Figure 3-3).

### 3.3.3 Polymer synthesis

**HEX-POP-93:** To a pressure tube containing **HEX-6I** (100 mg, 0.078mmol) and **TPM** (48.4 mg, 0.116 mmol) was added THF (3 mL) and  $\text{Et}_3\text{N}$  (1 mL). This was purged with nitrogen for 10 min before  $\text{Pd}(\text{PPh}_3)_4$  (13.4 mg, 0.012mmol) and  $\text{CuI}$  (2.2 mg, 0.012 mmol) were added and the tube was sealed. The reaction was then heated at 60 °C for 20 h. After that time a brown solid had formed which was collected by filtration, and washed with THF (100 mL), followed by hot DMSO (200 mL) until the filtrate was colorless. The polymer was then soaked in THF overnight. The solid was then collected by filtration again and washed with  $\text{CH}_2\text{Cl}_2$  (200 mL), and acetone (200 mL) until the filtrate was colorless. (87.4 mg, 98%)

**HBC-POP-98:** This procedure was adapted from a previously reported protocol for Sonogashira couplings using **HBC-6I**.<sup>33</sup> To a pressure tube containing **HBC-6I** (60 mg, 0.047 mmol) and **TPM** (29.3 mg, 0.071 mmol) was added piperidine (4 mL). This was purged with nitrogen for 10 min

before  $\text{Pd(PPh}_3)_4$  (8.1 mg, 0.070 mmol) and CuI (1.3 mg, 0.070 mmol) were added and the tube was sealed. The reaction was then heated at 52 °C for 20 h. After that time the reaction was filtered, and the resulting light brown solid was washed with 1M HCl (20 mL) followed by water (100 mL), hot DMSO (200 mL),  $\text{CH}_2\text{Cl}_2$  (200 mL), and acetone (200 mL) until the filtrate was colorless. (46.7 mg, 88%).

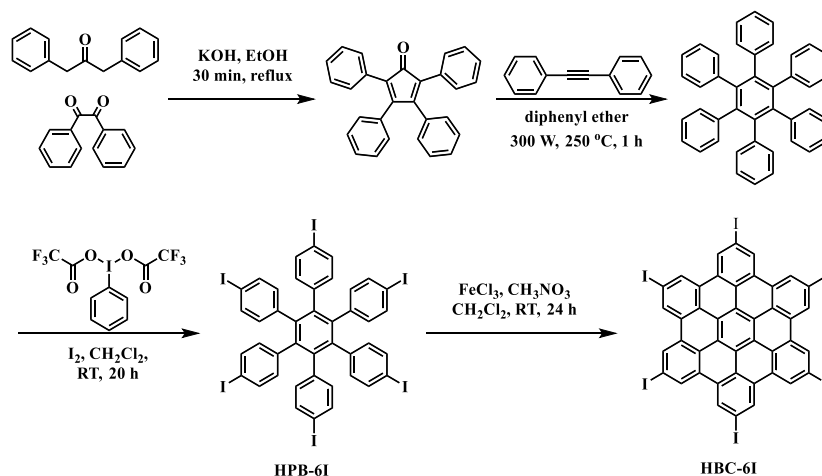


Figure 3-3. Synthesis of hexa(4-iodophenyl)benzene (HPB-6I) and hexakis(4-iodo)-peri-hexabenzocoronene (HBC-6I)

### 3.4 Result and discussion

#### 3.4.1 Synthesis and characterization

HPB-POP-93 and HBC-POP-98 were synthesized from HEX-6I and HBC-6I (Figure 3-2) respectively via co-polymerization with TPM. The products were insoluble in common organic solvents indicating the formation of a hyper-crosslinked skeletal structure. FT-IR spectra shows a significant reduction of alkyne C-H stretching in each of the two POPs compared to pre-polymerized TPM (Figure 3-4). This confirms the polymerization and indicates that there is little unreacted alkyne in the POP samples. In order of confirm their structures two POPs were

characterized with solid state NMR. Figure 3-5 shows  $^{13}\text{C}$ -CPMAS (solid line) and  $^{13}\text{C}$ -NQS (red line) spectra. The difference spectrum, which is a result of spectral subtraction of NQS from CPMAS, is shown as dotted line in the figure.  $^{13}\text{C}$ -NQS selects for the quaternary carbons and carbons without proton attached. NQS and difference spectra were used to confirm chemical shift assignments. EDX analysis (Figure 3-6, Table 3-1) indicates there are on average 0.91 and 0.86 unreacted iodine atoms per HEX or HBC units, respectively, in the polymers. The presence of unreacted iodides and alkynes is not unexpected owing to the steric hindrance of the **TPM** units which cause some of the halides to become too confined to react further.<sup>47</sup>

The TGA show that the 10% weight loss of HEX-POP-93 and HBC-POP-98 take place at 417 and 359 °C, respectively (Figure 3-7). The PXRD diffraction patterns (Figure 3-8) show both POPs to have largely amorphous structures. Interestingly, HBC-POP-98 shows a broad reflection at  $2\theta \sim 26^\circ$ . Our previous HBC-POPs<sup>29,30</sup> also showed this peak which is likely due to long range order arising from the face-to face  $\pi$ -stacking between the planar HBC components of the polymers. Face-to-face  $\pi$ -stacking of HBC is expected in both the solution and solid-state. Even with a tetrahedral linker the HBC units may be able to adopt face-to-face  $\pi$ -stacking interactions as observed in our previous work.<sup>29,30</sup> As expected, HEX-POP-93 did not show this peak, since the propeller shape of the HEX is less likely to participate in this kind of stacking.



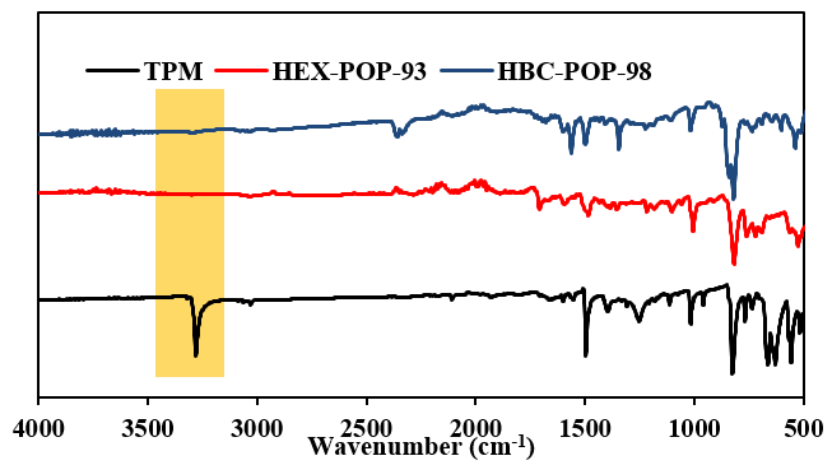


Figure 3-4. IR spectra of starting material: **TPM** and two POPs: HEX-POP-93 and HBC-POP-98

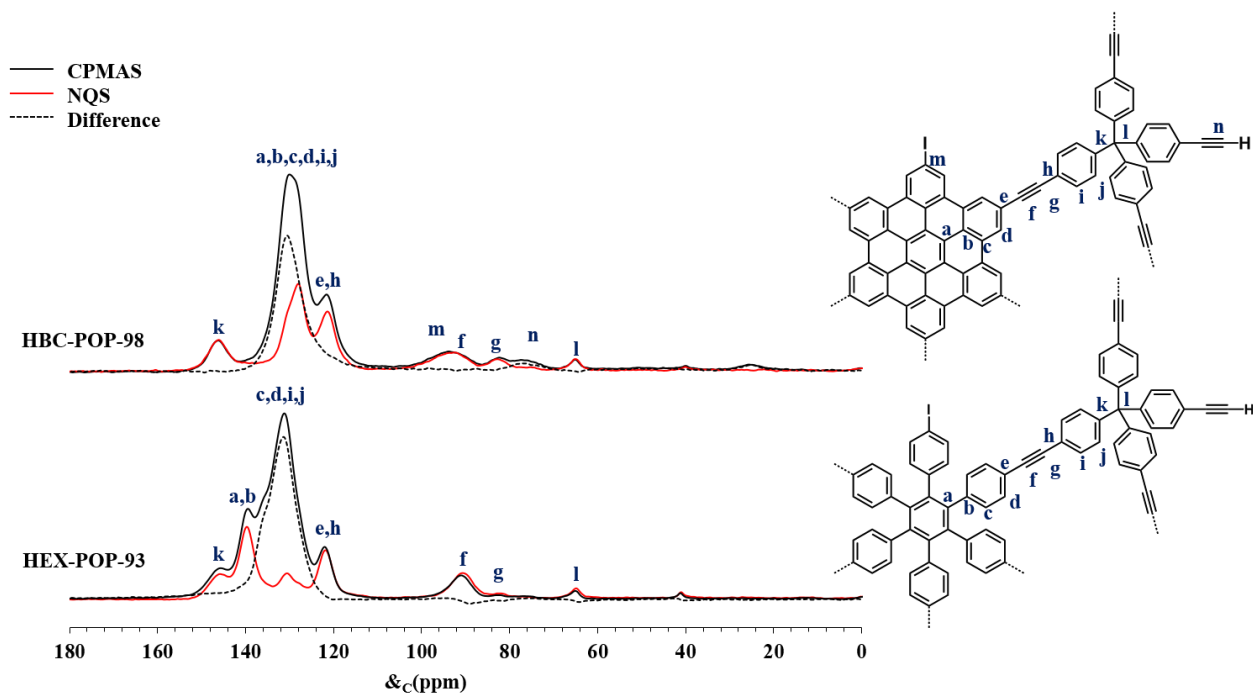


Figure 3-5. Solid state  $^{13}\text{C}$ -CPMAS and  $^{13}\text{C}$ -NQS NMR spectra

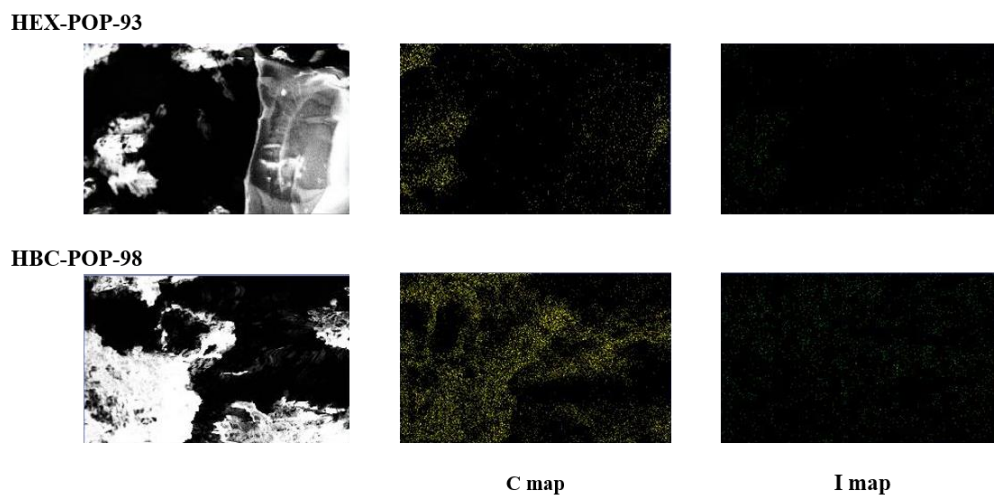


Figure 3-6. Carbon and iodine EDAX maps of HEX-POP-93 and HBC-POP-98

Table 3-1. Elemental ratios in HEX-POP-93 and HBC-POP-98 for carbon, iodine, and palladium based on EDX analysis

Sample	Weight %		
	C%	I%	Pd%
HEX-POP-93	89.90	9.50	0.60
HBC-POP-98	90.34	9.00	0.65

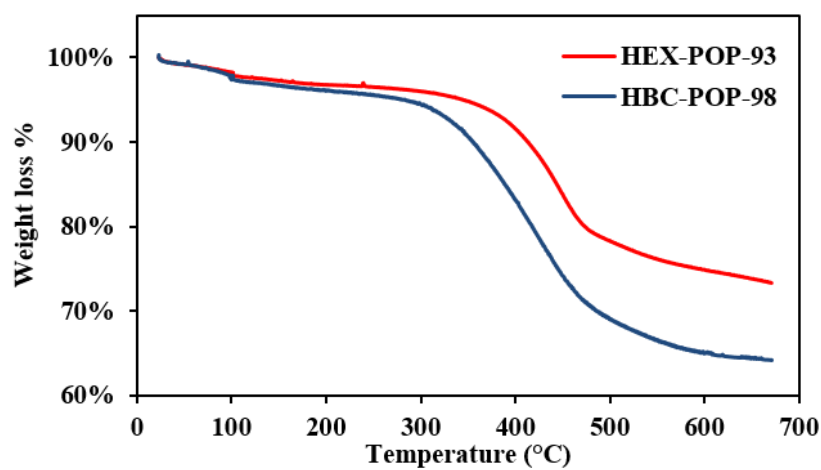


Figure 3-7. TGA curves of HEX-POP-93 and HBC-POP-98

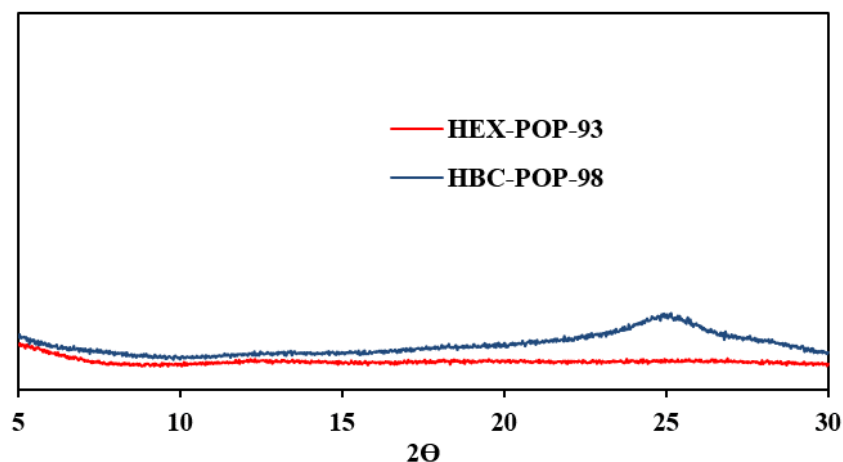


Figure 3-8. PXRD patterns of HEX-POP-93 and HBC-POP-98

### 3.4.2 Porosity measurements and gas uptake

The accessible surface areas and pore size distributions were determined for both HEX-POP-93 and HBC-POP-98 using N<sub>2</sub> adsorption measurements at 77 K. As seen in Figure 3-9, HEX-POP-93 and HBC-POP-98 have similar N<sub>2</sub> uptake capacities of 246 cm<sup>3</sup>/g and 242 cm<sup>3</sup>/g, respectively. The N<sub>2</sub> isotherms show rapid N<sub>2</sub> uptake at low relative pressures ( $P/P_0 < 0.01$ ), which is typical for microporous materials. Pore size distributions (Figure 3-9) also indicate both POPs are predominantly microporous (pore width < 2 nm), possessing two major micropore centers of approximately 1.2 nm and 1.7 nm. The Brunauer, Emmett and Teller (BET) and Langmuir surface areas for both POPs were calculated using the N<sub>2</sub> adsorption in the low-pressure range ( $P/P_0$  0.01-0.1) (Table 3-2). Both HPB and HBC POPs show moderate BET surface areas of 687 m<sup>2</sup>/g for HEX-POP-93 and 548 m<sup>2</sup>/g for HBC-POP-98. These surface areas are consistent with previously reported HEX and HBC based Sonogashira polymers.<sup>29,30,37</sup>

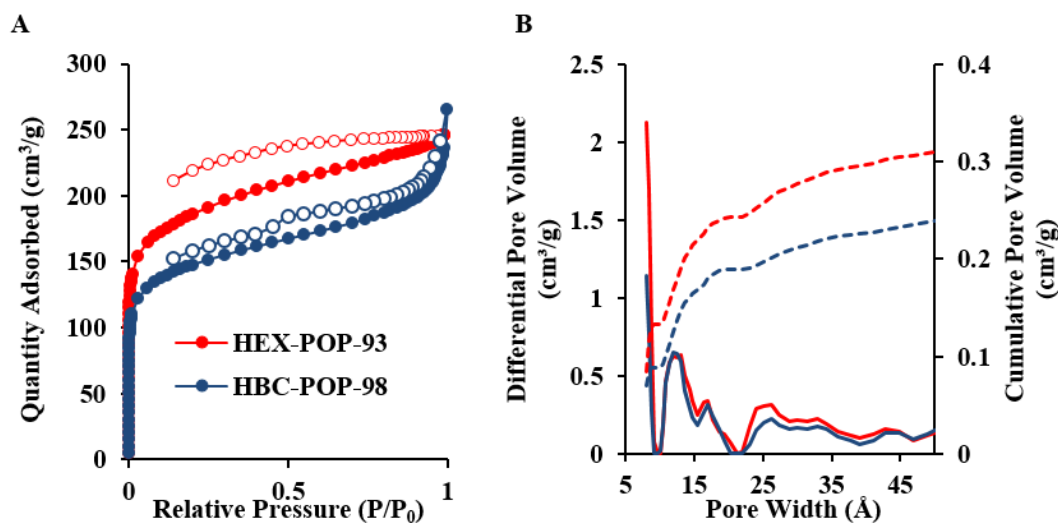


Figure 3-9. Nitrogen adsorption (solid symbols) and desorption (open symbols) isotherms at 77 K and pore size distribution (solid line) and cumulative pore volume (dash)

Table 3-2. Surface area and pore structure properties of polymers obtained by N<sub>2</sub> adsorption

Sample name	BET surface area	Langmuir	Horvath Kawazoe pore
	(m <sup>2</sup> /g)	surface area (m <sup>2</sup> /g)	volume (cm <sup>3</sup> /g)
HEX-POP-93	687	740	0.38
HBC-POP-98	548	589	0.41

The CO<sub>2</sub> adsorption isotherms for the two polymers were measured at 273 K and 298 K (Figure 3-10). The amount of CO<sub>2</sub> adsorbed continually increases with the pressure, implying that the CO<sub>2</sub> adsorption by the porous network has not reached its equilibrium or saturated state in the measured pressure range. Both POPs demonstrate similar uptake capacities of CO<sub>2</sub>. HEX-POP-93 and HBC-POP-98 show CO<sub>2</sub> uptake of 45 cm<sup>3</sup>/g (8.8 wt. %) and 41 cm<sup>3</sup>/g (8.0 wt. %), respectively at 273 K and 900 mmHg.

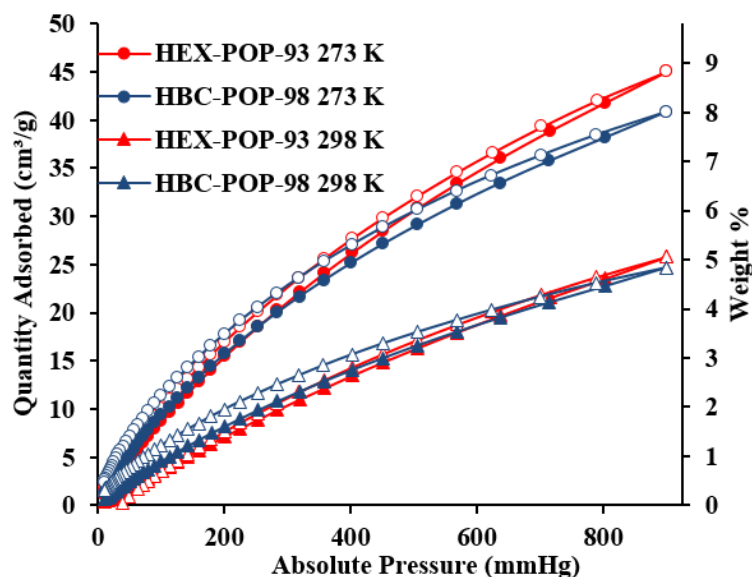


Figure 3-10. CO<sub>2</sub> adsorption-desorption isotherms at 273 K (circle) and 298 K (triangle)

### 3.4.3 Vapor adsorption measurements

In order to analyse the organic vapour adsorption properties of these two novel polymers, adsorption isotherms of benzene, toluene, cyclohexane and methanol were measured at 298 K. (Figure 3-11) The adsorption isotherm of water vapour at the same temperature was also measured for comparison. Both polymers exhibit good uptake of organic vapours while the water adsorption capacities are exceptionally low (1 % and 0.5 % for HEX-POP-93 and HBC-POP-98, respectively) (Figure 3-12, Figure 3-13).

The adsorption capacities for benzene, toluene and cyclohexane with HEX-POP-93 are 99.9, 47.1 and 25.4 wt. %, respectively (Figure 3-13). HEX-POP-93 displays remarkably high adsorption capacity for benzene that is nearly four times that of its aliphatic counterpart cyclohexane and two times that of toluene. The sorption capacity of HEX-POP-93 for benzene compares favorably with many other phenyl, biphenyl or naphthalene-based MOFs and POPs (Table 3-3). However, many of them possess higher surface areas and higher water adsorption capacities than that of HEX-

POP-93. High adsorption capacity for benzene compared to low surface area can be explained by the large amount of accessible  $\pi$ - $\pi$  interactions available between the HEX units and benzene. The adsorption capacity for toluene is less than that of benzene, probably due to the slightly larger kinetic diameter of toluene (6.1 Å) compared with benzene (5.9 Å).

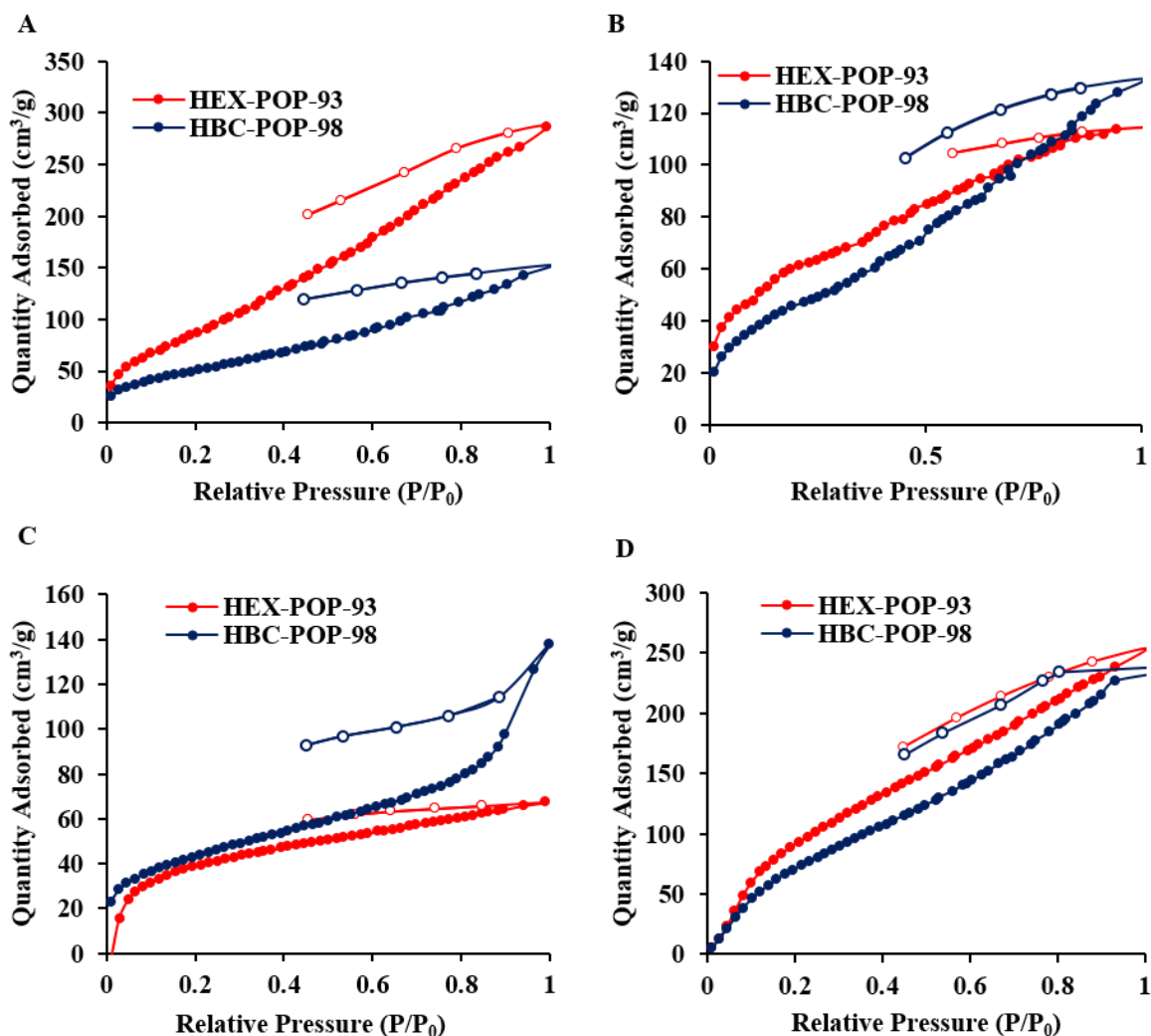


Figure 3-11. Adsorption and desorption isotherms of (A) benzene, (B) toluene, (C) cyclohexane and (D) methanol vapour for HEX-POP-93 and HBC-POP-98 at 298 K

The adsorption capacities for benzene, toluene and cyclohexane with HBC-POP-98 are 53.0, 54.6 and 51.7 wt%, respectively (Figure 3-13). The surface area of HBC-POP-98 is slightly lower than

HEX-POP-93, but the benzene adsorption capacity is nearly half. As indicated from the PXRD, HBC-POP-98 displays some long-range order, likely arising from  $\pi$ - $\pi$  interactions between HBC units. This arrangement could possibly reduce the amount of benzene adsorption in the polymer *via*  $\pi$ - $\pi$  interactions, leading to the lower observed adsorption capacity in HBC-POP-98. The pore volume of HBC-POP-98 is slightly larger than HEX-POP-93, which may account for the slightly higher adsorption of toluene and better adsorption of cyclohexane by HBC-POP-98 than that of HEX-POP-93.

Interestingly, though both the polymers have poor water uptake capacities, they have good adsorption capacities for methanol (36.2 wt% and 34.0 wt% for HEX-POP-93 and HBC POP-98, respectively). The adsorption of methanol for both is high (254 cm<sup>3</sup>/g and 238 cm<sup>3</sup>/g) and much larger than those of other organic vapors. This may be due to methanol having the smallest size among all four organic adsorbents.

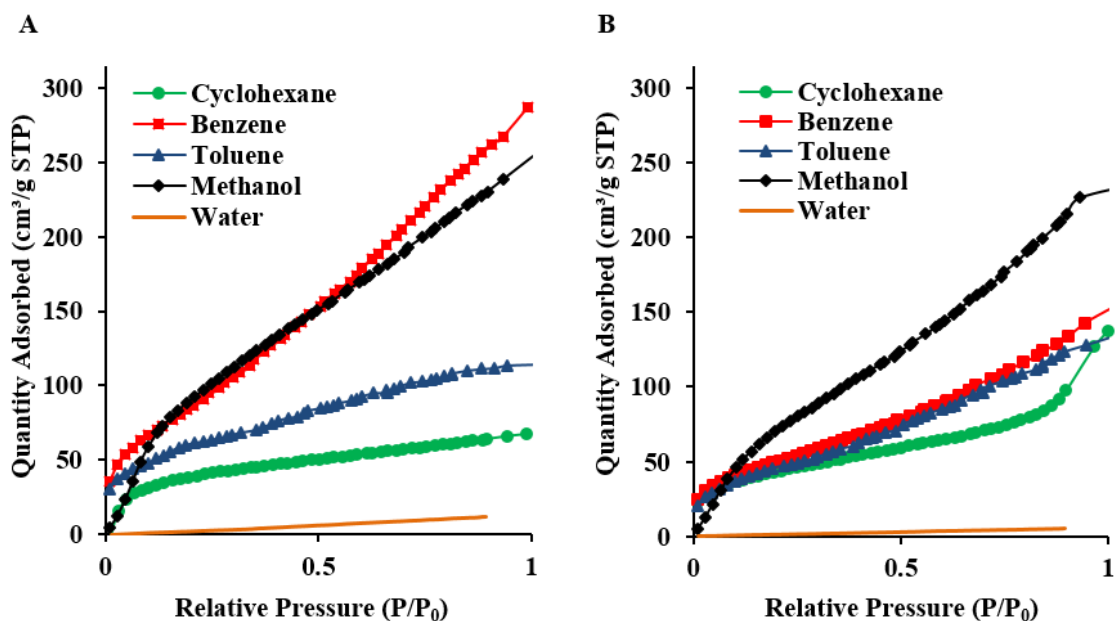


Figure 3-12. Adsorption isotherms of cyclohexane, benzene, toluene, methanol and water vapours at 298 K for (a) HEX-POP-93 and (b) HBC-POP-98

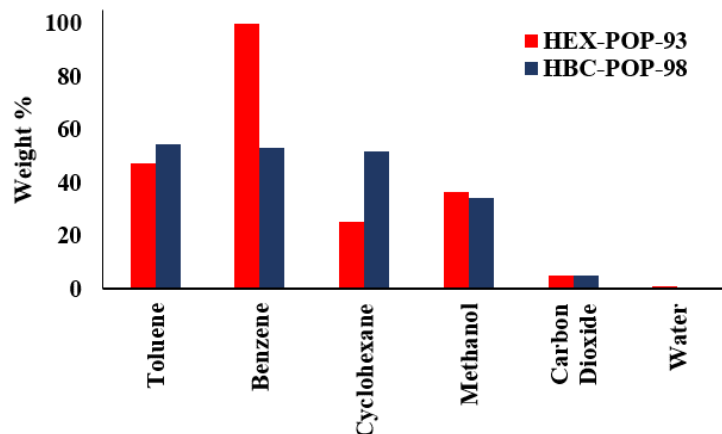


Figure 3-13. Adsorption weight percent of cyclohexane, benzene, toluene, methanol and water vapours at 298 K for HEX-POP-93 (red) and HBC-POP-98 (blue)

After each adsorption isotherm was measured, the samples were resubjected to the activation conditions (120 °C, vacuum, 12h) to remove the adsorbed solvent molecules. The adsorbed solvents could be completely removed as confirmed by measuring the mass of the sample before and after the adsorption analysis. Previous work has indicated that irreversible adsorption can potentially occur, even in cases where only physisorption is expected.<sup>48</sup> However, as the polymers are synthesized in organic solvents, we expect that if such sites were to exist in these materials, they would have become occupied during the polymerization reaction

Table 3-3. Adsorption capacities for POPs in this work and other materials

Material	BET surface area	Adsorption wt. %					Referen ce
		Benzene	Toluene	Cyclohexane	Methanol	Water	
HEX-POP-93	687	99.9	47.1	25.4	36.2	1.0	a
HBC-POP-98	548	53.0	54.6	51.7	34.0	0.5	a
MIL-101	3900	130.4 <sup>b</sup>	-	-	-	-	17



MIL-101	3980	129.1 <sup>c</sup>	109.6 <sup>c</sup>	-	-	-	18
PAF-1	5600	130.6 <sup>c</sup>	135.7 <sup>c</sup>	-	-	-	49
PAF-2	891	13.8 <sup>c</sup>	-	0.7 <sup>c</sup>	-	-	50
PAF-5	1503	128.6 <sup>c</sup>	111.4 <sup>c</sup>	-	94.9 <sup>c</sup>	-	22
PAF-11	704	87.4 <sup>c</sup>	78.0 <sup>c</sup>	-	65.4 <sup>c</sup>	3.5 <sup>c</sup>	51
SMPI-0	574.4	134.7	-	42.5	60	14.9	52
SMPI-10	112.0	104.7	-	42.8	83.4	30.4	52
CE-1	960	58.5	-	-	-	22.0	53
CE-2	588	35.1	-	-	-	6.9	53
PBI-1	62	54.4	-	-	-	32.9	54
MPI-1	1454	119.8	-	50.1	-	16.7	55
MPI-2	814	76.6	-	44.8	-	9.9	55
NPI-1	721	90.5	-	58.1	-	14.1	56
PI-ADPM	868	99.2	-	59.7	-	28.45	57
PSN-3	865	80.5	-	63.7	-	6.4	58
PSN-DA	1045	86.1	-	77.9	-		59
PCN-AD	843	98.0	-	57.4	-		60
PAN-1	925	72.6	-	52.7	-	8.4	61
PAN-2	1245	69.2	-	38.3	-	10.4	61
PBI-Ad-1	1023	98.0	-	53.6	-	-	62
PBI-Ad-2	926	76.5	-	46.3	-	-	62

<sup>a</sup> in this work, <sup>b</sup> calculate from given mmol g<sup>-1</sup> values, <sup>c</sup> calculated from given mg g<sup>-1</sup> values

### 3.5 Conclusion

In summary, we have successfully synthesized two novel porous organic polymers: HEX-POP-93 and HBC-POP-98 *via* a Sonogashira copolymerization reaction and confirmed it to be microporous by N<sub>2</sub> adsorption measurements. Both polymers possess moderate surface areas, but good organic vapour adsorption capacities. Moreover, HEX-POP-93 exhibits excellent adsorption capacity (99.9 wt. %) and preference for benzene over cyclohexane, toluene and water. HBC-POP-98 shows high adsorption capacities for benzene, toluene and cyclohexane. In contract, the water adsorption capacities were very low (<1 wt. %), making these POPs promising materials for adsorbing VOCs under practical conditions where water is present.

### 3.6 Acknowledgements

This research was carried out with support from the University of Texas at Dallas, and the American Chemical Society Petroleum Research Fund (52906-DNI10). We would like to acknowledge Dr. Gregory McCandless for assistance obtaining PXRD, Sahila Perananthan for assistance with thermal analysis, and Dr. William Hockaday for assistance with NQS analysis.

### 3.7 References

1. Salthammer, T. Emissions of Volatile Organic Compounds from Products and Materials in Indoor Environments. In *Indoor Air Pollution; The Handbook of Environmental Chemistry Series*; Pluschke, P., Ed.; Springer Berlin Heidelberg, 2004; *4F*, pp 113-127.
2. The original list of hazardous air pollutants. <http://www3.epa.gov/airtoxics/188polls.html> (accessed 11/13, 2015).
3. Bolden, A. L.; Kwiatkowski, C. F.; Colborn, T. New Look at BTEX: Are Ambient Levels a Problem? *Environ. Sci. Technol.* **2015**, *49*, 5261-5276.

4. Atkinson, R. Atmospheric chemistry of VOCs and NOx. *Atmos. Environ.* **2000**, *34*, 2063-2101.
5. Perez-Rial, D.; Lopez-Mahia, P.; Muniategui-Lorenzo, S.; Prada-Rodriguez, D. Temporal distribution, behaviour and reactivities of BTEX compounds in a suburban Atlantic area during a year. *J. Environ. Monit.* **2009**, *11*, 1216-1225.
6. Kampa, M.; Castanas, E. Human health effects of air pollution. *Environ. Pollut.* **2008**, *151*, 362-367.
7. Kim, K.; Jahan, S. A.; Kabir, E. A review on human health perspective of air pollution with respect to allergies and asthma. *Environ. Int.* **2013**, *59*, 41-52.
8. Wu, C.; Wu, S.; Wu, Y.; Cullen, A. C.; Larson, T. V.; Williamson, J.; Liu, L. J. Cancer risk assessment of selected hazardous air pollutants in Seattle. *Environ. Int.* **2009**, *35*, 516-522.
9. Mullaugh, K. M.; Hamilton, J. M.; Avery, G. B.; Felix, J. D.; Mead, R. N.; Willey, J. D.; Kieber, R. J. Temporal and spatial variability of trace volatile organic compounds in rainwater. *Chemosphere* **2015**, *134*, 203-209.
10. Volkamer, R.; Jimenez, J. L.; San Martini, F.; Dzepina, K.; Zhang, Q.; Salcedo, D.; Molina, L. T.; Worsnop, D. R.; Molina, M. J. Secondary organic aerosol formation from anthropogenic air pollution: Rapid and higher than expected. *Geophys. Res. Lett.* **2006**, *33*, L17811.
11. Hallquist, M.; Wenger, J. C.; Baltensperger, U.; Rudich, Y.; Simpson, D.; Claeys, M.; Dommen, J.; Donahue, N. M.; George, C.; Goldstein, A. H.; Hamilton, J. F.; Herrmann, H.; Hoffmann, T.; Iinuma, Y.; Jang, M.; Jenkin, M. E.; Jimenez, J. L.; Kiendler-Scharr, A.; Maenhaut, W.; McFiggans, G.; Mentel, T. F.; Monod, A.; Prévôt, A. S. H.; Seinfeld, J. H.; Surratt, J. D.; Szmigielski, R.; Wildt, J. The formation, properties and impact of secondary organic aerosol: current and emerging issues. *Atmos. Chem. Phys.* **2009**, *9*, 5155-5236.
12. Khan, F. I.; Kr. Ghoshal, A. Removal of Volatile Organic Compounds from polluted air. *J. Loss Prev. Process Ind.* **2000**, *13*, 527-545.
13. Ojala, S.; Koivikko, N.; Laitinen, T.; Mouammine, A.; Seelam, P.; Laassiri, S.; Ainassaari, K.; Brahmi, R.; Keiski, R. Utilization of Volatile Organic Compounds as an Alternative for Destructive Abatement. *Catalysts* **2015**, *5*, 1092-1151.
14. Ramos, M. E.; Bonelli, P. R.; Cukierman, A. L.; Ribeiro Carrott, M. M.; Carrott, P. J. Adsorption of volatile organic compounds onto activated carbon cloths derived from a novel regenerated cellulosic precursor. *J. Hazard. Mater.* **2010**, *177*, 175-182.

15. Baur, G.; Yuranov, I.; Renken, A.; Kiwi-Minsker, L. Activated carbon fibers for efficient VOC removal from diluted streams: the role of surface morphology. *Adsorption* **2015**, *21*, 479-488.
16. Das, D.; Gaur, V.; Verma, N. Removal of volatile organic compound by activated carbon fiber. *Carbon* **2004**, *42*, 2949-2962.
17. Jhung, S.; Lee, J. -H.; Yoon, J.; Serre, C.; Férey, G.; Chang, J. -S. Microwave Synthesis of Chromium Terephthalate MIL-101 and Its Benzene Sorption Ability. *Adv. Mater.* **2007**, *19*, 121-124.
18. Yang, K.; Sun, Q.; Xue, F.; Lin, D. Adsorption of volatile organic compounds by metal-organic frameworks MIL-101: Influence of molecular size and shape. *J. Hazard. Mater.* **2011**, *195*, 124-131.
19. Cheng, J.; Wang, P.; Ma, J.; Liu, Q.; Dong, Y. A nanoporous Ag(i)-MOF showing unique selective adsorption of benzene among its organic analogues. *Chem. Commun.* **2014**, *50*, 13672-13675.
20. Tan, D.; Fan, W.; Xiong, W.; Sun, H.; Li, A.; Deng, W.; Meng, C. Study on adsorption performance of conjugated microporous polymers for hydrogen and organic solvents: The role of pore volume. *Eur. Poly. J.* **2012**, *48*, 705-711.
21. Zhang, L.; Song, X.; Wu, J.; Long, C.; Li, A.; Zhang, Q. Preparation and characterization of micro-mesoporous hypercrosslinked polymeric adsorbent and its application for the removal of VOCs. *Chem. Eng. J.* **2012**, *192*, 8-12.
22. Ren, H.; Ben, T.; Sun, F.; Guo, M.; Jing, X.; Ma, H.; Cai, K.; Qiu, S.; Zhu, G. Synthesis of a porous aromatic framework for adsorbing organic pollutants application. *J. Mater. Chem.* **2011**, *21*, 10348-10353.
23. Dawson, R.; Cooper, A. I.; Adams, D. J. Nanoporous organic polymer networks. *Prog. Poly. Sci.* **2012**, *37*, 530-563.
24. Xu, Y.; Jin, S.; Xu, H.; Nagai, A.; Jiang, D. Conjugated microporous polymers: design, synthesis and application. *Chem. Soc. Rev.* **2013**, *42*, 8012-8031.
25. Liu, Q.; Tang, Z.; Wu, M.; Zhou, Z. Design, preparation and application of conjugated microporous polymers. *Polym. Int.* **2014**, *63*, 381-392.
26. Ben, T.; Qiu, S. Porous aromatic frameworks: Synthesis, structure and functions. *Cryst. Eng. Comm.* **2013**, *15*, 17-26.
27. McKeown, N. B. Polymers of Intrinsic Microporosity, *ISRN Mater. Sci.* **2012**, 16.

28. Byun, Y.; Coskun, A. Bottom-up Approach for the Synthesis of a Three-Dimensional Nanoporous Graphene Nanoribbon Framework and Its Gas Sorption Properties. *Chem. Mater.* **2015**, *27*, 2576-2583.
29. Thompson, C. M.; Li, F.; Smaldone, R. A. Synthesis and sorption properties of hexa-(peri)-hexabenzocoronene-based porous organic polymers. *Chem. Commun.* **2014**, *50*, 6171-6173.
30. Thompson, C. M.; McCandless, G. T.; Wijenayake, S. N.; Alfarawati, O.; Jahangiri, M.; Kokash, A.; Tran, Z.; Smaldone, R. A. Substituent Effects on the Gas Sorption and Selectivity Properties of Hexaphenylbenzene and Hexabenzocoronene Based Porous Polymers. *Macromolecules* **2014**, *47*, 8645-8652.
31. Alahakoon, S. B.; Thompson, C. M.; Nguyen, A. X.; Occhialini, G.; McCandless, G. T.; Smaldone, R. A. An azine-linked hexaphenylbenzene based covalent organic framework. *Chem. Commun.* **2016**, *52*, 2843-2845.
32. Wang, Z.; Dötz, F.; Enkelmann, V.; Müllen, K. "Double-Concave" Graphene: Permethoxylated Hexa-peri-hexabenzocoronene and Its Cocrystals with Hexafluorobenzene and Fullerene. *Angew. Chem. Int. Ed.* **2005**, *44*, 1247-1250.
33. Wu, J.; Baumgarten, M.; Debije, M. G.; Warman, J. M.; Müllen, K. Arylamine-Substituted Hexa-peri-hexabenzocoronenes: Facile Synthesis and Their Potential Applications as "Coaxial" Hole-Transport Materials. *Angew. Chem.* **2004**, *116*, 5445-5449.
34. Grimsdale, A. C.; Wu, J.; Mullen, K. New carbon-rich materials for electronics, lithium battery, and hydrogen storage applications. *Chem. Commun.* **2005**, 2197-2204.
35. Wang, L.; Sun, J.; Huang, Z.; Zheng, Q. Stepwise tuning of the substituent groups from mother BTB ligands to two hexaphenylbenzene based ligands for construction of diverse coordination polymers. *Cryst. Eng. Comm* **2013**, *15*, 8511-8521.
36. Chabre, Y. M.; Roy, R. Multivalent glycoconjugate syntheses and applications using aromatic scaffolds. *Chem. Soc. Rev.* **2013**, *42*, 4657-4708.
37. Chen, Q.; Luo, M.; Wang, T.; Wang, J.; Zhou, D.; Han, Y.; Zhang, C.; Yan, C.; Han, B. Porous Organic Polymers Based on Propeller-Like Hexaphenylbenzene Building Units. *Macromolecules* **2011**, *44*, 5573-5577.
38. Short, R.; Carta, M.; Bezzu, C. G.; Fritsch, D.; Kariuki, B. M.; McKeown, N. B. Hexaphenylbenzene-based polymers of intrinsic microporosity. *Chem. Commun.* **2011**, *47*, 6822-6824.

39. Carta, M.; Bernardo, P.; Clarizia, G.; Jansen, J. C.; McKeown, N. B. Gas Permeability of Hexaphenylbenzene Based Polymers of Intrinsic Microporosity. *Macromolecules* **2014**, *47*, 8320-8327.
40. Zhang, C.; Peng, L.; Li, B.; Liu, Y.; Zhu, P.; Wang, Z.; Zhan, D.; Tan, B.; Yang, X.; Xu, H. Organic microporous polymer from a hexaphenylbenzene based triptycene monomer: synthesis and its gas storage properties. *Polym. Chem.* **2013**, *4*, 3663-3666.
41. Dalapati, S.; Addicoat, M.; Jin, S.; Sakurai, T.; Gao, J.; Xu, H.; Irle, S.; Seki, S.; Jiang, D. Rational design of crystalline supermicroporous covalent organic frameworks with triangular topologies. *Nat. Commun.* **2015**, *6*.
42. Nguyen, P. T. K.; Nguyen, H. T. D.; Pham, H. Q.; Kim, J.; Cordova, K. E.; Furukawa, H. Synthesis and Selective CO<sub>2</sub> Capture Properties of a Series of Hexatopic Linker-Based Metal-Organic Frameworks. *Inorg. Chem.* **2015**, *54*, 10065-10072.
43. Pandey, P.; Farha, O. K.; Spokoyny, A. M.; Mirkin, C. A.; Kanatzidis, M. G.; Hupp, J. T.; Nguyen, S. T. A "click-based" porous organic polymer from tetrahedral building blocks. *J. Mater. Chem.* **2011**, *21*, 1700-1703.
44. Hirose, T.; Miyazaki, Y.; Watabe, M.; Akimoto, S.; Tachikawa, T.; Kodama, K.; Yasutake, M. Trialkylsilyl ethynyl-substituted triphenylenes and hexabenzocoronenes: highly soluble liquid crystalline materials and their hole transport abilities. *Tetrahedron* **2015**, *71*, 4714-4721.
45. Johnson, J. R.; Grummitt, O. Tetraphenylcyclopentadienone. *Org. Synth.* **1943**, *23*, 92.
46. Fieser, L. F. Hexaphenylbenzene. *Org. Synth.* **1966**, *46*, 44.
47. Bunz, U. H. F.; Seehafer, K.; Geyer, F. L.; Bender, M.; Braun, I.; Smarsly, E.; Freudenberg, J. Porous Polymers Based on Aryleneethynylene Building Blocks. *Macromol. Rapid Commun.* **2014**, *35*, 1466-1496.
48. Planchais, A.; Devautour-Vinot, S.; Giret, S.; Salles, F.; Trens, P.; Fateeva, A.; Devic, T.; Yot, P.; Serre, C.; Ramsahye, N.; Maurin, G. Adsorption of Benzene in the Cation-Containing MOFs MIL-141. *J. Phys. Chem. C* **2013**, *117*, 19393-19401.
49. Ben, T.; Ren, H.; Ma, S.; Cao, D.; Lan, J.; Jing, X.; Wang, W.; Xu, J.; Deng, F.; Simmons, J.; Qiu, S.; Zhu, G. Targeted Synthesis of a Porous Aromatic Framework with High Stability and Exceptionally High Surface Area. *Angew. Chem. Int. Ed.* **2009**, *48*, 9457-9460.
50. Ren, H.; Ben, T.; Wang, E.; Jing, X.; Xue, M.; Liu, B.; Cui, Y.; Qiu, S.; Zhu, G. Targeted synthesis of a 3D porous aromatic framework for selective sorption of benzene. *Chem. Commun.* **2010**, *46*, 291-293.

51. Yuan, Y.; Sun, F.; Ren, H.; Jing, X.; Wang, W.; Ma, H.; Zhao, H.; Zhu, G. Targeted synthesis of a porous aromatic framework with a high adsorption capacity for organic molecules. *J. Mater. Chem.* **2011**, *21*, 13498-13502.
52. Yang, Y.; Zhang, Q.; Zhang, Z.; Zhang, S. Functional microporous polyimides based on sulfonated binaphthalene dianhydride for uptake and separation of carbon dioxide and vapors. *J. Mater. Chem. A* **2013**, *1*, 10368-10374.
53. Yu, H.; Shen, C.; Tian, M.; Qu, J.; Wang, Z. Microporous Cyanate Resins: Synthesis, Porous Structure, and Correlations with Gas and Vapor Adsorptions. *Macromolecules* **2012**, *45*, 5140-5150.
54. Yu, H.; Tian, M.; Shen, C.; Wang, Z. Facile preparation of porous polybenzimidazole networks and adsorption behavior of CO<sub>2</sub> gas, organic and water vapors. *Polym. Chem.* **2013**, *4*, 961-968.
55. Li, G.; Wang, Z. Microporous Polyimides with Uniform Pores for Adsorption and Separation of CO<sub>2</sub> Gas and Organic Vapors. *Macromolecules* **2013**, *46*, 3058-3066.
56. Li, G.; Wang, Z. Naphthalene-Based Microporous Polyimides: Adsorption Behavior of CO<sub>2</sub> and Toxic Organic Vapors and Their Separation from Other Gases. *J. Phys. Chem. C* **2013**, *117*, 24428-24437.
57. Shen, C.; Bao, Y.; Wang, Z. Tetraphenyladamantane-based microporous polyimide for adsorption of carbon dioxide, hydrogen, organic and water vapors. *Chem. Commun.* **2013**, *49*, 3321-3323.
58. Li, G.; Zhang, B.; Wang, Z. Microporous Poly(Schiff Base) Constructed from Tetraphenyladamantane Units for Adsorption of Gases and Organic Vapors. *Macromol. Rapid Commun.* **2014**, *35*, 971-975.
59. Li, G.; Zhang, B.; Yan, J.; Wang, Z. Micro- and mesoporous poly(Schiff-base)s constructed from different building blocks and their adsorption behaviors towards organic vapors and CO<sub>2</sub> gas. *J. Mater. Chem. A* **2014**, *2*, 18881-18888.
60. Shen, C.; Yu, H.; Wang, Z. Synthesis of 1,3,5,7-tetrakis(4-cyanatophenyl)adamantane and its microporous polycyanurate network for adsorption of organic vapors, hydrogen and carbon dioxide. *Chem. Commun.* **2014**, *50*, 11238-11241.
61. Li, G.; Zhang, B.; Yan, J.; Wang, Z. Tetraphenyladamantane-Based Polyaminals for Highly Efficient Captures of CO<sub>2</sub> and Organic Vapors. *Macromolecules* **2014**, *47*, 6664-6670.

62. Zhang, B.; Li, G.; Yan, J.; Wang, Z. Tetraphenyladamantane-Based Microporous Polybenzimidazoles for Adsorption of Carbon Dioxide, Hydrogen, and Organic Vapors. *J. Phys. Chem. C* **2015**, *119*, 13080-13087.



**CHAPTER 4**

**HYPERCROSSLINKED NANOGRAFENE BASED POROUS POLYMERS VIA POST  
SYNTHETIC MODIFICATIONS**

Authors: Arosha A. K. Karunathilake, Christina M. Thompson, Amy X. Nguyen, Quang N. To,  
Ivana Q. Le and Ronald A. Smaldone

Department of Chemistry and Biochemistry, The University of Texas at Dallas,  
800 W Campbell Rd, Richardson, Texas, 75080

## 4.1 Abstract

Porous graphene possesses the combined properties of graphene and nanoporous materials making it an emerging material of interest for gas and energy storage applications. Expanded polycyclic aromatic hydrocarbons (PAHs), such as hexabenzocoronene (HBC) have gained renewed attention since the discovery of graphene, as they also possess some of the high stability and electrical conductivity of graphene. However, the synthesis of porous materials with PAHs is challenging due to their low solubility and reactivity. Hence, we have designed a bottom up synthesis of nanographene (NG) based porous polymers *via* the post-synthetic cyclodehydrogenation of highly porous hexaphenylbenzene (HEX) based POPs. The resulting NG based polymers possess good CO<sub>2</sub> adsorption capacities (22 wt. % for HEX-SO-DDQ-5d).

## 4.2 Introduction

Porous graphene is considered a promising material because of its high surface area, mechanical strength, excellent electrical conductivity, and good thermal stability making it a highly promising material not only for gas and energy storage<sup>1,2</sup> but also for energy conversion applications such as lithium batteries, supercapacitors, and dye-sensitized solar cells.<sup>3</sup> Strong  $\pi$ - $\pi$  stacking and Van der Waals interactions between sheets limits available surface area of graphene.<sup>4</sup> Hence, porous graphene should have designed to overcome these  $\pi$ - $\pi$  stacking to gain higher surface area. Today porous graphene are obtained mainly *via* templet-assisted methods such as aryl-aryl coupling of phenylene or non-templet methods such as by electron or helium ion beam irradiation. However, the controlled synthesis of porous graphene and other carbonaceous materials is challenging and

herein, stepwise bottom-up chemical synthesis emerged as a solution to the problem of structure control.<sup>2,5</sup>

Polycyclic aromatic hydrocarbons (PAHs) which are also sometimes referred to as nanographenes (NGs) have gained considerable attention as precursors for graphene through a bottom up synthetic approach.<sup>6</sup> Though their electronic structures differ from that of graphene due to their smaller size, they also possess high thermal and chemical stability and high charge-carrier mobility making themselves promising materials for applications in organic electronics. Hence, porous materials synthesized with PAHs such as hexa-*peri*-hexabenzocoronene (HBC) also possess high thermal stability, highly conductivity and better CO<sub>2</sub> and volatile organic compounds (VOCs) adsorption.<sup>7-10</sup> HBC (Figure 4-1) is considered to be the smallest nanographene.<sup>6</sup> However, incorporation of HBC in to porous materials is challenging due to its low solubility driven by strong  $\pi$ - $\pi$  stacking. HBC based porous materials also possess  $\pi$ - $\pi$  stacking limiting the available surface area for gas and VOCs adsorption *via* van der Waals interactions.<sup>7-10</sup>

On the other hand, hexaphenylbenzene (HEX), the precursor of HBC (Figure 4-1) has a propeller shape, soluble in variety of solvents and is easily functionalized.<sup>8-10</sup> In general, HBC can be synthesized through the oxidative cyclodehydrogenation, specifically a Scholl oxidation (SO), of HEX (Figure 4-1).<sup>11</sup> Herein, we demonstrate a bottom up synthetic approach for the synthesis of HBC or NG based porous organic polymers (POPs) *via* post synthetic cyclodehydrogenation of high surface area HEX based POPs to avoid the inherent  $\pi$ - $\pi$  stacking and to possess high surface area and high gas adsorption.

In recent years the synthesis of hypercrosslinked POPs (HCPs) using the Friedel–Crafts (FC) reaction has been reported as an efficient, economical and convenient strategy for making porous

materials.<sup>12</sup> Here aromatic monomers are polymerized with an external crosslinker such as formaldehyde dimethylacetal (FDA), in the presence of equivalent amounts of anhydrous  $\text{FeCl}_3$ .<sup>12,13</sup> In the resulting polymer structure the aromatic monomers are interconnected *via* methylene groups. Very recently, the direct coupling of aromatic monomers *via* Scholl oxidation (SO) in the presence of  $\text{AlCl}_3$  results in the formation of a porous aromatic framework (PAF) was reported as the most inexpensive method to synthesize POPs as it does not require an external cross linker.<sup>14,15</sup> Thus, these two approaches are low-cost and avoid the use of noble metal catalysts, and the need for monomers with a specific polymerizable functional group. Hence, we select these methods for synthesizing initial HEX based hydrocarbon porous polymers.

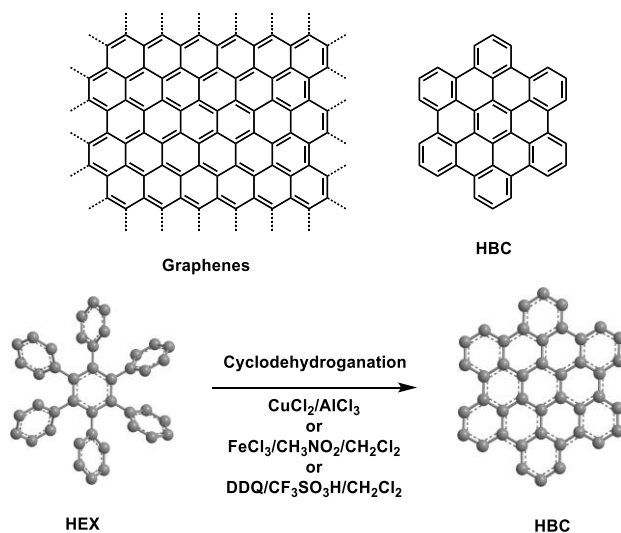


Figure 4-1. Structures of graphene, hexabenzocoronene (HBC) and hexaphenylbenzene (HEX) and synthesis of HBC via cyclodehydrogenation of HEX

Herein, a HEX based POP (HEX-FC) was synthesized *via* FC reaction in the presence of  $\text{FeCl}_3$  (6 equiv) and formaldehyde dimethyl acetal (FDA) (6 equiv) to obtain a high surface area. It has found that HBC does not undergo FC polymerization (Figure 4-2, **Method 1**). Also, polymerization reaction of HEX with excess of  $\text{FeCl}_3$  (60 equiv) in the presence of FDA for the

consecutive polymerization and cyclodehydrogenation also resulted only a low porosity (Figure 4-2, **Method 2**). Then, cyclodehydrogenation of HEX-FC with  $\text{FeCl}_3/\text{CH}_3\text{NO}_2$  or with  $\text{DDQ}/\text{CF}_3\text{SO}_3\text{H}$  for post polymerized SO (Figure 4-2, **Method 3 and 4**) was thus studied as a method of obtaining NG based porous system. The second HEX based conjugated POP synthesized based on direct SO of HEX (HEX-SO) was also subjected to post synthetic SO with  $\text{DDQ}/\text{CF}_3\text{SO}_3\text{H}$  to and post synthetically cyclodehydrogenated to obtained a NG based conjugated porous system (Figure 4-3).

Post polymerized cyclodehydrogenation has previously been used for other systems such as synthesis of graphene nano ribbon (GNRs)<sup>16-23</sup> and GNR based porous systems.<sup>5,24</sup> To the best of our knowledge this is the first report on using post polymerized cyclodehydrogenation for the synthesis of HBC-based porous polymers

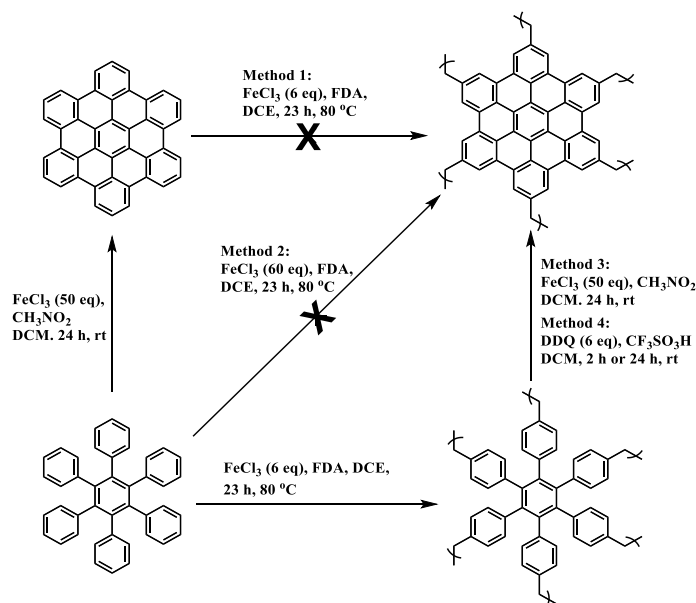


Figure 4-2. Different approaches for the synthesis of nanographene based POP via Friedel Crafts polymerization

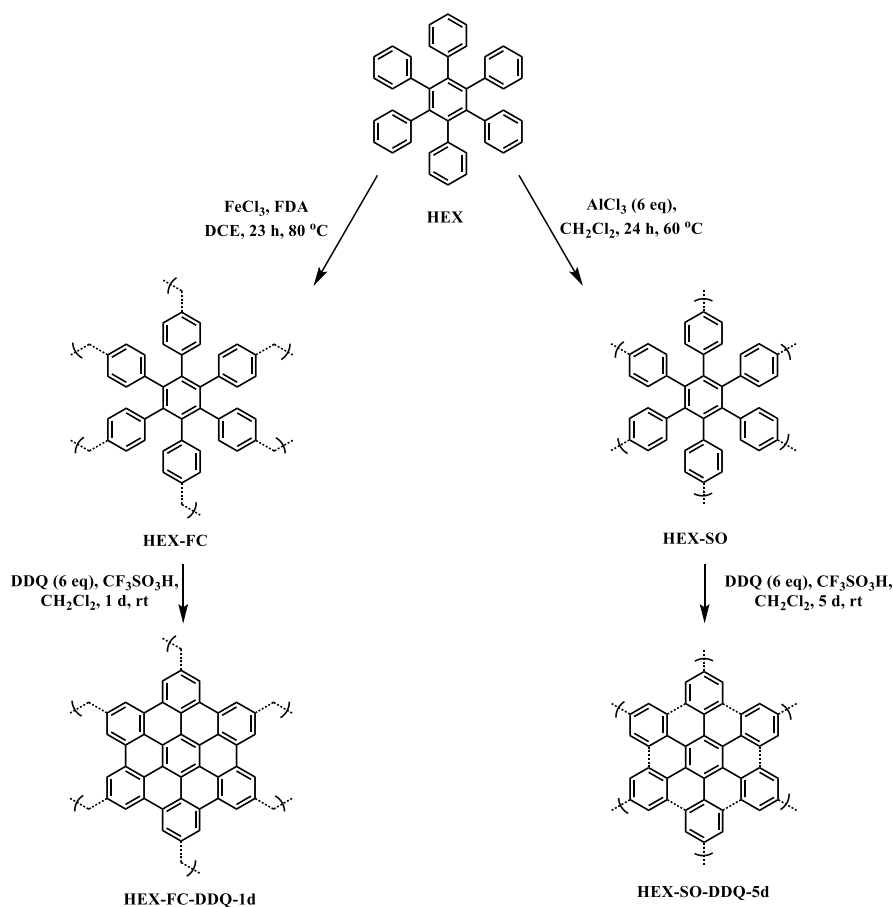


Figure 4-3. Synthesis of HEX-FC, HEX-SO and nanographene based POPs of each via cyclodehydrogenation

## 4.3 Experimental

### 4.3.1 Materials and methods

All reagents were purchased from commercial suppliers (Sigma-Aldrich and Fisher Scientific) and used as received. Low-pressure gas adsorption experiments (up to 760 torr) were carried out on a Micromeritics ASAP 2020 analyzer. Ultrahigh purity grade  $\text{N}_2$ ,  $\text{CO}_2$  and  $\text{CH}_4$  were obtained from Airgas Corporation. Samples were de-gassed under dynamic vacuum for 12 h at  $120^\circ\text{C}$  prior to each measurement.  $\text{N}_2$  isotherms were measured using a liquid nitrogen bath (77 K).  $\text{CO}_2$  was

measured using a room temperature water bath (298 K) and an ice water bath (273 K). Pore size distributions were calculated from the adsorption branch with the nonlocal density function theory (NLDFT) carbon slit-pore model in the Micromeritics software package. Raman analysis were performed on DXR Raman microscope from Thermo Scientific with a 532 nm laser. Fourier transform infrared (FT-IR) spectra were taken on Agilent Technology Carry 600 series FTIR spectrometer with a smart orbit diamond attenuated total reflectance (ATR) cell. The thermogravimetric analyses (TGA) were performed using a TA Instrument SDT Q600 Analyzer under nitrogen atmosphere with a heating rate of 10 °C min<sup>-1</sup> from 30-900 °C. Powder X-ray diffraction (PXRD) of polymers was carried out on a Bruker D8 Advance diffractometer with a sealed tube radiation source (Cu K $\alpha$ ,  $\lambda$  = 1.54184 Å), a no back-ground sample holder, and a Lynxeye XE detector. (SEM) images acquired on a Zeiss SUPRA40 SEM instrument. The samples were prepared on 15 mm aluminum stubs using double-sided adhesive copper tapes. Matrix-assisted laser desorption/ionization (MALDI) was performed on Shimadzu Biotech AXIMA Confidence MALDI-TOF Mass Spectrometer.

#### 4.3.2 Monomer synthesis

HEX and HBC was synthesized based on previously reported methods (Figure 4-4)<sup>25-27</sup>

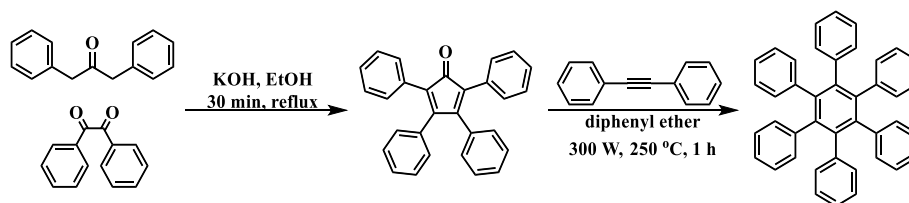


Figure 4-4. Synthesis of Hexaphenylbenzene

### 4.3.3 Polymer Synthesis

**HEX-FC:** To a round bottomed flask with HEX (53.5 mg, 0.1 mmol) FDA (52.9  $\mu$ L, 0.06 mmol) in 1,2-dichloroethane (DCE, 4 mL), anhydrous ferric chloride (97.3 mg, 0.6 mmol) was added. The resulting mixture was heated at 80 °C for 23 h under N<sub>2</sub> atmosphere. After cooling, the solid product was filtered and washed with methanol (100 mL) and dichloromethane (100 mL) with sonicating twice with each (20 mL) for 20 min until the filtrate was colorless, further purified by Soxhlet with methanol for 16 h, washed with acetone (100 mL) and dried. The polymer material was obtained as a light brown solid (45 mg, 79 %)

**HEX-SO:** To a round bottomed flask with HEX (300 mg, 0.56 mmol) in dichloromethane (DCM, 10 mL) AlCl<sub>3</sub> (449 mg, 3.37 mmol) was added. The resulting mixture was heated at 60 °C for 24 h under N<sub>2</sub> atmosphere. After cooling, the solid product was filtered and washed with methanol (100 mL) and dichloromethane (100 mL) with sonicating twice with each (20 mL) for 20 min until the filtrate was colorless, further purified by Soxhlet with methanol for 16 h, washed with acetone (100 mL) and dried. The polymer material was obtained as a pale yellow solid (240 mg, 81%)

**Method 1:** To a round bottomed flask with HBC (52.3 mg, 0.1 mmol) and FDA (52.9  $\mu$ L, 0.06 mmol) in 1,2-dichloroethane (DCE, 4 mL), anhydrous ferric chloride (97.3 mg, 0.6 mmol) was added. The resulting mixture was heated at 80 °C for 23 h under N<sub>2</sub> atmosphere. After cooling, the solid product was filtered and washed with methanol (100 mL) and dichloromethane (100 mL) with sonicating twice with each (20 mL) for 20 min until the filtrate was colorless, further purified by Soxhlet with methanol for 16 h, washed with acetone (100 mL) and dried. The polymer material was obtained as a light brown solid (24 mg, 43%).



**Method 2:** To a round bottomed flask with HEX (53.4 mg, 0.1 mmol) and FDA (52.9  $\mu$ L, 0.06 mmol) in 1,2-dichloroethane (DCE, 4 mL), anhydrous ferric chloride (973.2 mg, 6 mmol) was added. The resulting mixture was heated at 80  $^{\circ}$ C for 23 h under N<sub>2</sub> atmosphere. After cooling, the solid product was filtered and washed with methanol (100 mL) and dichloromethane (100 mL) with sonicating twice with each (20 mL) for 20 min until the filtrate was colorless, further purified by Soxhlet with methanol for 16 h, washed with acetone (100 mL) and dried. The polymer material was obtained as a light brown solid (47 mg, 84%).

**Method 3:** To a round bottomed flask with HEX-FC (50 mg) in dichloromethane (DCM, 25 mL), FeCl<sub>3</sub> (0.75 mg, 4.67 mmol) in nitromethane (3 mL) was added. The resulting mixture was stirred at room temperature for 24 h under N<sub>2</sub> atmosphere. The solid product was filtered and washed with methanol (100 mL) and dichloromethane (100 mL) sonicated twice with each (20 mL) for 20 min until the filtrate was colorless, further purified by Soxhlet with methanol for 16 h, washed with acetone (100 mL) and dried. The polymer material was obtained as brown solid (HEX-FC-FeCl<sub>3</sub>, 41 mg, 73%).

**Method 4:** To a round bottomed flask HEX-FC or HEX-SO (50 mg) in dichloromethane (DCM, 20 mL) DDQ (155 mg) and CF<sub>3</sub>SO<sub>3</sub>H (50  $\mu$ L) were added. The resulting mixtures were stirred at room temperature for 2 h and 24 h for HEX-FC and 24 h or 5 days for HEX-SO under N<sub>2</sub> atmosphere. Reactions were quenched with sat. K<sub>2</sub>CO<sub>3</sub> solution. The solid products were filtered and washed with water (100 mL) until the filtrate is neutral and then with methanol (100 mL) and dichloromethane (100 mL), sonicated twice with each (20 mL) for 20 min until the filtrate was colorless, further purified by soxhlet with methanol for 16 h, washed with acetone (100 mL) and dried. The polymer materials were obtained as a dark brown and reddish brown solid respectively

for HEX-FC-DDQs (HEX-FC-DDQ-2h, 40 mg, 71% and HEX-FC-DDQ-1d, 30 mg, 54%) and HEX-SO-DDQs (HEX-SO-DDQ-1d, 25 mg, 48% and HEX-SO-DDQ-5d, 38 mg, 73%).

## 4.4 Result and Discussion

### 4.4.1 Synthesis and characterization

Raman spectra of product were performed to confirmed the cyclodehydrogenation (Figure 4-5). HEX-FC-DDQ-1d clearly shows first-order D band (disorder band) and G band (graphite band) respectively at  $\sim 1330$  and  $\sim 1600\text{ cm}^{-1}$  that are standard for graphene-based materials. A broad 2D band was also obtained in  $2500\text{--}3000\text{ cm}^{-1}$  range. Bands are qualitatively consistent to the Raman spectra of previously reported bottom-up synthesized GNRs.<sup>16-23</sup> Peaks were fitted using a Lorentzian equation and the ratios of the integrated intensity of D band to G band ( $I_D/I_G$ ) were calculated to quantitate the extend of reaction (Table 4-1). HEX-FC-DDQ-2h, HEX-FC-FeCl<sub>3</sub> and products from **method 2** also shows a Raman D and G band but  $I_D/I_G$  ratios are higher than that of HEX-FC-DDQ-1d. In the product from **method 2**, D band is more intense than G band. HEX-FC or product from **method 1** does not show the D or G bands. Thus, it indicates that cyclodehydrogenation on HEX-FC is most efficient using the DDQ oxidation conditions for 24 h. Similarly, Raman spectra of both HEX-SO-DDQ-1d and HEX-SO-DDQ-5d shows the D and G bands with low  $I_D/I_G$  ratios (1.46 and 0.86, respectively) while the initial HEX-SO does not. The efficiency of the cyclodehydrogenation was also examined by FTIR spectroscopy. The FTIR spectrum of HEX-FC contains three characteristic peaks between  $3000\text{--}3100\text{ cm}^{-1}$ , that can be assigned to the aromatic C–H stretches and a strong out-of plane (*opla*) C-H deformation band at around  $700\text{ cm}^{-1}$ . These peaks are attenuated in HEX-FC-FeCl<sub>3</sub> and HEX-FC-DDQ-2h have

completely disappeared in HEX-FC-DDQ-1d (Figure 4-6). Thus, it indicates that after a 24 h reaction with DDQ/CF<sub>3</sub>SO<sub>3</sub>H, HEX-FC is successfully cyclodehydrogenated. Similarly, the three characteristic peaks at between 3000-3100 cm<sup>-1</sup> for aromatic C-H of HEX-SO is also reduced in HEX-SO-DDQ-1d while completely retarded for HEX-SO-DDQ-5d indicating complete cyclodehydrogenation. HEX-SO required a longer time than HEX-FC for complete cyclodehydrogenation. This is probably due to the higher steric effect in HEX-SO than that of HEX-FC as HEX group have directly connected each other in HEX-SO, while in HEX-FC, HEX groups are connected *via* methylene groups, where the methylene group will allow the steric flexibility for the propeller HEX to undergo a cyclodehydrogenation forming planer NG like structure. Thus, two initial polymers and HEX-FC and HEX-SO and two best photosynthetically modified polymers HEX-FC-DDQ-1d and HEX-SO-DDQ-5d were selected for future studies.

Thus, two initial polymers (HEX-FC and HEX-SO) and two best post-synthetically modified polymers (HEX-FC-DDQ-1d and HEX-SO-DDQ-5d) were selected for future studies. Powder X-ray diffraction (PXRD) indicates all the polymers are amorphous in nature. (Figure 4-7). The cyclodehydrogenated polymers do not display any broad peaks at ~26° 2 $\theta$  indicative of turbostratic carbon, while our previously reported HBC based polymers synthesized using direct polymerization methods do  $\pi$  stacking. Thermogravimetric analysis of POPs indicates polymers are thermally stable with less than 20 wt.% up to 800 °C at N<sub>2</sub> atmosphere (Figure 4-8). SEM analysis indicate the morphology of initial polymers retain in the post synthetic modified polymers (Figure 4-9).

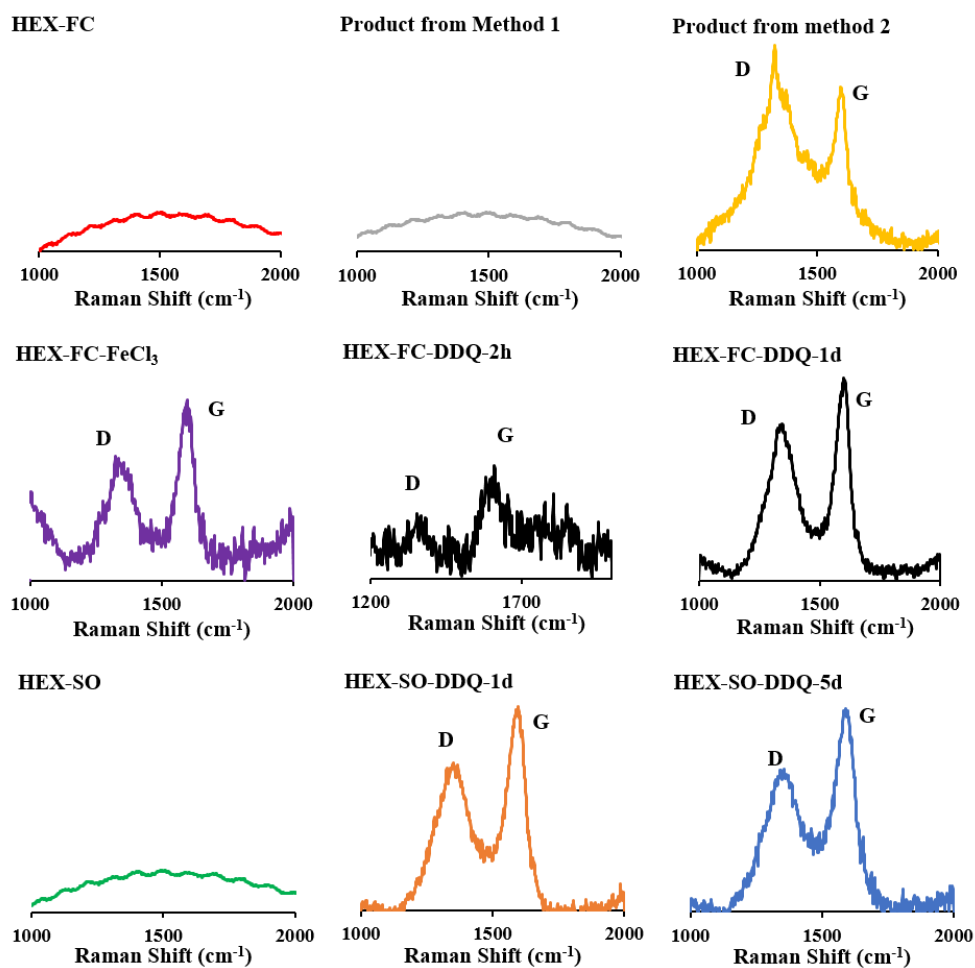


Figure 4-5. Raman spectra of polymers

Table 4-1.  $I_D/I_G$  ratio based on Raman analysis

Sample	$I_D/I_G$ ratio
Method 2	3.87
HEX-FC-FeCl <sub>3</sub>	3.54
HEX-FC-DDQ-1d	3.01
HEX-SO-1d	1.46
HEX-SO-5d	0.86

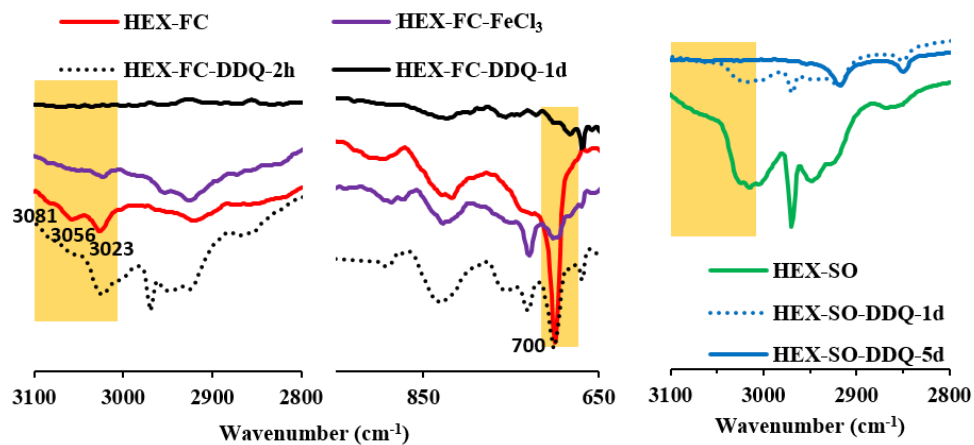


Figure 4-6. FT-IR spectra of polymers

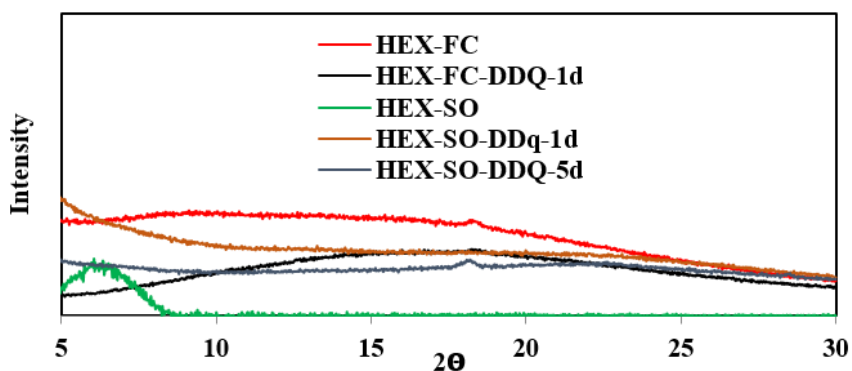


Figure 4-7. Powder X-ray diffraction (PXRD) of polymers

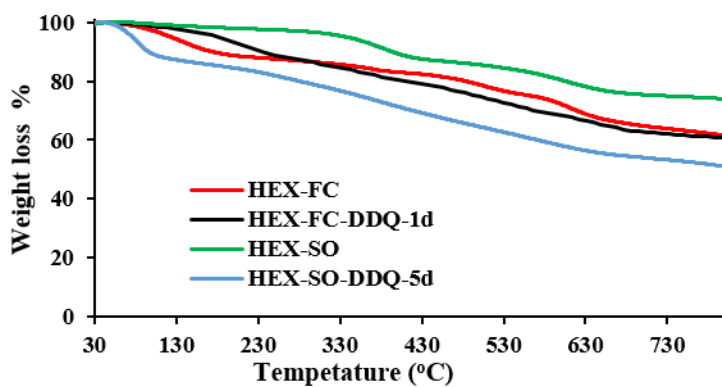


Figure 4-8. TGA of polymers

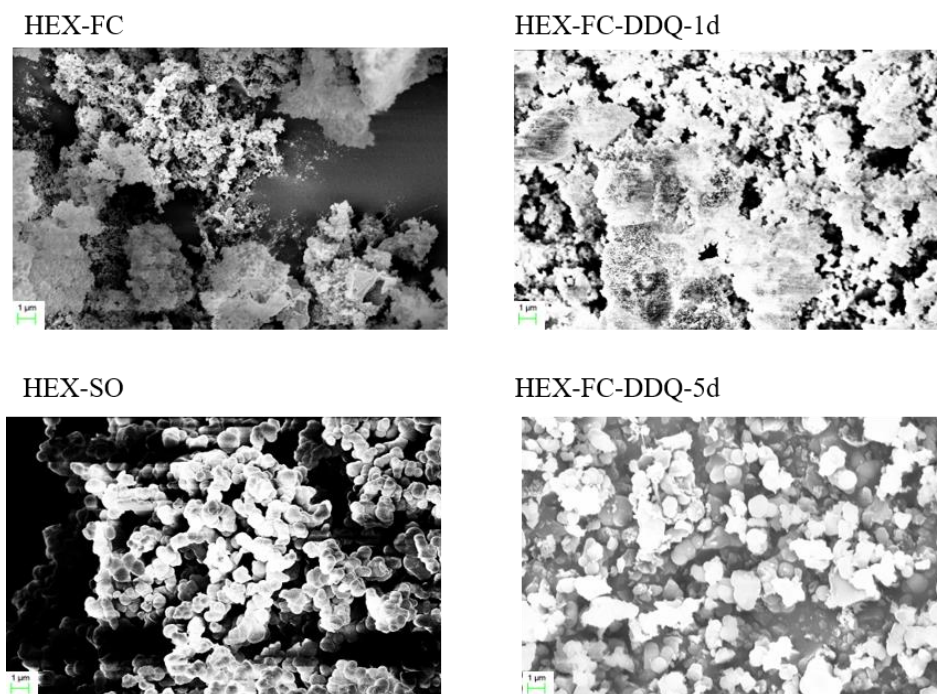


Figure 4-9. SEM images of initial polymers and corresponding NG polymers

#### 4.5 Porosity and surface area

N<sub>2</sub> adsorption measurements at 77 K were used to measure the accessible surface areas and pore size distributions of each POP (Figure 4-10). The product obtained from direct FC polymerization of HBC (**Method 1**) has a low surface area (57 m<sup>2</sup>/g). This is possibly because polymerization might not have occurred owing to the poor reactivity of HBC under FC conditions, or its poor solubility. MALDI analysis of the product of this polymerization indicates that unreacted HBC is present. The product obtained *via* FC reaction on HEX with excess FeCl<sub>3</sub> (60 equiv) (**Method 2**) shows moderate N<sub>2</sub> adsorption capacity of 243 cm<sup>3</sup>/g and BET surface area of 517 m<sup>2</sup>/g. The presence of excess amount of FeCl<sub>3</sub> should definitely support the cyclodehydrogenation of HEX and oligomers of HEX, limiting the progress of FC polymerization parallel to HBC formation.

However, the same reaction with FeCl<sub>3</sub> (6 equiv) yielded a highly porous polymer, HEX-FC with high N<sub>2</sub> adsorption capacity of 1422 cm<sup>3</sup>/g and BET surface area 1958 m<sup>2</sup>/g.

For the cyclodehydrogenation we used two approaches: *via* mild oxidizing conditions FeCl<sub>3</sub>/CH<sub>3</sub>NO<sub>2</sub> (**method 3**, HEX-FC-FeCl<sub>3</sub>) and strong conditions DDQ/CF<sub>3</sub>SO<sub>3</sub>H for 2 h and 24 h (**method 4**, HEX-FC-DDQ-2h and HEX-FC-DDQ-1d). Based on Raman and FTIR analysis DDQ/CF<sub>3</sub>SO<sub>3</sub>H method for 24 h was found to do the complete cyclodehydrogenation resulting product HEX-FC-DDQ-1d which also shows excellent N<sub>2</sub> adsorption capacity of 1394 cm<sup>3</sup>/g and BET surface area 1722 m<sup>2</sup>/g (Langmuir 1886 m<sup>2</sup>/g) (Figure 4-10).

Table 4-2. Pore structure parameters of polymers obtained by N<sub>2</sub> adsorption

Sample	BET surface area (m <sup>2</sup> /g)	Langmuir surface area (m <sup>2</sup> /g)	Horvath Kawazoe pore volume (cm <sup>3</sup> /g)
HEX-FC	1958	2046	2.20
Method 1	57	59	0.30
Method 2	509	512	0.38
HEX-FC-FeCl <sub>3</sub>	1677	1814	1.75
HEX-FC-DDQ-2h	1803	1971	2.05
HEX-FC-DDQ-1d	1772	1886	1.07
HEX-SO	2222	2370	2.16
HEX-SO-1d	1332	1448	0.64
HEX-SO-5d	1042	1134	0.56

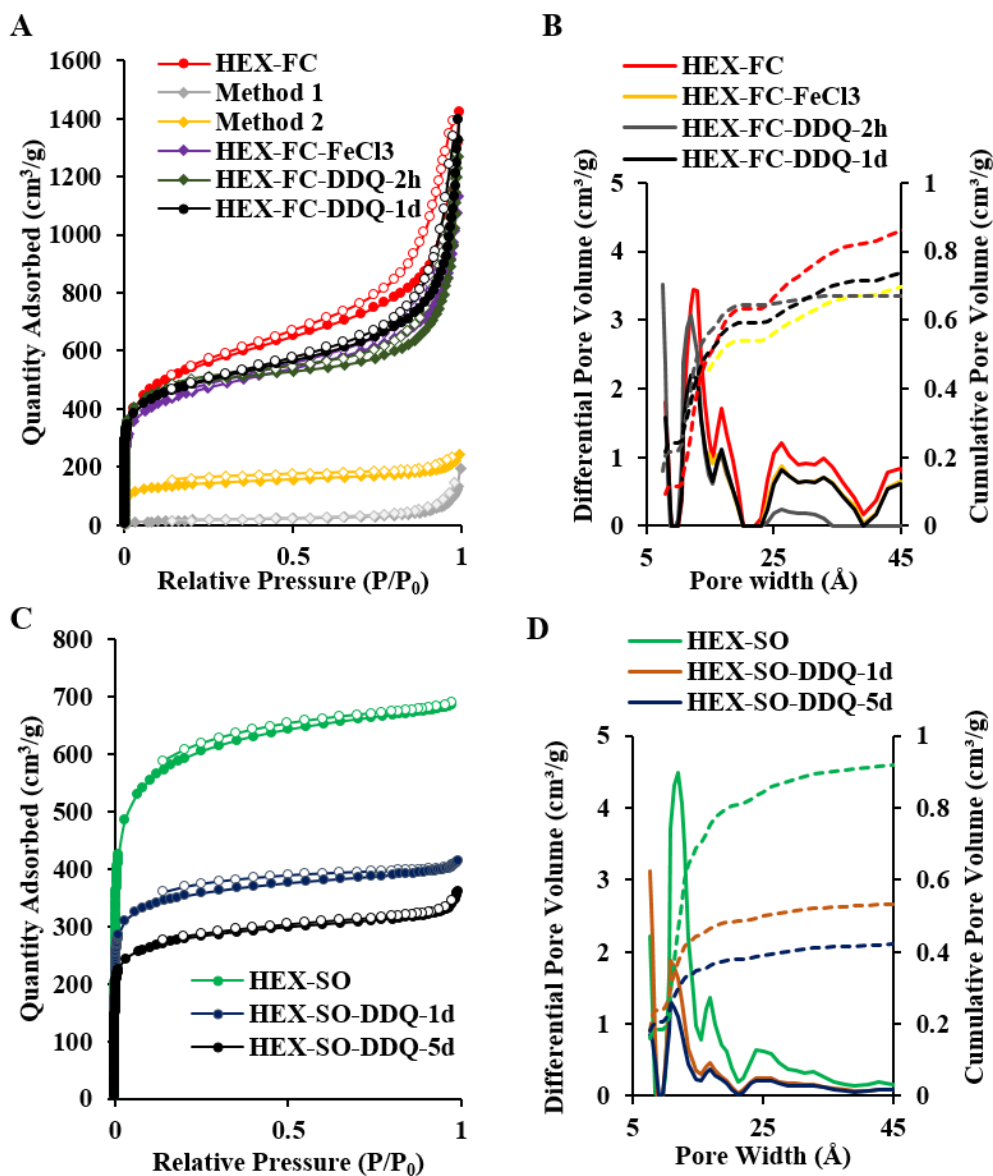


Figure 4-10. Nitrogen adsorption (solid symbols) and desorption (open symbols) isotherms at 77 K and pore size distribution (solid line) and cumulative pore volume (dash) of POPs

The direct SO on HEX with AlCl<sub>3</sub> also resulted in a highly porous polymer, HEX-SO, with a BET surface area of 2222 m<sup>2</sup>/g and N<sub>2</sub> adsorption capacity of 689 cm<sup>3</sup>/g, which exceeds the reported literature value (BET surface area of 1795 m<sup>2</sup>/g)<sup>28</sup> of a similar POP synthesized with HEX under similar conditions. Either careful polymerization or activation process might have increased our



surface area and in three different trials we have been able to reproduce our surface area (BET surface area 2222, 2240, 2272 m<sup>2</sup>/g). The second SO for post polymerized cyclodehydrogenation with strong oxidizing agent DDQ/CF<sub>3</sub>SO<sub>3</sub>H for 1d and 5 d resulted in two HEX-SO-DDQs: HEX-SO-DDQ-1d and HEX-SO-DDQ-5d. HEX-SO-DDQ-1d has BET surface area of 1332 m<sup>2</sup>/g (Langmuir 1448 m<sup>2</sup>/g) while HEX-SO-DDQ-5d has BET surface area of 1042 m<sup>2</sup>/g (Langmuir 1134 m<sup>2</sup>/g) (Figure 4-10).

Interestingly, polymers synthesized *via* SO has a type I isotherm on N<sub>2</sub> adsorption while POPs synthesized *via* FC has type II isotherm mean SO polymers are mostly microporous while FC polymers are micro and mesoporous. This can be observed in porosity distribution as well (Figure 4-10). Thus, it indicates that the direct polymerization of HEX *via* SO provides a uniform crosslinking with higher surface area than using a tetrahedral spacer group as in FC. To the best of our knowledge BET surface area of HEX-SO is the highest reported surface area for any HEX based porous organic material while the HEX-FC is the second.<sup>7,9,28,29</sup> Further, BET surface area of HEX based polymers we are reporting here are higher than many other POPs synthesized *via* FC or SO<sup>28</sup> methods with other aromatic hydrocarbon molecules, for example tetraphenyl methane based PAF-32 (BET-1679 m<sup>2</sup>/g)<sup>30</sup> and PAF-42 (BET- 640 m<sup>2</sup>/g)<sup>14</sup> synthesized *via* FC and SO approaches.

Both HEX-FC-DDQ-1d and HEX-SO-DDQ-5d have lower surface area than that of their precursor polymers while this reduction is much more prominent in the HEX-SO-DDQ. HEX has a propeller like shape and cyclodehydrogenation should planarized the aromatic system reducing the accessible surface area for N<sub>2</sub>. In FC polymers, the external cross-linker may provide a tetrahedral methylene spacer group which might help support the high surface area even after planarization.

#### 4.5.1 CO<sub>2</sub> and CH<sub>4</sub> adsorption

CO<sub>2</sub> adsorption isotherms for the POPs were measured at 273 K and 298 K. The amount of CO<sub>2</sub> adsorbed continually increases with the pressure, implying that the CO<sub>2</sub> adsorption by the porous network has not reached its equilibrium or saturated state in the measured pressure range. Despite the lower surface area, NG based POPs demonstrate higher CO<sub>2</sub> uptake capacities (HEX-FC-DDQ-1d=16.7 wt.%, HEX-SO-DDQ-1d 22.2 wt.% and HEX-SO-DDQ-5d 21.9 wt. %) than that of corresponding initial POPs HEX-FC and HEX-SO (16.4 wt.% and 20.7 wt.% respectively). CO<sub>2</sub> adsorption capacity of HEX-SO is much higher than any other HEX based porous materials.<sup>29</sup> To get further inside in to this, isostatic heats of adsorption ( $Q_{st}$ ) were calculated based on adsorption data at 273 and 298 K (Figure 4-11). Initial  $Q_{st}$  of NG based POPs are much higher than the  $Q_{st}$  of initial POPs. However,  $Q_{st}$  decrease rapidly for NG based POPs while initial POPs show a stabilizing trend. However, the initial  $Q_{st}$  for NG based POPs is higher than that of initial POPs. This indicates that the graphitization facilitates improved affinity for CO<sub>2</sub> adsorption. CH<sub>4</sub> adsorption isotherms for the POPs were also measured at 273 K and 298 K (Figure 4-12). Despite the lower surface area, NG based POPs demonstrate higher CH<sub>4</sub> uptake capacities as well as that of the corresponding initial POPs.

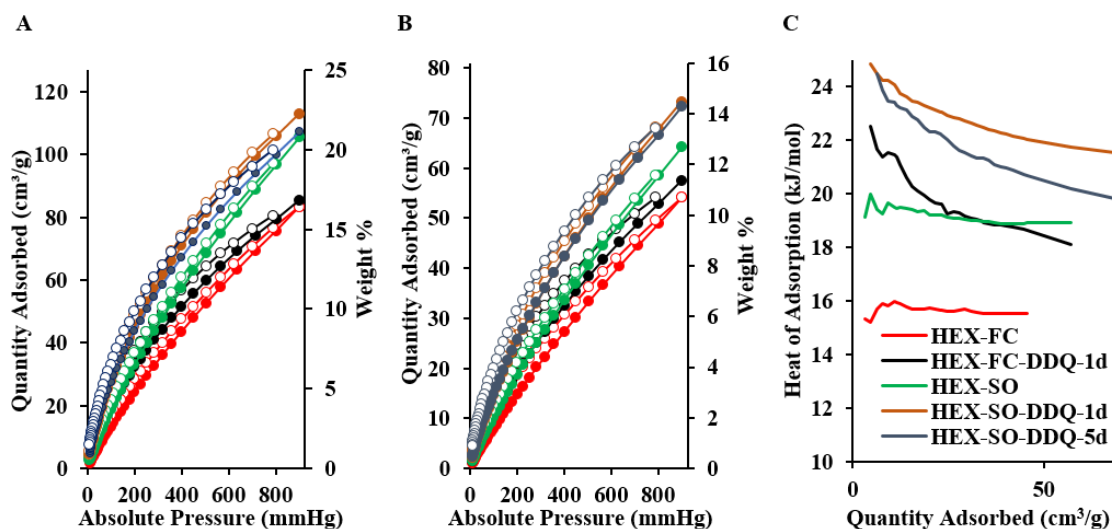


Figure 4-11. CO<sub>2</sub> adsorption isotherms at (a) 273 K, (b) 298 K and (c) heat of adsorption for CO<sub>2</sub>

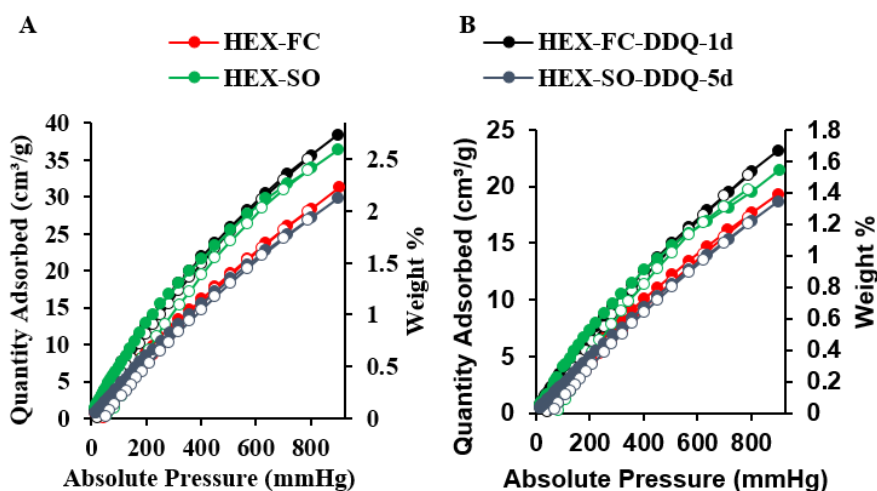


Figure 4-12. CH<sub>4</sub> adsorption isotherms at (a) 273 K and (b) 298 K

## 4.6 Conclusion

Several methods to post-synthetically cyclodehydrogenate HEX-based polymers were evaluated on POPs synthesized using both Friedel-Crafts and Scholl polymerizations. We found that cyclodehydrogenation with DDQ/CF<sub>3</sub>SO<sub>3</sub>H on hypercrosslinked HEX based polymers was the most effective method to convert these polymers to the corresponding hypercrosslinked

nanographene based polymers. While the cyclodehydrogenation reaction decreased the BET surface areas it increased the CO<sub>2</sub> adsorption capacity (up to 22.2 wt.% for HEX-SO-DDQ-1d) indicating that the presence of the HBC units within the POP influence the properties of the material.

#### 4.7 Acknowledgements

This research was carried out with the support of University of Texas at Dallas, and the American Chemical Society Petroleum Research Fund (52906-DNI10). We would like to acknowledge Dr. Y. J. Chabal, Dr. M. A. Quevedo-Lopez, N. Shafiq and M. I. Pintor-Monroy for Raman spectroscopy facilities and assist and Nimali C. Abeykoon, and Sahila Perananthan for valuable discussions.

#### 4.8 References

1. Russo, P.; Hu, A.; Compagnini, G. Synthesis, Properties and Potential Applications of Porous Graphene: A Review. *Nano-Micro Lett.* **2013**, *5*, 260-273.
2. Gadipelli, S.; Guo, Z. X. Graphene-based materials: Synthesis and gas sorption, storage and separation. *Prog. in Mater. Sci.* **2015**, *69*, 1-60.
3. Wasalathilake, C. K.; Ayoko, G.; Yan, C. Porous Graphene Materials for Energy Storage and Conversion Applications. In *Recent Advances in Graphene Research*, Nayak, P. Ed., InTech: **2016** Available from: <http://www.intechopen.com/books/recent-advances-in-graphene-research/porous-graphene-materials-for-energy-storage-and-conversion-applications>
4. Guo, F.; Creighton, M.; Chen, Y.; Hurt, R.; Kulaots, I. Porous Structures in Stacked, Crumpled and Pillared Graphene-Based 3D Materials. *Carbon* **2014**, *66*, 476-484.
5. Byun, Y.; Coskun, A. Bottom-up Approach for the Synthesis of a Three-Dimensional Nanoporous Graphene Nanoribbon Framework and Its Gas Sorption Properties. *Chem. Mater.* **2015**, *27*, 2576-2583.

6. Narita, A.; Wang, X.; Feng, X.; Müllen, K. New advances in nanographene chemistry. *Chem. Soc. Rev.* **2015**, *44*, 6616-6643.
7. Dalapati, S.; Addicoat, M.; Jin, S.; Sakurai, T.; Gao, J.; Xu, H.; Irle, S.; Seki, S.; Jiang, D. Rational design of crystalline supermicroporous covalent organic frameworks with triangular topologies. *Nat. Commun.* **2015**, *6*, 8.
8. Thompson, C. M.; Li, F.; Smaldone, R. A. Synthesis and sorption properties of hexa-(peri)-hexabenzocoronene-based porous organic polymers. *Chem. Commun.* **2014**, *50*, 6171-6173.
9. Thompson, C. M.; McCandless, G. T.; Wijenayake, S. N.; Alfarawati, O.; Jahangiri, M.; Kokash, A.; Tran, Z.; Smaldone, R. A. Substituent Effects on the Gas Sorption and Selectivity Properties of Hexaphenylbenzene and Hexabenzocoronene Based Porous Polymers. *Macromolecules* **2014**, *47*, 8645-8652.
10. Karunathilake, A. A. K.; Chang, J.; Thompson, C. M.; Nguyen, C. U.; Nguyen, D. Q.; Rajan, A.; Sridharan, A.; Vyakaranam, M.; Adegboyega, N.; Kim, S. J.; Smaldone, R. A. Hexaphenylbenzene and hexabenzocoronene-based porous polymers for the adsorption of volatile organic compounds. *RSC Adv.* **2016**, *6*, 65763-65769.
11. Seyler, H.; Purushothaman, B.; Jones, D.; Holmes, A.; Wong, W. Hexa-peri-hexabenzocoronene in organic electronics. *Pure Appl. Chem.*, **2012**, *84*(4), 1047-1067.
12. Xu, S.; Luo, Y.; Tan, B. Recent Development of Hypercrosslinked Microporous Organic Polymers. *Macromol. Rapid Commun.* **2013**, *34*, 471-484.
13. Li, B.; Gong, R.; Wang, W.; Huang, X.; Zhang, W.; Li, H.; Hu, C.; Tan, B. A New Strategy to Microporous Polymers: Knitting Rigid Aromatic Building Blocks by External Cross-Linker. *Macromolecules* **2011**, *44*, 2410-2414.
14. Li, L.; Ren, H.; Yuan, Y.; Yu, G.; Zhu, G. Construction and adsorption properties of porous aromatic frameworks via AlCl<sub>3</sub>-triggered coupling polymerization. *J. Mater. Chem. A* **2014**, *2*, 11091-11098.
15. Li, B.; Guan, Z.; Yang, X.; Wang, W. D.; Wang, W.; Hussain, I.; Song, K.; Tan, B.; Li, T. Multifunctional microporous organic polymers. *J. Mater. Chem. A* **2014**, *2*, 11930-11939.
16. Schwab, M. G.; Narita, A.; Hernandez, Y.; Balandina, T.; Mali, K. S.; De Feyter, S.; Feng, X.; Müllen, K. Structurally Defined Graphene Nanoribbons with High Lateral Extension. *J. Am. Chem. Soc.* **2012**, *134*, 18169-18172.
17. Kim, K. T.; Lee, J. W.; Jo, W. H. Charge-Transport Tuning of Solution-Processable Graphene Nanoribbons by Substitutional Nitrogen Doping. *Macromol. Chem. Phys.* **2013**, *214*, 2768-2773.

18. Kim, K. T.; Jung, J. W.; Jo, W. H. Synthesis of graphene nanoribbons with various widths and its application to thin-film transistor. *Carbon* **2013**, *63*, 202-209.
19. El Gemayel, M.; Narita, A.; Dossel, L. F.; Sundaram, R. S.; Kiersnowski, A.; Pisula, W.; Hansen, M. R.; Ferrari, A. C.; Orgiu, E.; Feng, X.; Mullen, K.; Samori, P. Graphene nanoribbon blends with P3HT for organic electronics. *Nanoscale* **2014**, *6*, 6301-6314.
20. Narita, A.; Verzhbitskiy, I. A.; Frederickx, W.; Mali, K. S.; Jensen, S. A.; Hansen, M. R.; Bonn, M.; De Feyter, S.; Casiraghi, C.; Feng, X.; Mullen, K. Bottom-Up Synthesis of Liquid-Phase-Processable Graphene Nanoribbons with Near-Infrared Absorption. *ACS Nano*. **2014**, *8*, 11622-11630.
21. Vo, T. H.; Shekhirev, M.; Kunkel, D. A.; Orange, F.; Guinel, M. J. -; Enders, A.; Sinitskii, A. Bottom-up solution synthesis of narrow nitrogen-doped graphene nanoribbons. *Chem. Commun.* **2014**, *50*, 4172-4174.
22. Vo, T. H.; Shekhirev, M.; Lipatov, A.; Korlacki, R. A.; Sinitskii, A. Bulk properties of solution-synthesized chevron-like graphene nanoribbons. *Faraday Discuss.* **2014**, *173*, 105-113.
23. Vo, T. H.; Shekhirev, M.; Kunkel, D. A.; Morton, M. D.; Berglund, E.; Kong, L.; Wilson, P. M.; Dowben, P. A.; Enders, A.; Sinitskii, A. Large-scale solution synthesis of narrow graphene nanoribbons. *Nat. Commun.* **2014**, *5*, 3189.
24. Byun, Y.; Cho, M.; Kim, D.; Jung, Y.; Coskun, A. Edge-Functionalized Graphene Nanoribbon Frameworks for the Capture and Separation of Greenhouse Gases. *Macromolecules* **2017**, *50*, 523-533.
25. Johnson, J. R.; Grummitt, O. Tetraphenylcyclopentadienone. *Org. Synth.* **1943**, *23*, 92.
26. Clar, E.; Ironside, C. T. Hexabenzocoronene. *Proc. Chem. Soc.* **1958**, 150-150.
27. Zhai, L.; Shukla, R.; Rathore, R. Oxidative C-C Bond Formation (Scholl Reaction) with DDQ as an Efficient and Easily Recyclable Oxidant. *Org. Lett.* **2009**, *11*, 3474-3477.
28. Msayib, K. J.; McKeown, N. B. Inexpensive polyphenylene network polymers with enhanced microporosity. *J. Mater. Chem. A* **2016**, *4*, 10110-10113.
29. Alahakoon, S. B.; Thompson, C. M.; Nguyen, A. X.; Occhialini, G.; McCandless, G. T.; Smaldone, R. A. An azine-linked hexaphenylbenzene based covalent organic framework. *Chem. Commun.* **2016**, *52*, 2843-2845.
30. Jing, X.; Zou, D.; Cui, P.; Ren, H.; Zhu, G. Facile synthesis of cost-effective porous aromatic materials with enhanced carbon dioxide uptake. *J. Mater. Chem. A* **2013**, *1*, 13926-13931.

## **BIOGRAPHICAL SKETCH**

Arosha Aruni Kumari Karunathilake was born in Kandy, Sri Lanka. She received her bachelor's degree in chemistry in June 2007 from University of Peradeniya, Sri Lanka. After graduating she worked as a demonstrator and then as a research assistant at University of Peradeniya for another year. Then she joined Uva Wellassa University of Sri Lanka as a demonstrator in August 2008 and was promoted as a lecturer in April 2009. She entered The University of Texas at Dallas in fall 2012 to pursue her PhD in Chemistry under the supervision of Dr. Ronald A. Smaldone.

## CURRICULUM VITAE

### Arosha A. K. Karunathilake

Email: axk113330@utdallas.edu

---

#### Personal Summary

- Skilled organic/materials chemist with extensive hands-on experience on organic synthesis and materials characterization.
- Enthusiastic individual with eight years' experience in teaching chemistry in higher education.
- PhD candidate expecting to graduate in spring 2017.

#### Education

##### PhD in Chemistry - Candidate

The University of Texas at Dallas, TX, USA

August 2012-present

Thesis title: Expanded aromatic monomers for functional porous polymers

##### BSc Special in chemistry (Hons)

University of Peradeniya

2003-2007

Major: Chemistry

Minor: Biology, Molecular biology and biotechnology

Thesis title: Antibiotic activity of tea catechins against *Pseudomonas aeruginosa* and Enterococci.

##### Certificates and Courses

Graduate Teaching Certificate

The University of Texas at Dallas, TX, USA

2016-present

Certificate Course on Teaching in Higher Education

The Staff Development Centre of Uva Wellassa University of Sri Lanka

2011-2012

Higher Diploma in Information Technology

University of Colombo, Sri Lanka

2008

#### Teaching and Research Experience

##### Graduate Teaching/Research Assistant

The University of Texas at Dallas, TX, USA

August 2012-present

Teaching Assistant: General chemistry - 2012 Fall, 2013 Spring, 2014 Summer

Organic chemistry - 2013 Fall, 2014 Spring, 2015 Fall

- Conducting practical classes, and pre-lab lectures
- Grading pre-lab, post lab assignments and quizzes
- Proctoring and grading exams for lecture courses

Research Assistant:

- Advisor: Prof. Ronald A. Smaldone
- Research interest: Synthesis of novel functional porous polymers
- Skills: Organic synthesis, Porosity analysis, SEM, EDX, EPS, PXRD, MALDI-TOF, NMR, UV/Vis, FTIR, Fluorescence Spectroscopy, Raman spectroscopy, TGA



**Lecturer**

Uva Wellassa University of Sri Lanka, Badulla, Sri Lanka April 2009-July 2012

- Lecturing and Instructing laboratory classes on organic chemistry
- Co-supervising undergraduate research projects -Natural products chemistry
- Curriculum and Laboratory development in Chemistry and Material Science and Technology
- Faculty board member - Faculty of Science and Technology
- Resource person for high school science camps in the Uva province

**Demonstrator**

Uva Wellassa University of Sri Lanka, Badulla, Sri Lanka August 2008-April 2009

- Lecturing on organic Chemistry
- Instructing laboratory classes –general, organic and analytical chemistry

**Research Assistant**

University of Peradeniya, Sri Lanka February 2008-July 2008

- Research Advisor: Prof. B.M.R. Bandara
- Skills: Natural products extraction and isolation, HSCCC, Microbiology techniques and antibiotic assay

**Demonstrator**

University of Peradeniya, Sri Lanka July 2007-January 2008

Teaching assistant for general chemistry laboratories.

**Undergraduate Researcher**

University of Peradeniya, Sri Lanka August 2012-July 2013

Advisor: Prof. B.M.R. Bandara

**Publications**

3. S. B. Alahakoon, G.T. McCandless, **A. A. K. Karunathilake**, C. M. Thompson and R. A. Smaldone, Enhanced Structural Organization in Covalent Organic Frameworks Through Fluorination, *Chem. Eur. J.*, **2017**, 23,4255-4259.
2. **A. A. K. Karunathilake**, C. M. Thompson, S. Peranathan, J. P. Ferraris and R. A. Smaldone, Electrochemically active porous organic polymers based on corannulene, *Chem. Commun.*, **2016**, 52, 12881-12884.
1. **A. A. K. Karunathilake**, J. Chang, C. M. Thompson, C. U. Nguyen, D. Q. Nguyen, A. Rajan, A. Sridharan, M. Vyakaranam, N. Adegboyega, S. J. Kim and R. A. Smaldone, Hexaphenylbenzene and Hexabenzocoronene-based Porous Organic Polymers for Adsorption of Volatile Organic Compounds, *RSC Adv.*, **2016**, 6, 65763-65769.

**Presentations**

7. **Arosha A.K. Karunathilake**, Ronald A. Smaldone, Hexaphenylbenzene based Conjugated Porous Organic Polymers through Cu Catalyzed Homopolymerization of Alkynes and Alkynylsilanes, 49th Annual Meeting-in-Miniature, Dallas-Fort Worth Section of the American Chemical Society, Denton, TX, USA, April, 2016
6. **Arosha A.K. Karunathilake**, Christina M. Thompson, Ronald A. Smaldone, Hexaphenylbenzene and Hexabenzocoronene- based Porous Polymers for Selective Adsorption of Volatile Organic Compounds, ACS National Meeting, San Diego, CA, USA, March 13-17, 2016

5. **Arosha A.K. Karunathilake**, Christina M. Thompson, Ronald A. Smaldone, Corannulene-Based Porous Organic Polymers, 48th Annual Meeting-in-Miniature, Dallas-Fort Worth Section of the American Chemical Society, Arlington, TX, USA April, 2015
4. **A. A. Karunathilake**, R. A. Smaldone, *Microwave-assisted* synthesis of polyaromatic compounds, ACS National Meeting, Dallas, TX, USA, March 16-20, 2014
3. W. W. Kumbukgolla, **A. A. K. Karunathilake**, V. Thevenesam, G.J. Panagoda N.S. Kumar and B.M.R. Bandara, Antimicrobial Activity of Tea Polyphenols against Some Clinically Important Pathogens. NPAHA 2011, Int. Symposium, Natural Products, IFS, Kandy, Sri Lanka, October 3-8, 2011
2. **A. A. K. Karunathilake**, S. R. W. A. B. M. N. S. Kandepola, G.J. Panagoda, V. Thevenesam, N.S. Kumar, B.M.R. Bandara. Anti-Candida Activity of Catechins Isolated from Fresh Tea Flush, Mature Tea Leaves and Green Tea, Peradeniya University Research Session, Peradeniya, Sri Lanka 2009.
1. **A. A. K. Karunathilake**, W. W. Kumbukgolla, E. W. M. A. Ekanayake, V. Thevenesam, N. S. Kumar and B. M. R. Bandara. Screening for antibiotic activity of tea catechins against *Pseudomonas aeruginosa* and Enterococci. Peradeniya University Research Session, Peradeniya, Sri Lanka 2007.

## Awards

PhD Small Research Grant,	2016
The Office of Vice President for Research at UT Dallas	
Graduate Studies Scholarship, University of Texas at Dallas	2012-2017

## Other Affiliations and Activities

Member, American Chemical Society	Since 2013
Sri Lankan Student Association, University of Texas at Dallas	Since 2012
Vice President of SLSA, UTD	2015-2016
Assistant Secretary - Organizing committee	
Uva Wellassa University Research Symposium	2011